UNIVERSITY OF CALIFORNIA

Santa Barbara

Endocrine modulation of large-scale brain networks — implications for women's brain health

A dissertation submitted in partial satisfaction of the

requirements for the degree Doctor of Philosophy

in Psychological and Brain Sciences

by

Laura A. Pritschet

Committee in charge:

Professor Emily G. Jacobs, Chair

Professor Scott T. Grafton

Professor Thomas Sprague

Professor Michael Gazzaniga

September 2023

The dissertation of Laura A. Pritschet is approved.

_____

Scott T. Grafton

_____

Michael Gazzaniga

_____

Thomas Sprague

_____

Emily G. Jacobs, Committee Chair

September 2023

Endocrine modulation of large-scale brain networks — implications for women's brain health

For my guiding lights, Jeanette & Brian Pritschet.
In my life, I love you more

ACKNOWLEDGEMENTS

"Women are born with pain built in. It's our physical destiny: period pains, sore boobs, childbirth, you know. We carry it within ourselves throughout our lives, men don't. We have it all going on in here inside, we have pain on a cycle for years and years and years and then just when you feel you are making peace with it all, what happens? The menopause comes, the [bleep] menopause comes, and it is the most wonderful thing in the world. And yes, your entire pelvic floor crumbles and you get hot and no one cares, but then you're free, no longer a slave, no longer a machine with parts. You're just a person."

Phoebe Waller-Bridge, 2019

I will never forget sitting in my behavioral neuroscience lab course junior year of college, a sense of disdain growing at the remarkably consistent exclusion of females from every animal study the curriculum had us discuss. It came to a head one day when I asked my professor about this lack of representation. I received the disheartening "female hormones are too complicated to study" excuse. I thought to myself, *half of the world's population is made up of females, how are we a disqualification from scientific inquiry?* Frustration with this misguided dogma has fueled my commitment to use my voice and leverage the broader impact of my work to advance women's health. In doing this, I stand on the shoulders of giants — the women and allies who have dedicated their lives to making the world a better, more equitable place. Thank you to those that have come before, those fighting now, and

the future generation of advocates who know women deserve better and will stand for no less. Thank you to all who have shared your experiences with the world. Each story is worthy.

Rosalind Franklin famously wrote, *"science and everyday life cannot and must not be separated".* Thank you to the individuals who took time *out of their everyday lives* to help us better understand the brain. You were busy being parents, spouses, employees, menopausal, and occasionally claustrophobic. But on that day, you chose to prioritize our science and I am forever indebted to you.

I am not one to put my faith in destiny, but I do believe having Emily Jacobs as my graduate mentor was an act of fate. After our first meeting in 2017, I knew I had to work with her. It was clear after *one* discussion that Emily is a scientist who cares first and foremost about the greater good, having been an advocate for women's health and equality her entire life. Emily is not motivated by trophies, impact factors, or flag planting. She cares to identify the disparities and do whatever it takes to correct course, all so that women can live better lives. She inspires everyone she encounters, and we are not just better scientists for it, we are better people.

Emily, I've been fortunate enough to witness your magic over the last six years. You are an excellent teacher and mentor who leads with creativity, passion, energy, thoughtfulness, and brilliance. You make UCSB a renowned place to receive an education — the best decision *anyone* could make. Thank you for answering every frantic call with patience, offering up every opportunity a mentee could ask for,

entertaining wild dreams and making them a reality, giving me the space to realize my ideas were bad on my own, making science fun, *redefining* the very notion of a 'hype-woman', and providing an environment where I could thrive and feel excited every single day. From growing up two miles from each other in same small Illinois town, to graduate school in California, and now postdoc'ing on the east coast, I have always been trying to follow in your footsteps. And who better to follow? Thank you for being the best example of a well-rounded scientist, advocate, boss, mother, partner, and friend. I am so fortunate to be molded by you not only as an academic, but as an individual finding their way in this world. Your star has *already gone supernova* a million times over — it's your universe and we are all lucky to be living in it. You're the hero drawn on my wall.

To my nearest and dearest, Caitlin Taylor. You are the next exception to my opposition of destiny. I knew you were my soulmate the day I met you — spending an ungodly amount of time fawning over Emily's fancy refrigerator with me. You have not only been an academic mentor to me, but a role model and guiding light in all aspects of my life. Just like your dad, you are an artist in your own right. Your ability to visualize the complex world, the messy science, the nuanced problems we face *and eloquently* pave a way forward, well I have never seen anything quite like it. I always have and always will count on your honest opinion, because even though it saddens me when you vehemently oppose my celebrity crushes (for one), I know you are always right. Guiding me in the right direction, looking out for me. You make every person around you feel seen and heard, and I hope you recognize how very *rare* and *special* it is to possess *that* skill — a real life superpower.

Caitlin, thank you for fixing every single one of my figures, replacing my beloved em-dashes with the more appropriate commas, and always lifting me up when the imposter syndrome would creep in. Most importantly, thank you for keeping a permanent smile on my face — I have *cackled* more in past six years than I have in my whole life combined. With your unparalleled dance moves, pronunciations, ‘isms (‘do not shatter me’), and hilarious *slash spot-on* hot takes, you light up every room. You’re my favorite collaborator, conference buddy, hotel roommate, and bartender. Even though I am soon flying the nest, I will always be there to spend hours going over the presentations you make to choose the perfect throw pillow, sneakily wallpaper your office, spend every first Monday of May rating Met Gala outfits together, consume inedible shortcake and deem it amazing, and join your bubble in all future epidemiological crises. I value you and our friendship more than you could ever know. I love you, I love your family, and I cannot wait for all our future clowning.

Emily and Caitlin. Thank you for all the laughs — from unstealthily escaping packed events via a hill of loose dirt, carelessly running across busy intersections to find our car, being the loudest table at every restaurant, spending countless hours meticulously perfecting color schemes and single words in a manuscript, and being the only people on the dance floor — I will cherish our trio forever. Thank you for guiding me through my twenties and giving me endless advice on all the forks in the roads and insecurities I faced. I couldn’t have done any of this journey without you both. I will end my love letter by recognizing the blood, sweat, and tears you two have put into the Ann S. Bowers Women’s Brain Initiative over this past half decade.

A thank you barely covers it, but on behalf of all women everywhere — we are grateful.

I would like to thank my committee members — Drs. Scott Grafton, Michael Gazzaniga, and Thomas Sprague — for their guidance and support over the past six years. I have become a better scientist not only because of your helpful insight, but by pondering the critical questions you have presented before me. Even though I may not have cracked the answers to every question yet, I have developed the tools necessary to tackle them *because of* your mentorship. I'd like to give an extra special thanks to Scott Grafton, the inaugural *Jacobs Lab Honorary Cycling Female* award winner. Scott, thank you for the planting the seed that became the 28andMe project over a simple lunch back in 2019. I appreciate you green-lighting each crazy dense-sampling project request even after we promise '*this will be the last one*'. Your support, in all its forms, means so much.

The biggest lesson I have learned thus far in my academic career is that collaborative science is critical for impactful discovery. Thank you to my fellow Jacobs Lab graduate students — Shuying Yu, Elle Murata, and Hannah Grotzinger — for sharing and exchanging your knowledge with me over these past several years. Whether commiserating over the difficulties of data collection or derailing each lab meeting with more entertaining gossip and pop culture discussions, I've had such a wonderful time with our team. I feel very fortunate to be surrounded by such hard-working scientists, each with their own unique motivations and goals for improving women's health. I've become a better scientist and advocate by knowing you. Also, this work would not have been completed without the help of some

insanely brilliant and driven research assistants: Morgan Fitzgerald, Courtney Kenyon, Aidan Galati, Christine Shoemaker, Michaela Bostwick, and Ella Carllson. You each have the world in the palm of your hands; I can't wait to see how much better it becomes with all of you at the helm.

Thank you to my colleagues in PBS for providing me the opportunity to push the creative bounds of scientific thinking with such a fun and intelligent group of individuals. To the Miller Lab team, especially Tyler Santander and Evan Layher, thank you for coming on board to help us execute these challenging, time-consuming experiments. It wouldn't have been accomplished without you. Tyler, I owe you an entire brewery's worth of beers for all your help over the past six years. Thank you for patiently and repetitively explaining the ins-and-outs of MRI methods to me. You remain a core member of my training team and I hope you'll accept this rose to be a collaborator on women's brain health forever. Another big thank you to my collaborators beyond PBS, including Rachel Buckley, Joshua Mueller, Jean Carlson, Joshua Faskowitz, Daniel Handwerker, Elizabeth Chrastil, Daniela Cossio, Magdalena Martínez-García, Susana Carmona, and Rachel Schroeder. I will never take for granted the privilege it is to know and work with you. I also wouldn't be here today without those who introduced me to research as a bright-eyed and bushy-tailed undergraduate: Sepideh Sadaghiani, Max Egan, Zachary Horne, Larisa Hussak, Christina Tworek, Shelbie Sutherland, and Andrei Cimpian. I'm so grateful you took me under your wing.

To the heroes of PBS: Chris McFerron, Katherine Lowe, Shane Zheng, and Mario Mendoza. Thank you for keeping every graduate student's head above water,

making our lives easier by giving us the resources to succeed, advocating for us, and cheering on the science. Chris, thank you serving as our third-party representative for each dense-sampling project, ensuring that us guinea pigs were healthy, happy, and heard. Mario, thank you for immediately jumping on board these crazy dense-sampling projects. It took just as much dedication and time from you as it did the participant, and yoour care and attention to our well-being meant the world. As such, I am deeply sorry that I almost kicked you in the face when we tried to take blood from my foot. Additionally, a special thanks to the NRI grants management team, including Julia Niessen, Kyle Hekhuis, and Rosa Soriano, for kindly taking those frantic *Friday at 4pm* phone calls and providing endless grant support. It simply would not have happened without any of you.

To the friendships I have made in Santa Barbara that I will cherish forever. Katy, Jonathan, Abby, Cris, Devi, Cate, Julian, and Kevin: from laughing so hard we fall to the floor, to drunk mac and cheese nights, dancing at O'Malleys, hiding in uncomfortable positions for 30 minutes while waiting to surprise people on their birthdays, letting our intensities shine during innocent games of fishbowl, and showing up for each other when it mattered most…you are my people. I'd especially like to thank my "Santa Barbara bff", Katy Walter, who has been there with me every step of the way since graduate orientation. Although we unintentionally twin and people can never tell us apart, you and I both know how different we are from each other. And there's beauty to this difference — we can always be what the other needs. Thank you for your constant loyalty, confidence, encouragement, and support. My best memories in graduate school are with you: pasta nights at San

Clemente, being called ‘two girls on a budget’ when shopping for apartment furniture, venting after hard days, Jane dinners to celebrate milestones, self-care nights, and co-hosting parties with our inner circle. I will forever copy everything you do because you are more than a friend, you are a role model.

I’d also like to thank the people who have been a big source of support, joy, and comfort my whole life. To my best friend Ashtan — and now her husband Robert, an honorary bestie — as well as my favorite Charleston natives, Maddy, Linnea, and Alex: I love that we can chat for hours as well as give each other the silence that only comes when two people understand each other. To my siblings, Sara and Michael: my earliest memories in life are with you two by my side. Thank you for being my earliest protectors, supporters, comedic relief, and role models. Although we are each so different, the ties that bind us are strong. Megan and Juraj, thank you for joining this family circus, we are better off for it. Shiloh, Sophia, & James, I’ll always be in your corner. I love you.

I will end the world’s longest acknowledgements section by trying to put into words the appreciation I have for three of the most important people in my life. To my parents, Jeanette and Brian, fierce champions of science and my unwavering support system. I am who I am because of your unique molding, a blend of both your passions. To my mom, the social scientist. You are the fiercest, most independent, quick-witted person I know. Growing up in a time when the expectations for a woman were rooted in outdated traditions, you ignored the noise and continued to be your authentic ‘*always challenge the status-quo and make your opinions known’* self. Indeed, my first foray into feminism was watching *you* navigate this world. You

juggled graduate school, babies, and full-time social work all while being there for extended friends and family — you have always been able to do it all. I hope you know just how frequently I brag about your intellect and introspection. I take great pride in being referred to as a 'mini-Jeanette', which (to me) means being able to know when to speak up for myself or laugh something off and move forward. Thank you for your daily check-ins, lending a shoulder when I need to decompress, and making me laugh like no other. No matter how old I get, I'll always need you.

Behind every extrovert exists an introvert trying to keep the peace. To my dad, the biological scientist. Some of my earliest memories with you were spending hours at the public library together. You'd leave me in the children's section and come back with a stack of 10 books that you'd get through in a single week. I love asking you questions because I love knowing you'll have the answer. As such, I wanted to become an expert in *something* just so I could do the same. And even though you like to rile me up and be contrarian, I'll have you know that you have been one of the most prominent feminists in my life. I knew I could never tell you (or mom) that I felt like I couldn't achieve something because of my gender — the colorful response that would ensue would be enough to squash anyone's imposter syndrome. You are the best girl dad in the game. And now that you are passing on the Dr. Pritschet title to me, I promise to represent our name with the utmost respect and care, with just a little more flair.

Simply, thank you to my parents for always *being there*. Every single game, performance, milestone. Every night at the dinner table. Every day. Thank you for encouraging me to be myself, through and through, from the very beginning.

Finally, to my fiancé, Pavel. To know you is to love you. I could count all the stars in every galaxy, and it still wouldn't be close to capturing how lucky I feel to be your partner. The only good thing to come out of participating in an intramural UCSB softball league. It has been such a fun journey to go through graduate school with you, from our humble beginnings of coffee dates at Nano Cafe to me becoming a Mrs. and Dr. in the same week. You're my go-to editor, reviewer, illustrator, therapist, mentor, programmer, cheerleader, and test subject, always helping me to become a better scientist because of your vast skill set, brilliance, and supernatural patience.

Thank you for being the He to my Me, subjecting yourself to 40 MRI scans and blood draws — *during the busiest time of your graduate career no less* — to help push our lab's science forward. You are unmatched. Thank you for closing my computer and forcing me to log off Slack when I needed to rest. For going line-by-line to check for typos in each and every grant, manuscript, application, and slide deck. For sneakily running across campus to catch my presentations just so you could hug me afterwards. For those times I catch you ranting about the lack of women's health research with random strangers at a party. But mostly, thank you for taking care of me when I can't take care of myself. I promise, for the rest of our lives, to return the favor. Every step, every way, with you.

It would be ridiculous to finish my acknowledgments without a proper shoutout to Taylor Swift for providing the soundtrack to my PhD. To sum it up how it feels:

"I have this thing where I get older but just never wiser"

VITA OF LAURA A. PRITSCHET
September 2023

Education

University of California – Santa Barbara, Santa Barbara CA 2023
Ph.D., Psychological and Brain Sciences

University of Illinois – Urbana-Champaign, Urbana, IL 2017
B.S., Psychology

National University of Ireland – Galway, Galway, IE 2016
Visiting Student, Cognitive Neuroscience

Appointments

Graduate Researcher, UCSB 2017 - 2023
Advisor: Dr. Emily G. Jacobs
Thesis: Endocrine modulation of large-scale functional brain networks

Undergraduate Research Assistant, UIUC 2016 – 2017
Advisor: Dr. Sepideh Sadaghiani
Senior Project: Dynamic changes in perception and oscillatory spectral analysis

Undergraduate Research Assistant, UIUC 2014 – 2017
Advisor: Dr. Andrei Cimpian
Thesis: Effortful vs. prosocial empathy: a development study in children

Funding

National Institutes of Health F99/K00 Award	2022 – 2027
National Institutes of Health F31 NRSA Award	2021 – 2022
UCSB Graduate Division Dissertation Fellowship	2021
Neuroscience Research Institute Travel Award	2019
Carle Hospital Neuroscience Research Award	2017
Fresenius Medical Scholarship	2013 – 2017

Awards & Honors

Michael D. Young Engaged Scholar Award	2023
Fiona and Michael Goodchild Graduate Mentoring Award	2023
Lindau Nobel Laurate Meeting, UC Representative	2021, 2023
NIH ORWH Science Policy Scholar Travel Award	2020, 2022
Women's Health Research Cluster Trainee Award	2021
Undergraduate Excellence in Cognitive Neuroscience	2017
UIUC Liberal Arts & Sciences James Scholar	2013 – 2017

Publications

**denotes equal authorship*

Pritschet L., Taylor C., Cossio, D., Santander, T., Grotzinger, H., Faskowitz, J., Handwerker, D., Layher, E., Chrastil, E.R., & Jacobs E.G., Neuroanatomical changes observed over the course of a human pregnancy (2023). *Under Review*

Greenwell, S., Faskowitz, J., **Pritschet, L.**, Santander, T., Jacobs, E.G., & Betzel, R.F. (2023) High-amplitude network co-fluctuations linked to variation in hormone concentrations over menstrual cycle. *Network Neuroscience* 1-40

Taylor C., **Pritschet L.,** & Jacobs E.G. (2021) The scientific body of knowledge—whose body does it serve? A spotlight on oral contraceptives and women's health factors in neuroimaging. *Frontiers in Neuroendocrinology*, 100874. Special Issue: Beyond Sex Differences: A Spotlight on Women's Brain Health

Mueller J.*, **Pritschet L.*,** Santander T., Taylor C.M, Grafton S.T., Jacobs E.G, & Carlson J.M. (2021) Dynamic community detection reveals transient reorganization of functional brain networks across a female menstrual cycle. *Network Neuroscience* 5(1):125-144

Pritschet L., Taylor, C.M., Santander T., & Jacobs E.G. Applying dense-sampling methods to reveal dynamic endocrine modulation of the nervous system (2021). *Current Opinion in Behavioral Sciences,* 40:72-78.

Pritschet L.*, Santander T.*, Taylor C.M., Layher E., Yu S., Miller M.B., Grafton S.T., & Jacobs E.G. (2020) Functional reorganization of brain networks across the human menstrual cycle. *Neuroimage*, 220, 117091. +***Cover Image***

Taylor C.M, **Pritschet L.,** Olsen R., Layher E., Santander T., Grafton S.T., & Jacobs E.G. (2020) Progesterone shapes medial temporal lobe volume across the human menstrual cycle. *Neuroimage*, 220*,* 117125. +**Featured Review and Editors' Choice** in *Science Translational Medicine.* Ref: Stevens J. (2020) Brain structural changes in sync with the cycle *12, 553*

Fitzgerald M.*, **Pritschet L.*,** Santander T., Grafton S.T., & Jacobs E.G. (2020) Dynamic cerebellar network organization across the human menstrual cycle. *Scientific Reports, 10,* 20732

Taylor, C. M., **Pritschet, L.,** Yu, S., & Jacobs, E. G. (2019). Applying a women's health lens to the study of the aging brain. *Frontiers in human neuroscience*, *13*, 224

Pritschet, L., Powell, D., & Horne, Z. (2016). Marginally significant effects as evidence for hypotheses: Changing attitudes over four decades. Psychological Science, 27(7), 1036-1042.

Select Presentations

Lindau Nobel Laureate Meeting, Next Gen Science Symposium 2023
Talk: Endocrine modulation of the brain as revealed by precision imaging

Massachusetts General Hospital / Harvard Medical School 2023
Talk: Endocrine modulation of large-scale brain networks: implications for women's brain health

Organization for Human Brain Mapping & Whistler Brain Meetings 2023
Poster: The impact of endocrine aging on intrinsic functional brain architecture in healthy, midlife women

Cognitive Neuroscience Society Annual Meeting 2023
Poster: Brain structure changes observed over the course of a human pregnancy

Organization for the Study of Sex Differences Annual Meeting 2022
Talk: Applying dense-sampling to reveal endocrine modulation of the central nervous system

Organization for the Study of Sex Differences Annual Meeting 2022
Talk: The scientific body of knowledge – whose body does it serve? A spotlight on human neuroscience

Organization for Human Brain Mapping Annual Meeting 2019
Poster: Estradiol shapes resting-state functional connectivity over a complete reproductive cycle

Society for Neuroscience Annual Meeting 2018
Poster: Reproductive aging shapes top-down, goal-directed modulation of visual processing

Teaching

PBS Behavioral Endocrinology, TA	2020
PBS Memory and Cognition Lab, TA	2019
PBS Hormones and Cognition, TA	2018 – 2019

Service & Membership

Mentor, Access Grads (Co-President, 2021– 2022)	2018 – 2022
Organizer, Connectivity Tutorial Workshop	2019 – 2021
Panelist, PNAS Journal Club	2021
Member, Women's Health Research Cluster	2020 –
Member, Organization for Human Brain Mapping	2019 –
Member, Organization of the Study of Sex Differences	2018 –

ABSTRACT

Endocrine Modulation of large-scale brain networks —

implications for women's brain health

by

Laura A. Pritschet

Since its inception, the field of neuroendocrinology has provided evidence for a tightly coupled relationship between the nervous and endocrine systems. In rodents and nonhuman primates, estrogen and progesterone's impact on the brain is evident across a range of spatiotemporal scales. Yet, the influence of sex hormones on the structural and functional architecture of the human brain is largely unknown. The body of work presented in my dissertation aims to advance our understanding of the human brain through the lens of neuroendocrinology by examining how distinct hormonal transition periods shape brain morphology and function. In Study 1, I present findings from my keystone '28andMe' precision imaging experiment, in which a participant underwent brain imaging and venipuncture every 24 hours over 30 consecutive days across a complete menstrual cycle and again, one year later, while on an oral hormonal contraceptive regimen. The results from this study reveal the rhythmic nature in which brain networks reorganize across the cycle, with transient increases in estradiol enhancing global efficiency of several large-scale networks. In Study 2, this approach was expanded by conducting the first precision imaging experiment on pregnancy, in which a primiparous woman underwent 26 MRI scans and venipuncture

beginning 3 weeks pre-conception through two years postpartum. Pronounced decreases in gray matter volume and cortical thickness paired with increases in white matter microstructure were evident across the brain, with few regions untouched by the transition to motherhood. Finally, in Study 3, I present findings from our Midlife Hormones and Cognition Study, where a highly characterized sample of 85 midlife women (ages 43–60) in various states of ovarian decline underwent MRI scanning and venipuncture to establish how endocrine aging influences whole-brain intrinsic network organization. Results suggest that the frequency of menopause-related vasomotor and neurological symptoms exacerbate network connectivity decline in postmenopausal women, especially among higher-order cognitive networks. Together, these studies provide novel insight into the spatiotemporal extent of human brain–hormone relationships over the lifespan, a severely understudied area in cognitive neuroscience with significant implications for women's health.

TABLE OF CONTENTS

1

Prelude

Adapted from the following article: Taylor, C. M., **Pritschet, L.,** & Jacobs, E. G. (2021). The scientific body of knowledge–Whose body does it serve? A spotlight on oral contraceptives and women's health factors in neuroimaging. *Frontiers in neuroendocrinology*, *60*, 100874.

Ensuring women benefit equally in the biological sciences

We are at an exciting scientific and technological inflection point in human history; we now have unprecedent insight into the human brain, with rapidly expanding knowledge of the metabolic, neurochemical, neurophysiological, and morphological basis of brain function. However, some of the most basic questions — with the farthest-reaching implications — remain underexplored and unanswered (Taylor, Pritschet, & Jacobs, 2021). Women undergo ~400 menstrual cycles throughout their reproductive lives, 100 million women worldwide use oral hormonal contraceptives, ~140 million women undergo pregnancy *annually*, 10% of the female population suffer from endocrine disorders, and women spend 1/3rd of their lives in a post-menopausal state. Each of these neuroendocrine events comes with significant shifts in the hormonal milieu, often tethered to brain-related changes in cognition, behavior, and health (Brinton et al., 2015; Schiller et al., 2016; Beltz and Mozer, 2019). Since the mid-1990s, the number of studies leveraging brain imaging to

understand a wide range of phenomena has exploded into the tens of thousands. Yet, the topic of women's brain health — despite implications for half the world's population — has not kept pace in the slightest. Why is that? Where do we go from here?

Historical overview

Over the past half century, males have been treated as the representative sex as females were deemed "too variable" to be studied due to their reproductive cycle, failing to appreciate that sex hormones are critical neuromodulators deserving attention in both sexes. This decades long oversight, driven by an untested and now debunked presumption of *greater* variability (Prendergast et al., 2014), was a driving reason for why females were excluded from a large portion of preclinical studies in domains at the nexus of brain health, such as pharmacology and neuroscience (Beery et al., 2011). These survey projects from Annelise Beery and Brian Prendergast catalyzed one of the most powerful policy shifts in the health sciences. In 2016, Dr. Janine Clayton, Director of the NIH Office of Research on Women's Health, pioneered the federal *Sex as a Biological Variable (SABV)* mandate requiring the inclusion of both sexes in taxpayer-funded preclinical research (Clayton and Collins, 2014). This in turn created a new standard of practice towards encouraging the discovery of similarities and differences between the sexes with hopes to shine a light on sex-specific health outcomes. The SABV mandate is already making tangible headway. A recent comparison of articles published in 2019 versus 2009 among neuroscience and psychiatry journals revealed a 30% increase in the number of studies including both sexes in their designs (Rechlin et al., 2022).

However, in human neuroscience, the biases are different. Although we tend to recruit both sexes equally in our research designs, women are not benefitting equally from our scientific efforts. The advent of large neuroimaging databases has further advanced the field of cognitive neuroscience by providing datasets of 100s–1000s of participants. Sex differences research has benefited from these datasets, with the statistical power to identify sex differences across the lifespan (Lotze et al., 2019; Ritchie et al., 2018). While considering SABV has become increasingly common in human neuroimaging (Sacher et al., 2013), looking beyond sex differences to study women's brain health remains uncommon (Taylor et al., 2019, 2021).

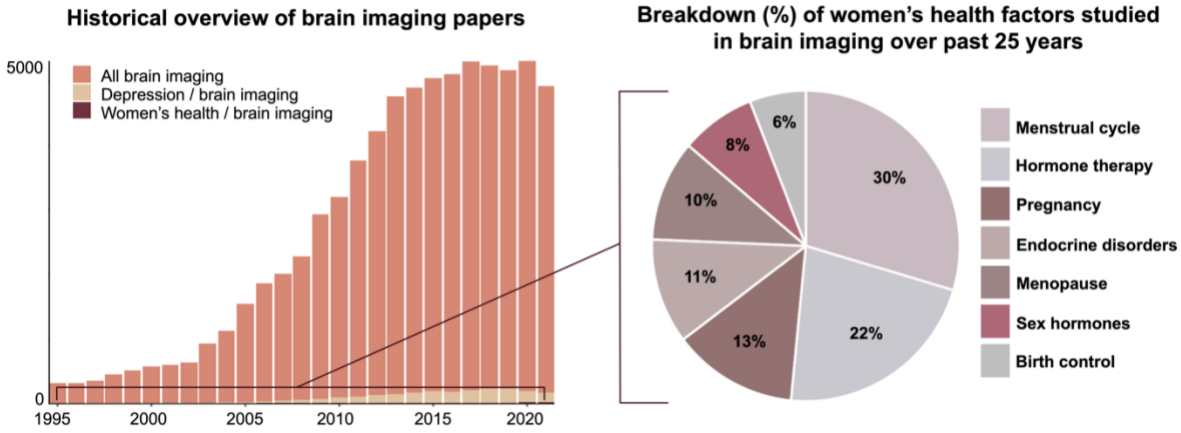

Figure 1.1. A spotlight on women's health factors in brain imaging. **Left |** Major aspects of women's lives have been overlooked in human neuroscience research over the past 25 years. **Right |** The majority of women's brain health studies have focused on the brain's response to the menstrual cycle and menopausal hormone replacement therapy.

Identifying the blind spots in cognitive neuroscience

Over the last five years, I have led several survey projects to quantify the extent to which human brain imaging overlooks major aspects of the human condition specific to women (e.g., menstrual cycles, hormonal contraceptive use, pregnancy, menopause). First, a historical survey of neuroimaging papers published

from 1995–2021 revealed the persistence of this oversight across all journals. Of the >50,000 human neuroimaging articles published over the last 25 years, fewer than 250 were focused on women's health. The number of articles dedicated to understanding the neural impact of major neuroendocrine transition states barely registers on the graph — accounting for ~0.5% of total publications — even in comparison to a smaller sub-topic within human brain imaging (**Fig 1.1**).

Zooming in, I followed this up with an in-depth exploration among all articles (~1,200) published in 2018 across six top brain imaging journals to investigate the extent to which *any* mention of women's health factors was present throughout a given paper. I found that fewer than 3% of these articles considered anything pertaining to women's health in their study design – half of which were used as justification to exclude women due to 'added variability of the menstrual cycle' (**Fig 1.2**).

Major hormonal transition periods are central to half the world's population, yet we lack an understanding of the endocrine basis of human brain function. Moving forward, it is imperative that the human brain imaging community increase its commitment to advancing knowledge of the brain with a women's health focus so that both sexes are benefitting equally from our scientific efforts.

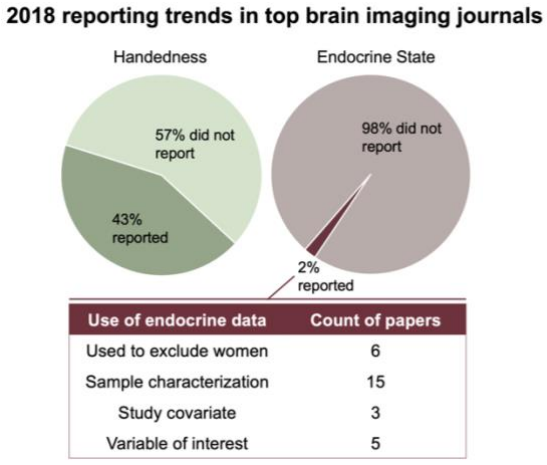

Figure 1.2. In 2018, only 2% of neuroimaging articles published in leading neuroscience journals mentioned women's health factors. Of those, 20% merely did so to *exclude* women and justify conducting a male-only study. Less than 0.5% of articles directly studied sex hormones or a sex hormone–related topic. *Figure adapted from Taylor, Pritschet, & Jacobs, 2021.*

2

Introduction

Broad overview of sex hormone action in mammalian physiology

The brain is a “complex temporally and spatially multiscale structure that gives rise to elaborate molecular, cellular, and neuronal phenomena that form the physical and biological basis of cognition” (Bassett & Gazzaniga, 2011). As such, neuroscientists have plumbed the depths of the mind and brain to extraordinary lengths in order to understand how 86 billion neurons work together to lay the foundation for the mind and drive human behavior. Yet, in doing this, we often forget that the brain is part of a larger, integrated biological system. Since its inception, the field of neuroendocrinology has provided evidence for a tightly coupled relationship between the nervous and endocrine systems (Galea et al., 2017; Frick, 2019), operating as a cohesive unit through reciprocal communication of the brain and periphery via neural and hormonal pathways. A central feature of the mammalian endocrine system is that hormone secretion varies over time (**Fig. 2.1**), and this rhythmicity is essential for sustaining many physiological processes. How does the brain respond to the continuous wax and wane of hormone secretion? And critically, what happens when these systems begin to decouple in midlife? In this dissertation, I present findings from three unique studies that work to answer these questions by

investigating endocrine modulation of large-scale brain networks across the menstrual cycle, over the course of pregnancy, and in response to ovarian depletion in menopause. The goal of this work is to demonstrate that probing the dynamic interplay between the nervous and endocrine systems has the potential to transform both our understanding of the brain and women's health at large.

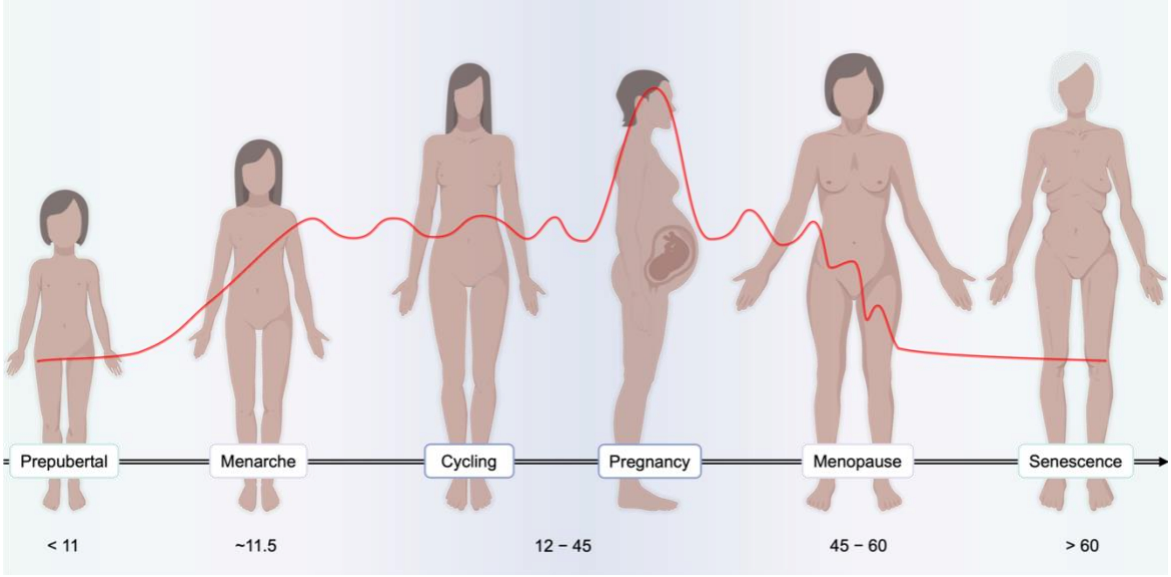

Figure 2.1. A broad schematic of sex steroid hormone fluctuations (red line) across the female lifespan characterized by endocrine stage and average age. Sex steroid hormones come online during puberty, with menarche marking the beginning of menstrual cycles that will occur every ~25-35 days across reproductive years, barring exogenous hormone exposure or major endocrine disorders. Most women will experience pregnancy at least once in their lifetime, involving a hundred- to thousand-fold increase in sex hormones over the gestational window. Women then undergo a complex hormonal transition at midlife, marked by high fluctuations in steroid hormone production during the perimenopausal phase and culminating in ovarian senescence at the end of menopause — a decline of up to 90% for both estradiol and progesterone. *Figure partially created with BioRender.com*

Hormonal feedback systems

A hormone is a chemical messenger synthesized in an endocrine gland, secreted into the circulatory system, and transported through the body via the bloodstream to act upon receptors and exert a specific physiological action on a target cell

(Wilkinson and Brown, 2015). Steroid hormones — corticosteroids and sex hormones — are synthesized from cholesterol in the adrenal cortex and gonads, respectively. In the following studies, I will focus exclusively on the actions of sex hormones in females (see Frick et al., 2018 for a review on both sexes). Androgens, estrogens, and progesterone work synergistically to coordinate the physiological changes that occur across hormonal transition periods, such as puberty, menstrual cycles, pregnancy, and menopause. Sex hormones exert influence on the brain via the hypothalamic-pituitary-gonadal axis (HPG) feedback system (**Fig 2.2**). Sex steroids are released from the gonads (female, ovaries; males, testes) to reduce gonadotropin-releasing hormone (GnRH) secretion from the hypothalamus and subsequent inhibition of gonadotropins (luteinizing hormone, LH; follicle-stimulating hormone, FSH) from the pituitary. In both sexes this feedback system is predominantly negative to prevent overstimulation of the gonads. However, in females, these feedback signals become positive midway through the reproductive cycle when a

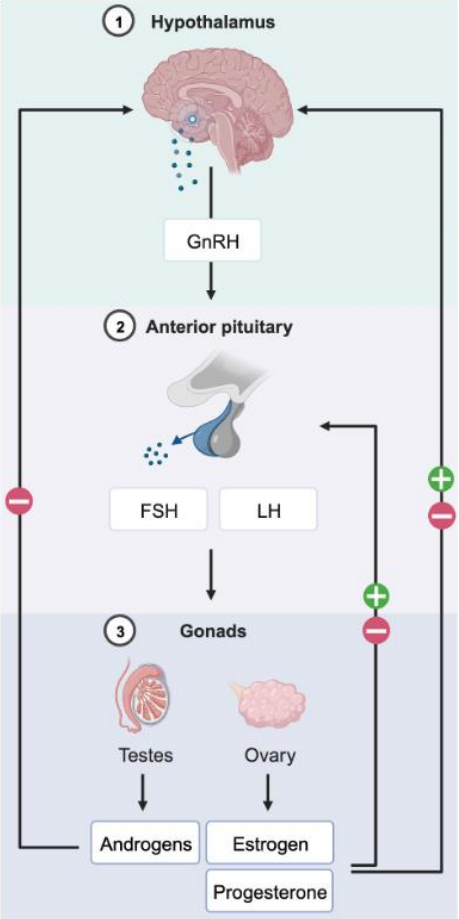

Figure 2.2. Sex hormones exert influence on the brain via the hypothalamic-pituitary-gonadal axis (HPG) feedback system. Gonadotropin-releasing hormone (GnRH) is secreted from the hypothalamus. The anterior pituitary produces luteinizing hormone (LH) and follicle-stimulating hormone (FSH), and the gonads produce sex steroid hormones. *Adapted from "Hypothalamic-Pituitary-Adrenal Axis" by BioRender.com (2023). Retrieved from https://app.biorender.com/biorender-templates*

surge of estrogen leads to increased GnRH, LH, and FSH to prepare for ovulation. Once ovulation has occurred, the corpus luteum begins to release progesterone and negative feedback returns. If conception does not occur, the uterine lining is shed, menses occurs, and the cycle then repeats. The onset of this biological rhythm occurs in puberty with menarche and comes to an end with ovarian senescence in menopause.

Mechanisms of hormone action

Hormones are lipid soluble, allowing for diffusion through the cell membrane to bind to intracellular receptors in the cytoplasm or nucleus (**Fig. 2.3**). This hormone-receptor complex then binds to a hormone response element (e.g., estrogen receptor element, ERE) to act as a transcription regulator by controlling the synthesis of mRNA molecules of specific genes to ultimately change that cell's function (Frick and Kim, 2018). Sex hormones can also exert effects through rapid, non-classical mechanisms. Estrogen, for example, can interact with metabotropic glutamate and membrane-bound receptors to rapidly change gene expression, via

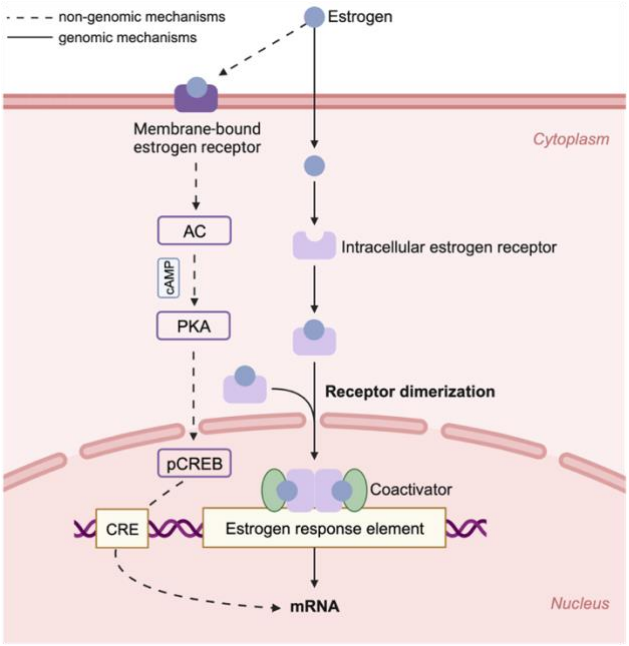

Figure 2.3. Sex hormones act through both genomic and non-genomic mechanisms to change the function of a cell. Abbreviations: AC, adenyl cyclase; PKA, protein kinase A; pCREB, phosphorylated response element binding protein; mRNA, messenger RNA; CRE, cAMP-responsive elements; cAMP, cyclic adenosine monophosphate *Adapted from "Estrogen signaling in breast cancer" by BioRender.com (2023). Retrieved from: https://app.biorender.com/biorender-templates*

“stimulation of cyclic adenosine monophosphate (cAMP) formation, protein kinase A (PKA) and the transcription factor phosphorylated response element binding protein (pCREB)” (derived from Wilkinson and Brown, 2015; see also Frick and Kim, 2018). Sex hormones act as regulators to ensure the brain is responding rapidly and appropriately across timescales of seconds to days, coordinating the signaling and transcriptional pathways regulating energy metabolism, neurogenesis, synaptic activity, and behavior (Galea et al., 2017; Frick and Kim, 2018). Advances in characterization techniques, such as fluorescence immunocytochemistry and in situ hybridization, has allowed for the tagging of cells with estrogen receptors (ER) alpha, beta, and the G-protein coupled GPER-1 receptor in the brain — predominantly in rodent and non-human primates. This has revealed an abundance of hormone receptor expression throughout the cerebrum and cerebellum, with enriched expression in extra-hypothalamic regions such as the hippocampus and prefrontal cortex (PFC) (Almey et al., 2015).

In sum, estrogen and progesterone signaling are critical components of cell survival and plasticity, exerting excitatory and inhibitory effects that are evident across multiple spatial and temporal scales in the brain (Frick and Kim, 2018; Taxier et al., 2020). Naturally, one pressing question comes to mind: *what does this mean for brain morphology and function?* When we think about sex hormones, we typically associate them with classical reproductive behaviors: breastfeeding, infant cue responses, maternal bonding, aggression, affect, and sexual behavior. While this is true — sex hormones are a central facet of reproductive life — they exert effects in regions beyond the hypothalamus in areas that act as key hubs of information

processing for the whole brain. Below, I highlight major discoveries from the past 20 years establishing sex hormones' action in higher-order cognitive regions in the brain.

Sex hormones regulate brain morphology across species

Animal studies offer unambiguous evidence that sex steroid hormones shape the synaptic organization of the brain, particularly within the hippocampus and PFC (Woolley and McEwen, 1993; Hara et al., 2015; Frick et al., 2015; Galea et al., 2017; Frick and Kim, 2018). At the epigenetic level, estradiol induces chromatin modifications that promote hippocampal plasticity (Fortress and Frick, 2014). At the synaptic level, estradiol and progesterone regulate spine proliferation in the hippocampus (Hara et al., 2015). Pioneering work from Catherine Woolley and Bruce McEwen (1992, 1993) showed that the density of dendritic spines on hippocampal CA1 pyramidal cells is dependent on circulating E and progesterone (P) levels, with dendritic spines varying by ~30% over the 4-5 day rodent estrous cycle. Hormone deprivation (via gonadectomy) in the rat (Gould et al., 1990; Woolley and McEwen, 1993) and African green monkey (Leranth et al., 2002) leads to a pronounced loss of spines on CA1 neurons, which is reversed by estrogen replacement. At the macroscopic level, total hippocampal volume is related to plasma estradiol levels in the meadow vole (Galea et al., 1999) and fluctuates across the estrous cycle in the mouse (Qiu et al., 2013). Also in mice, in-vivo magnetic resonance imaging (MRI) demonstrates estrous stage–related hippocampal volume changes are detectable within a 24-hour period (Qiu et al., 2013). In humans, hippocampal volume has been shown to increase from the early-

to late-follicular phase of the menstrual cycle (Lisofsky et al., 2015; Protopopescu et al., 2008). Recent evidence from our team suggests that progesterone dynamically shapes medial temporal lobe morphology across a ~28-day menstrual cycle, with volumetric changes in CA2/3, parahippocampal cortex, entorhinal cortex and perirhinal cortex—effects that were blocked by progesterone suppression (Taylor et al., 2020). During pregnancy, the changes in sex hormone production throughout gestation modulate hippocampal plasticity in rodents (Kinsley and Lambert, 2008; Workman et al., 2012; Galea et al., 2014) and likely mediates the transient decline in hippocampal volume observed in humans post-pregnancy (Hoekzema et al., 2017). Finally, the abrupt hormonal changes associated with surgical menopause lead to structural changes in the medial temporal lobe, including thinning of the parahippocampus and entorhinal cortex (Zeydan et al., 2019), while estradiol administration in postmenopausal women increases hippocampal volume (Albert et al., 2017). Together, these findings provide converging cross-species evidence that sex hormones induce structural changes in the hippocampus across rapid and protracted timescales.

Non-human primate studies have established similar relationships within the PFC (Hao et al., 2006; Morrison et al., 2006). In female rhesus macaques, ~50% of PFC pyramidal neurons express estrogen receptors (ER-β) and those with enriched expression show stronger working memory performance (Wang et al., 2010). At the synaptic level, cyclic estradiol administration in ovariectomized rhesus macaques leads to increased spine density in PFC neurons (Hao et al., 2006) and improved working memory performance relative to estradiol-depleted controls (Rapp et al.,

2003). Sellers and colleagues (2015) found that the presence of ER-β in the synapses of primary cortical neurons was a requirement for rapid spinogenesis. Spines are the main site for excitatory glutamatergic input, especially among pyramidal neurons and decades of neuroendocrinology research has shown that spine distribution, number, and morphology fluctuate in a hormone-dependent manner. Taking this together, there is mounting evidence suggesting that sex hormones contribute to the remodeling of neuronal circuits, wielding the power to shape cognitive function (Frick and Kim, 2018).

In the following chapters, I will touch upon recent neuroimaging studies offering additional evidence towards ovarian hormone modulation of human brain morphology and function. Briefly here, this literature builds upon pioneering work from (Berman et al., 1997) and (Shaywitz et al., 1999), who used pharmacological blockade and hormone replacement techniques to illustrate the influence of estradiol and progesterone on regional activity in memory circuitry — particularly dorsolateral PFC. An emerging theory, driven in part by pivotal work from Emily Jacobs, is that estradiol increases the efficiency of cortical circuits within the PFC. In young women performing a working memory task, PFC activity is exaggerated under low estradiol conditions and reduced under high estradiol conditions (Jacobs and D'Esposito, 2011). The same pattern is observed decades later in life: as estradiol production declines over the menopausal transition, working memory–dependent PFC activity becomes exaggerated despite no deficit in performance (Jacobs et al., 2016; Jacobs and Goldstein, 2018). Thus, one principle of estradiol's action may be that it helps generate efficiency in cortical circuits, particularly within PFC. An intriguing

possibility is that these effects are mediated through dopamine signaling and/or (Williams and Goldman-Rakic, 1995; Becker, 1990; Jacobs and D'Esposito, 2011; Almey et al., 2015;) a number of other estrogen-linked neuromodulatory pathways such as serotonin, norepinephrine, and acetylcholine (Amin et al., 2005; Epperson et al., 2012). Findings from cross-sectional and traditional longitudinal studies support a role for ovarian hormones in shaping the brain across the life course (McEwen, 2018). However, new approaches with improved temporal resolution are needed to illuminate the time-sensitive coupling between hormone fluctuations and the brain.

Novelty of this dissertation

Scientists have routinely pushed the bounds of experimental creativity to tease apart the inherently complex nature of brain–hormone interactions. Traditional approaches to studying human brain–hormone interactions rely largely on cross-sectional designs that, by nature, cannot capture fluctuations in sex hormone production. A growing trend in human neuroimaging is to flip the cross-sectional model, densely-sampling individuals over timescales of days, weeks, months, or years to provide greater insight into the dynamic properties of the human brain. Dense-sampling (i.e., precision imaging) extends longitudinal designs by collecting multiple phenotypic measurements at a higher frequency and/or duration in individuals over a larger number of sessions (> 10 time points). In Studies 1 and 2, I address a new set of methodological innovation for probing estrogen and progesterone action in the human brain — the application of dense-sampling to reveal endocrine modulation of the human brain.

In cognitive neuroscience, a classic approach for studying the brain involves collecting data from a number of individuals at a *single* time point and then group-averaging, thus increasing the ability to generalize findings to a broader population. One strength of this cross-sectional approach is that it allows researchers to isolate how reproductive stage, over and above chronological age, shapes the brain (Jacobs and Goldstein, 2018). Longitudinal studies offer valuable clues about how the brain responds to periods of significant hormonal change, such as sampling women before and after major pregnancy (Hoekzema et al., 2017) or across discrete stages of the menopausal transition (Mosconi et al., 2018). Several studies have also applied this approach to the menstrual cycle, sampling women several (e.g., 2–3) times in order to compare brain structure and function by cycle stage (Weis et al., 2019; Pletzer et al., 2019). However, inconsistences emerge due to the inherent

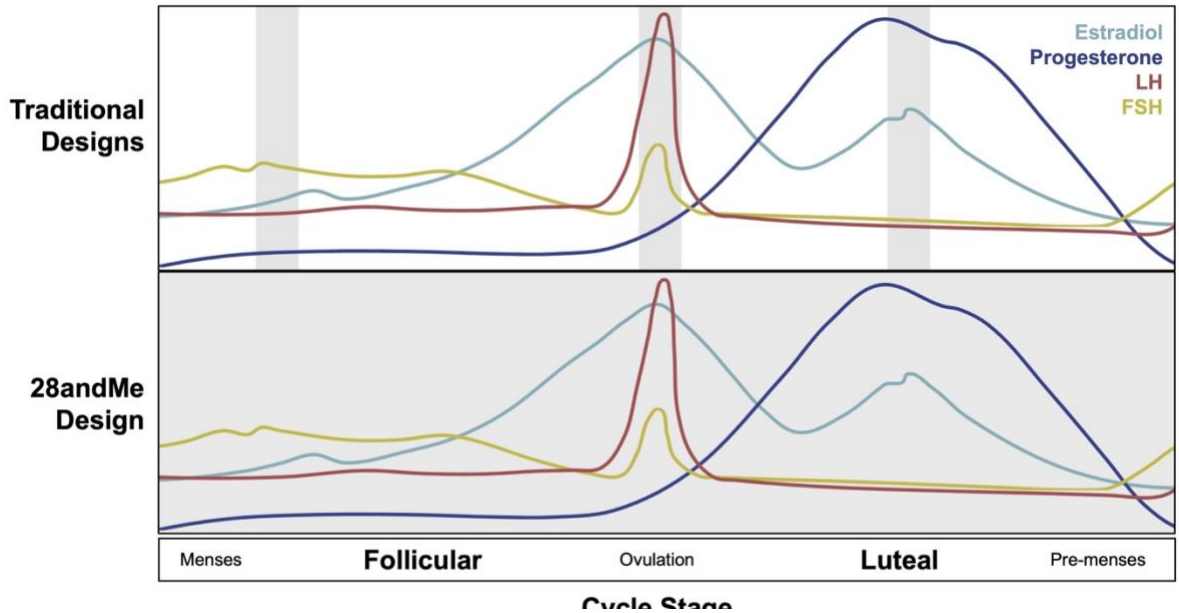

Figure 2.4. **Top |** Traditional brain–hormone designs typically involve bringing women in to be tested 2–3 times at distinct stages of their cycle (vertical gray bars): menses, ovulatory window, and mid-luteal phases. These designs are good for examining brain differences with respect to absolute concentrations of sex hormones. However, they are unable to capture the brain's response to dynamic hormonal fluctuations. **Bottom |** In our 28andMe study, a woman underwent MRI scanning every 24 hours over 30 consecutive days to capture a complete menstrual cycle.

limitation of applying a static sampling rate to the study of a dynamical system. Two to four time points remain insufficient to explore how the brain responds to *transient changes* in sex hormones, a critical feature of the endocrine system (**Fig. 2.4**) (Schmidt et al., 2017; Pritschet et al., 2020, 2021; Mueller et al., 2021). While human neuroimaging studies that densely sample the individual connectome have begun to transform our understanding of the dynamics of human brain organization (see Gratton and Braga, 2021 for special issue on 'deep imaging'), they routinely omit sex steroid hormones as variables of interest. This approach is uniquely well-suited, however, to test hypotheses and build models of nervous and endocrine system interactions across the lifespan, capturing details of brain–hormone coupling that may be overlooked by traditional cross-sectional or sparse-sampling approaches (Pritschet et al., 2021). As such, our team recently completed a set of precision imaging studies that work to uncover dynamic endocrine modulation of the nervous system. In **Study 1**, I present findings from my keystone '28andMe' project, in which a participant underwent brain imaging and venipuncture every 24 hours over 30 consecutive days across a complete menstrual cycle and again, one year later, while on an oral hormonal contraceptive regimen. We then extended this approach to a different endocrine state, pregnancy, where the traditional method is to compare the brains of women pre versus post pregnancy, overlooking the neural changes that unfold during the gestational window. Our team conducted the first precision imaging study of pregnancy in which a healthy 38-year-old primiparous woman underwent 26 MRI scans and venipuncture beginning 3 weeks pre-conception through two years postpartum (**Study 2**). These findings provide novel insight into the spatiotemporal

extent of brain-hormone relationships, allowing us to examine both short- and long-term effects of sex hormones across the brain.

Lastly, I probed the brain's response to the *decoupling* of the nervous and endocrine systems during the midlife transition to menopause. Our current understanding of how female reproductive aging impacts the brain stems from studies identifying fairly coarse regional differences in brain activity or morphology as a function of women's menopausal status. The application of network science techniques to the study of the brain has allowed neuroscientists to move beyond examining individual regions in isolation, granting us the ability to understand how functional networks distributed across broad swaths of cortex support cognition. In **Study 3**, I worked to fill a major gap in the literature by applying computational techniques to a large, highly characterized sample of midlife women (ages 43–60) to establish how endocrine aging influences the brain at the macroscopic scale of whole-brain intrinsic network organization.

In summary, the body of work presented here aims to advance our understanding of the human brain through the lens of neuroendocrinology by examining how different hormonal transition periods shape brain morphology and function.

3

Functional organization of brain networks across the human menstrual cycle

Adapted from the following article: Pritschet, L.*, Santander, T.*, Taylor, C. M., Layher, E., Yu, S., Miller, M. B., Grafton, S.T., & Jacobs, E. G. (2020). Functional reorganization of brain networks across the human menstrual cycle. *Neuroimage*, *220*, 117091. **Authors contributed equally to this work*

Authorship Contributions: The work presented in this study was highly collaborative. The overall study was conceived by L.P., C.M.T., and E.G.J.; L.P., T.S., E.L., C.M.T., S.Y., and E.G.J. performed the experiments; data analysis strategy was conceived by T.S. and L.P. and implemented by T.S.; L.P., T.S., and E.G.J. wrote the manuscript; E.L., C.M.T., S.Y., M.B.M., and S.T.G. edited the manuscript.

A. Introduction

The brain is an endocrine organ whose day-to-day function is intimately tied to the action of neuromodulatory hormones (Woolley and McEwen, 1993; Frick et al., 2015; Hara et al., 2015; Galea et al., 2017). Yet, the study of brain-hormone interactions in human neuroscience has often been woefully myopic in scope: the classical approach of interrogating the brain involves collecting data at a single time point from multiple subjects and averaging across individuals to provide evidence for a hormone-brain-behavior relationship. This cross-sectional approach obscures the rich, rhythmic nature of endogenous hormone production. A promising trend in network neuroscience is to flip the cross-sectional model by tracking small samples

of individuals over timescales of weeks, months, or years to provide insight into how biological, behavioral, and state-dependent factors influence intra- and inter-individual variability in the brain's intrinsic network organization (Poldrack et al., 2015; Gordon et al., 2017; Gratton et al., 2018a). Neuroimaging studies that densely sample the individual connectome are beginning to transform our understanding of the dynamics of human brain organization. However, these studies commonly overlook sex steroid hormones as a source of variability—a surprising omission given that sex hormones are powerful neuromodulators that display stable circadian, infradian, and circannual rhythms in nearly all mammalian species. In the present study, we illustrate robust, time-dependent interactions between functional network dynamics and the sex steroid hormones 17β-estradiol and progesterone during a complete menstrual cycle. A within-subject replication study further confirms the robustness of these effects. These results offer compelling evidence that sex hormones modulate widespread patterns of connectivity in the human brain.

Converging evidence from rodent (Woolley et al., 1993; Frick et al., 2015; Frick et al., 2018), non-human primate (Hao et al., 2006; Wang et al., 2010), and human neuroimaging studies (Berman et al., 1997; Jacobs & D'Esposito, 2011; Petersen et al., 2014; Lisofky et al., 2015; Jacobs et al., 2016a,b) has established the widespread influence of 17β-estradiol and progesterone on regions of the mammalian brain that support higher level cognitive functions. Estradiol and progesterone signaling are critical components of cell survival and plasticity, exerting excitatory and inhibitory effects that are evident across multiple spatial and temporal scales (Galea et al., 2017; Frick et al., 2018). The dense expression of estrogen and

progesterone receptors (ER; PR) in cortical and subcortical tissue underscores the widespread nature of hormone action. For example, in non-human primates, ~50% of pyramidal neurons in prefrontal cortex (PFC) express ER (Wang et al., 2010) and estradiol regulates dendritic spine proliferation in this region (Hara et al., 2015). Across the rodent estrous cycle (occurring every 4-5 days), fluctuations in estradiol enhance spinogenesis in hippocampal CA1 neurons, while progesterone inhibits this effect (Woolley and McEwen, 1993).

During an average human menstrual cycle, occurring every 25-32 days, women experience a ~12-fold increase in estradiol and an ~800-fold increase in progesterone. Despite this striking change in endocrine status, we lack a complete understanding of how the large-scale functional architecture of the human brain responds to rhythmic changes in sex hormone production across the menstrual cycle. Much of our understanding of cycle-dependent changes in brain structure (Woolley et al.,1993; Sheppard et al., 2019) and function (Hampson et al., 2014; Warren and Juraska, 1997; Kim & Frick, 2017) comes from rodent studies, since the length of the human menstrual cycle (at least 5x longer than rodents' estrous cycle) presents experimental hurdles that make longitudinal studies challenging. A common solution is to study women a few times throughout their cycle, targeting stages that roughly correspond to peak/trough hormone concentrations. Using this 'sparse-sampling' approach, studies have examined resting-state connectivity in discrete stages of the cycle (Petersen et al., 2014; Hjelmervik et al., 2014; Lisofsky et al., 2015; De Bondt et al., 2015; Syan et al., 2017; Weis et al., 2019) however, some of these findings are undermined by inconsistencies in cycle staging methods,

lack of direct hormone assessments, or limitations in functional connectivity methods.

In this dense-sampling, deep phenotyping study, we determined whether day-to-day variation in sex hormone concentrations impacts connectivity states across major intrinsic brain networks. First, we assessed brain-hormone interactions over 30-consecutive days representing a complete menstrual cycle (Study 1). To probe the reliability of these findings, procedures were then repeated over a second 30-day period, providing a within-subject controlled replication (Study 2). Results reveal that intrinsic functional connectivity is linearly dependent on hormonal dynamics across the menstrual cycle at multiple spatiotemporal scales. Estradiol and progesterone were associated with spatially-diffuse changes in connectivity, both at time-synchronous and time-lagged levels of analysis, demonstrating that intrinsic fluctuations in sex hormones—particularly the ovulatory surge in estradiol—may contribute to dynamic variation in the functional network architecture of the human brain. We further highlight this sensitivity to estradiol in a controlled replication study. Together, these findings provide insight into how brain networks reorganize across the human menstrual cycle, suggesting that consideration of the hormonal milieu is critical for fully understanding the intrinsic dynamics of the human brain.

B. Methods

Participant

The participant (author L.P.) was a right-handed Caucasian female, aged 23 years for the duration of the study. The participant had no history of neuropsychiatric

diagnosis, endocrine disorders, or prior head trauma. She had a history of regular menstrual cycles (no missed periods, cycle occurring every 26-28 days) and had not taken hormone-based medication in the 12 months prior to the first study. The participant gave written informed consent and the study was approved by the University of California, Santa Barbara Human Subjects Committee.

Study design

The participant underwent testing for 30 consecutive days, with the first test session determined independently of cycle stage for maximal blindness to hormone status (Study 1). One year later, as part of a larger parent project, the participant repeated the 30-day protocol while on a hormone regimen (0.02mg ethinyl-estradiol, 0.1mg levonorgestrel, Aubra, Afaxys Pharmaceuticals), which she began 10 months prior to the start of data collection (Study 2). The general procedures for both studies were identical (**Fig. 3.1**). The pharmacological regimen used in Study 2 chronically and selectively suppressed progesterone while leaving estradiol dynamics largely indistinguishable from Study 1. This provided a natural replication dataset in which to test the reliability of the estradiol associations observed in the first study. The participant began each test session with a daily questionnaire (see **Behavioral Assessments**), followed by an immersive reality spatial navigation task (not

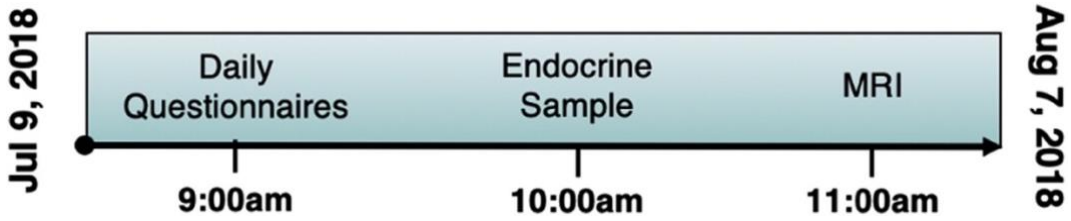

Figure 3.1. Timeline of data collection for the 30 experiment sessions. Endocrine and MRI assessments were collected at the same time each day to minimize time-of-day effects.

reported here). Time-locked collection of serum and whole blood started each day at 10:00am in Study 1 and 11:00am in Study 2 (±30 min), when the participant gave a blood sample. Endocrine samples were collected, at minimum, after two hours of no food or drink consumption (excluding water). The participant refrained from consuming caffeinated beverages before each test session. The MRI session lasted one hour and consisted of structural and functional MRI sequences.

Behavioral assessments

To monitor state-dependent mood and lifestyle measures throughout the two studies, the following scales (adapted to reflect the past 24 hours) were administered each morning: Perceived Stress Scale (PSS; Cohen et al., 1983), Pittsburgh Sleep Quality Index (PSQI; Buysse et al., 1989), State-Trait Anxiety Inventory for Adults (STAI; Spielberger and Vagg, 1984), and Profile of Mood States (POMS; Pollock et al., 1979). The participant had moderate levels of anxiety as determined by STAI reference ranges; however, all other measures fell within the 'normal' standard range. Self-reported stress was marginally higher in Study 2 (M_{diff} = 3.9, $t(58) = 2.66$, $p = .046$); no other differences in mood or lifestyle measures were observed between the two studies. Few significant relationships were observed between hormones and state-dependent measures following FDR-correction for multiple comparisons ($q < .05$)—and critically, none of these state-dependent factors were associated with estradiol (**Fig. 3.2A**). Furthermore, performance on a daily selective attention task (Cohen et al., 2014) was stable across the experiment

(*M*=98%, *SD*=. 01) (**Fig 3.2B**). Taken together, there were no indications of significant shifts in behavior across the cycle.

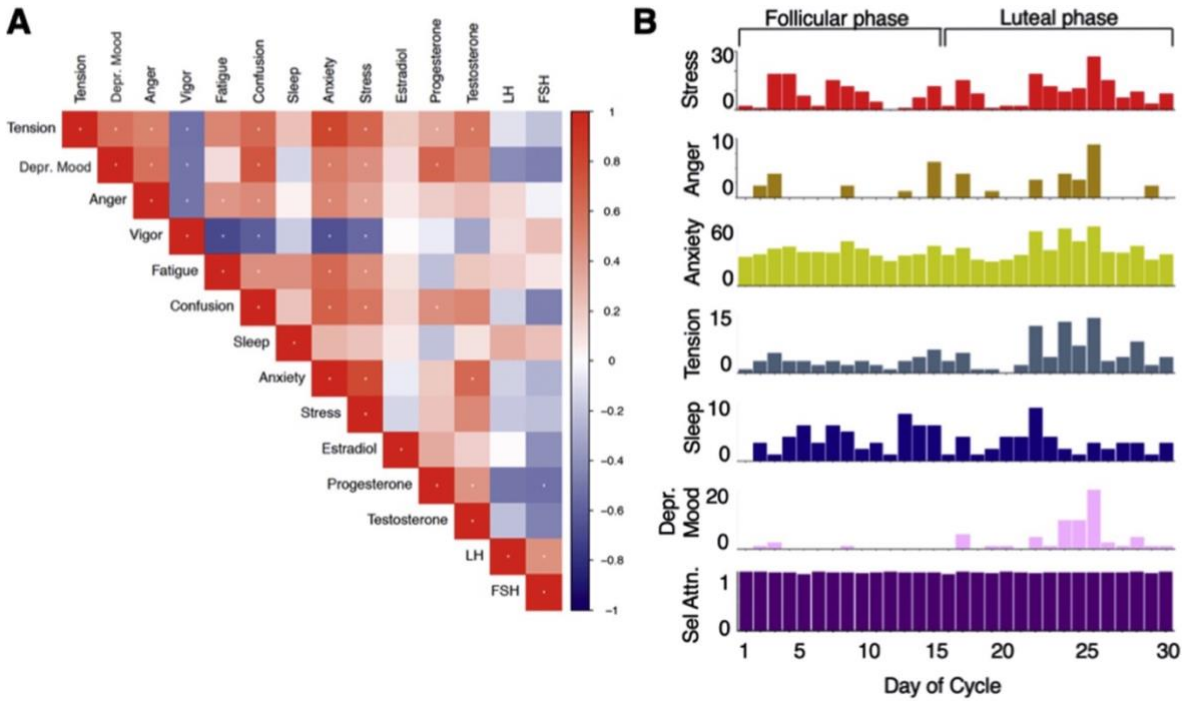

Figure 3.2. Behavioral variation across the first 30-day experiment. **A)** Correlation plot showing relationships between mood, lifestyle measures, and sex steroid hormone concentrations. Cooler cells indicate negative correlations, warm cells indicate positive correlations, and white cells indicate no relationship. Asterisks indicate significant correlations after FDR-correction (q<.05). **B)** Mood and lifestyle measure vary across the cycle; cognitive performance (selective attention task) does not. 'Day 1' indicates first day of menstruation, not first day of experiment. Abbreviations: LH, Luteinizing hormone; FSH, Follicle-stimulating hormone.

Endocrine procedures

A licensed phlebotomist inserted a saline-lock intravenous line into the dominant or non-dominant hand or forearm daily to evaluate hypothalamic-pituitary-gonadal axis hormones, including serum levels of gonadal hormones (17β-estradiol, progesterone and testosterone) and the pituitary gonadotropins luteinizing hormone (LH) and follicle stimulating hormone (FSH). One 10cc mL blood sample was collected in a vacutainer SST (BD Diagnostic Systems) each session. The sample

clotted at room temperature for 45 min until centrifugation (2000 × *g* for 10 minutes) and were then aliquoted into three 1 mL microtubes. Serum samples were stored at -20°C until assayed. Serum concentrations were determined via liquid chromatography-mass spectrometry (for all steroid hormones) and immunoassay (for all gonadotropins) at the Brigham and Women's Hospital Research Assay Core. Assay sensitivities, dynamic range, and intra-assay coefficients of variation (respectively) were as follows: estradiol, 1 pg/mL, 1-500 pg/mL, < 5% relative standard deviation (*RSD*); progesterone, 0.05 ng/mL, 0.05-10 ng/mL, 9.33% *RSD*; testosterone, 1.0 ng/dL, 1-2000 ng/dL, <4% *RSD*. FSH and LH levels were determined via chemiluminescent assay (Beckman Coulter). The assay sensitivity, dynamic range, and the intra-assay coefficient of variation were as follows: FSH, 0.2 mIU/mL, 0.2-200 mIU/mL, 3.1-4.3%; LH, 0.2 mIU/mL, 0.2-250 mIU/mL, 4.3-6.4%. Importantly, we note that LC-MS assessments of *exogenous* hormone concentrations (attributable to the hormone regimen itself) showed that serum concentrations of ethinyl estradiol were very low (*M* = 0.01 ng/mL; range 0.001–0.016 ng/mL) and below 1.5 ng/mL for levonorgestrel (*M* = 0.91 ng/mL; range = 0.03–1.43 ng/mL*)*: this ensures that the brain-hormone associations reported in Study 2 are still due to *endogenous* estradiol action*.*

MRI acquisition

The participant underwent a daily magnetic resonance imaging scan on a Siemens 3T Prisma scanner equipped with a 64-channel phased-array head coil. First, high-resolution anatomical scans were acquired using a T_1-weighted

magnetization prepared rapid gradient echo (MPRAGE) sequence (TR = 2500 ms, TE = 2.31 ms, TI = 934 ms, flip angle = 7º, 0.8 mm thickness) followed by a gradient echo fieldmap (TR = 758 ms, TE_1 = 4.92 ms, TE_2 = 7.38 ms, flip angle = 60º). Next, the participant completed a 10-minute resting-state fMRI scan using a T_2^*-weighted multiband echo-planar imaging (EPI) sequence sensitive to the blood oxygenation level-dependent (BOLD) contrast (72 oblique slices, TR = 720 ms, TE = 37 ms, voxel size = 2 mm^3, flip angle = 56º, multiband factor = 8). In an effort to minimize motion, the head was secured with a custom, 3D-printed foam head case (https://caseforge.co/) (days 8-30 of Study 1 and days 1-30 of Study 2). Overall motion (mean framewise displacement) was negligible (**Appendix A Fig. 1**), with fewer than 130 microns of motion on average each day. Importantly, mean framewise displacement was not correlated with estradiol concentrations (Study 1: Spearman r = -0.06, p = .758; Study 2: Spearman r = -0.33, p = .071). Note that physiological recordings were not collected during scanning.

fMRI preprocessing

Initial preprocessing was performed using the Statistical Parametric Mapping 12 software (SPM12, Wellcome Trust Centre for Neuroimaging, London) in Matlab. Functional data were realigned and unwarped to correct for head motion and geometric deformations due to motion and magnetic field inhomogeneities; the mean motion-corrected image was then coregistered to the high-resolution anatomical image. All scans were then registered to a subject-specific anatomical template created using Advanced Normalization Tools' (ANTs) multivariate template

construction (**Appendix A Fig. 2**). A 4 mm full-width at half-maximum (FWHM) isotropic Gaussian kernel was subsequently applied to smooth the functional data. Further preparation for resting-state functional connectivity was implemented using in-house Matlab scripts. Global signal scaling (median = 1,000) was applied to account for fluctuations in signal intensity across space and time, and voxelwise timeseries were linearly detrended. Residual BOLD signal from each voxel was extracted after removing the effects of head motion and five physiological noise components (CSF + white matter signal). Motion was modeled based on the Friston-24 approach, using a Volterra expansion of translational/rotational motion parameters, accounting for autoregressive and nonlinear effects of head motion on the BOLD signal (Friston et al., 1996). Our use of coherence allows for the estimation of frequency-specific covariances in spectral components below the range contaminated by physiological noise. Nevertheless, to ensure the robustness of our results, we re-analyzed the data with global signal regression included. This had little bearing on the overall findings. For completeness, results from the GSR-based processing pipeline are provided in **Appendix A.**

Functional connectivity estimation

Functional network nodes were defined based on a 400-region cortical parcellation (Schaefer et al., 2018) and 15 regions from the Harvard-Oxford subcortical atlas (http://www.fmrib.ox.ac.uk/fsl/). For each day, a summary timecourse was extracted per node by taking the first eigenvariate across functional volumes (Friston et al., 2006). These regional timeseries were then decomposed

into several frequency bands using a maximal overlap discrete wavelet transform. Low-frequency fluctuations in wavelets 3-6 (~0.01-0.17 Hz) were selected for subsequent connectivity analyses (Patel and Bullmore, 2016). We estimated the *spectral* association between regional timeseries using magnitude-squared coherence: this yielded a 415 × 415 functional association matrix each day, whose elements indicated the strength of functional connectivity between all pairs of nodes (FDR-thresholded at $q < .05$). Coherence offers several advantages over alternative methods for assessing connectivity: 1) estimation of *frequency-specific* covariances, 2) *simple interpretability* (values are normalized to the [0,1] interval), and 3) *robustness to temporal variability in hemodynamics* between brain regions, which can otherwise introduce time-lag confounds to connectivity estimates via Pearson correlation.

Statistical analysis

First, we assessed time-synchronous variation in functional connectivity associated with estradiol and progesterone through a standardized regression analysis. Data were *Z*-transformed and edgewise coherence was regressed against hormonal timeseries to capture day-by-day variation in connectivity relative to hormonal fluctuations. For each model, we computed robust empirical null distributions of test statistics via 10,000 iterations of nonparametric permutation testing: under the null hypothesis of no temporal association between connectivity and hormones, the coherence data at each edge were randomly permuted, models were fit, and two-tailed *p*-values were obtained as the proportion of models in which

the absolute value of the permuted test statistics equaled or exceeded the absolute value of the 'true' test statistics. We report edges surviving a threshold of $p < .001$. We did not apply additional corrections in an effort to maximize power in our small sample size; Study 2 instead offers an independent validation of the observed whole-brain effects.

Next, we sought to capture linear dependencies between hormones and network connectivity *directed in time* using vector autoregressive (VAR) models. Here we chose to focus exclusively on estradiol for two reasons: 1) the highly-bimodal time-course of progesterone over a natural cycle confers a considerably longer autocorrelative structure, requiring many more free parameters (i.e. higher-order models, ultimately affording fewer degrees of freedom); and 2) progesterone lacks an appreciable pattern of periodicity in its autocovariance with network timeseries, suggesting less relevance for time-lagged analysis over a single cycle. In contrast, estradiol has a much smoother time-course that is well-suited for temporal evolution models such as VAR.

In short, VAR solves a simultaneous system of equations that fits *current* states of the brain and estradiol from the *previous* states of each (see Eq. (1)). For consistency, we considered only *second-order* VAR models, given a fairly reliable first zero-crossing of brain/hormone autocovariance functions at lag two (this was based on common criteria noted in other instances of time-delayed models; Boker et al., 2014). Fit parameters for each VAR therefore reflect the following general form:

$$Brain_t = b_{1,0} + b_{1,1}Brain_{t-1} + b_{1,2}Estradiol_{t-1} + b_{1,3}Brain_{t-2} + b_{1,4}Estradiol_{t-2} + \epsilon_{1,t}$$

$$Estradiol_t = b_{2,0} + b_{2,1}Brain_{t-1} + b_{2,2}Estradiol_{t-1} + b_{2,3}Brain_{t-2} + b_{2,4}Estradiol_{t-2} + \epsilon_{2,t} \quad (1)$$

where error terms, $\epsilon_{i,t}$, are assumed to be uncorrelated and normally-distributed. Given that the design matrix is identical for each outcome measure, they can be combined in matrix form, and a least-squares solution to the system of equations can be obtained via maximum likelihood.

With respect to brain states, we modeled both edgewise coherence and factors related to macroscale network topologies. Specifically, we computed measures of *between-network* integration (the participation coefficient; i.e. the average extent to which network nodes are communicating with other networks over time) and *within-network* integration (global efficiency, quantifying the ostensible ease of information transfer across nodes inside a given network). These were derived using the relevant functions for weighted graphs in the Brain Connectivity toolbox (Rubinov and Sporns, 2010). Estimation of participation coefficients took the full (415 x 415) FDR-thresholded coherence matrices along with a vector of network IDs, quantifying the extent to which each node was connected to other nodes outside of its own network; summary, mean participation coefficients were then obtained for each network across its constituent nodes. For global efficiencies, the 415 x 415 matrices were subdivided into smaller network-specific matrices as defined by our parcellation, yielding estimates of integration *only* among within-network nodes. Ultimately, regardless of brain measure, each VAR was estimated similarly to the time-synchronous analyses described above: data were *Z*-scored, models were fit, and model-level stats (test-statistics, R^2, and *RMSE*) were empirically-thresholded against 10,000 iterations of nonparametric permutation testing. Here, however, both brain and hormonal data were permuted under the null

hypothesis of temporal stochasticity (i.e. no autoregressive trends and no time-lagged dependencies between variables). As before, we did not apply additional corrections and offer Study 2 as an independent validation set.

Finally, for each set of edgewise models (time-synchronous and time-lagged), we attempted to disentangle both the general *direction* of hormone-related associations and whether certain networks were more or less *sensitive* to hormonal fluctuations. Toward that end, we took the thresholded statistical parametric maps for each model (where edges are test statistics quantifying the magnitude of association between coherence and hormonal timeseries) and estimated *nodal association strengths* per graph theory's treatment of signed, weighted networks. That is, positive and negative association strengths were computed independently for each of the 415 nodes by summing the suprathreshold positive/negative edges linked to them. We then simply assessed mean association strengths ($\pm$ 95% confidence intervals) in each direction across the various networks in our parcellation.

Here, networks were defined by grouping the subnetworks of the 17-network Schaefer parcellation, such that (for example), the A, B, and C components of the Default Mode Network were treated as one network. We chose this due to the presence of a unique Temporal Parietal Network in the 17-network partition, which is otherwise subsumed by several other networks (Default Mode, Salience/Ventral Attention, and SomatoMotor) in the 7-network partition. The subcortical nodes of the Harvard-Oxford atlas were also treated as their own network, yielding a total of nine

networks. These definitions were thus used for computation of participation coefficients and global efficiencies in network-level VAR models.

C. Results

Endocrine Assessments

Analysis of daily sex hormone (by liquid-chromatography mass-spectrometry; LC-MS) and gonadotropin (by chemiluminescent immunoassay) concentrations from Study 1 confirmed the expected rhythmic changes of a typical menstrual cycle, with a total cycle length of 27 days. Serum levels of estradiol and progesterone were lowest during menses (day 1-4) and peaked in late follicular (estradiol) and late luteal (progesterone) phases (**Fig. 3.3; Table 3.1**). Progesterone concentrations surpassed 5 ng/mL in the luteal phase, signaling an ovulatory cycle (Ecochard et al., 2015). In Study 2, the participant was placed on a pharmacological regimen (0.02

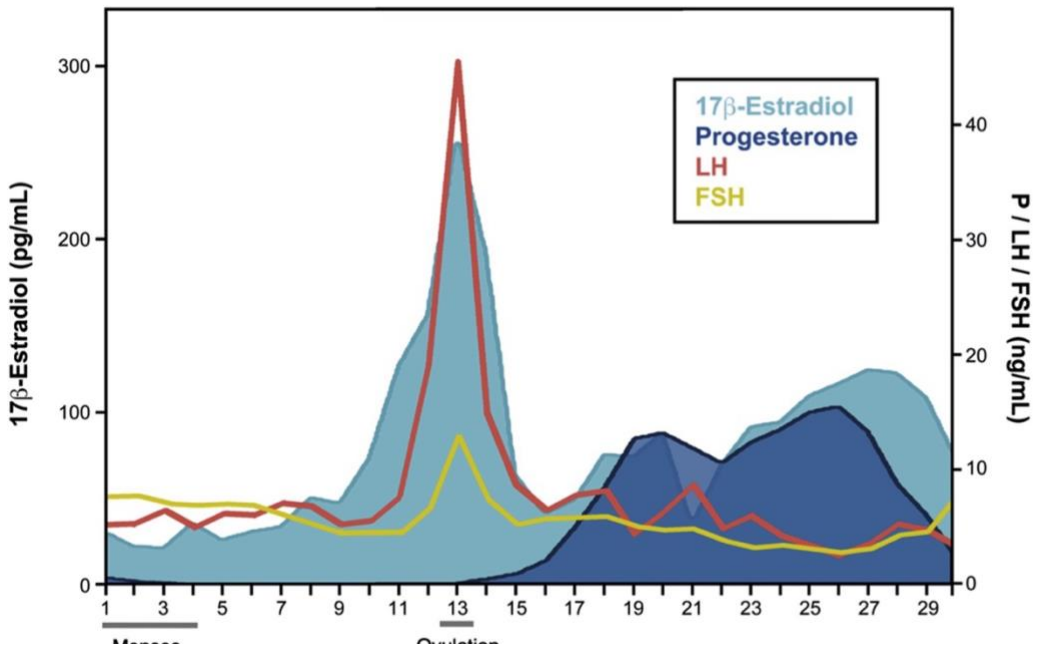

Figure 3.3. Participant's hormone concentrations plotted by day of cycle (Study 1). 17β-estradiol, progesterone, luteinizing hormone (LH), and follicle stimulating hormone (FSH) concentrations fell within standard ranges.

mg ethinyl-estradiol, 0.1 mg levonorgestrel) that chronically and selectively suppressed circulating progesterone, while leaving endogenous estradiol concentrations largely untouched. Estradiol dynamics in Study 2 (*M* = 66.2 pg/mL, *range*: 5–246 pg/mL) were highly similar to Study 1 (*M* = 82.8 pg/mL, *range:* 22–264 pg/mL; *t*(58)= -1.01, *p* = .32), offering us a second dataset in which to test the reliability of estradiol's influence on intrinsic brain networks.

Table 3.1. Gonadal and pituitary hormones by cycle stage (Study 1).

	Follicular	**Ovulatory**	**Luteal**
	Mean (SD) *standard range*	Mean (SD) *standard range*	Mean (SD) *standard range*
Estradiol (pg/mL)	37.9 (15.9) *12.5-166.0*	185.3 (59.0) *85.8-498.0*	85.4 (26.4) *43.8-210.0*
Progesterone (ng/mL)	0.2 (0.2) *0.1-0.9*	0.2 (.2) *0.1-120*	9.5 (4.8) *1.8-23.9*
LH (mIU/mL)	5.9 (0.7) *2.4-12.6*	21.7 (16.4) *14.0-95.6*	5.5 (2.0) *1.0-11.4*
FSH (mIU/mL)	6.5 (1.2) *3.5-12.5*	8.1 (3.6) *4.7-21.5*	4.8 (1.3) *1.7-7.7*

Note. Standard reference ranges based on aggregate data from Labcorp: https:/www.labcorp.com/

Time-synchronous associations between sex hormones and whole-brain functional connectivity

Inspection of day-to-day similarity in whole-brain patterns of coherence (via pairwise Pearson correlation) revealed moderate-to-high levels of reliability between different stages of the cycle. Notably, however, one session in Study 1 (day 26) was markedly dissimilar to the other sessions. Removal of this day from the analysis below did not impact the results (**Appendix A Fig. 4**).

To further explore cycle-dependent variability, we tested the hypothesis that whole-brain functional connectivity at rest is associated with intrinsic fluctuations in estradiol and progesterone in a *time-synchronous* (i.e. day-by-day) fashion. Based on the enriched expression of ER in frontal cortex (Wang et al., 2010), we predicted

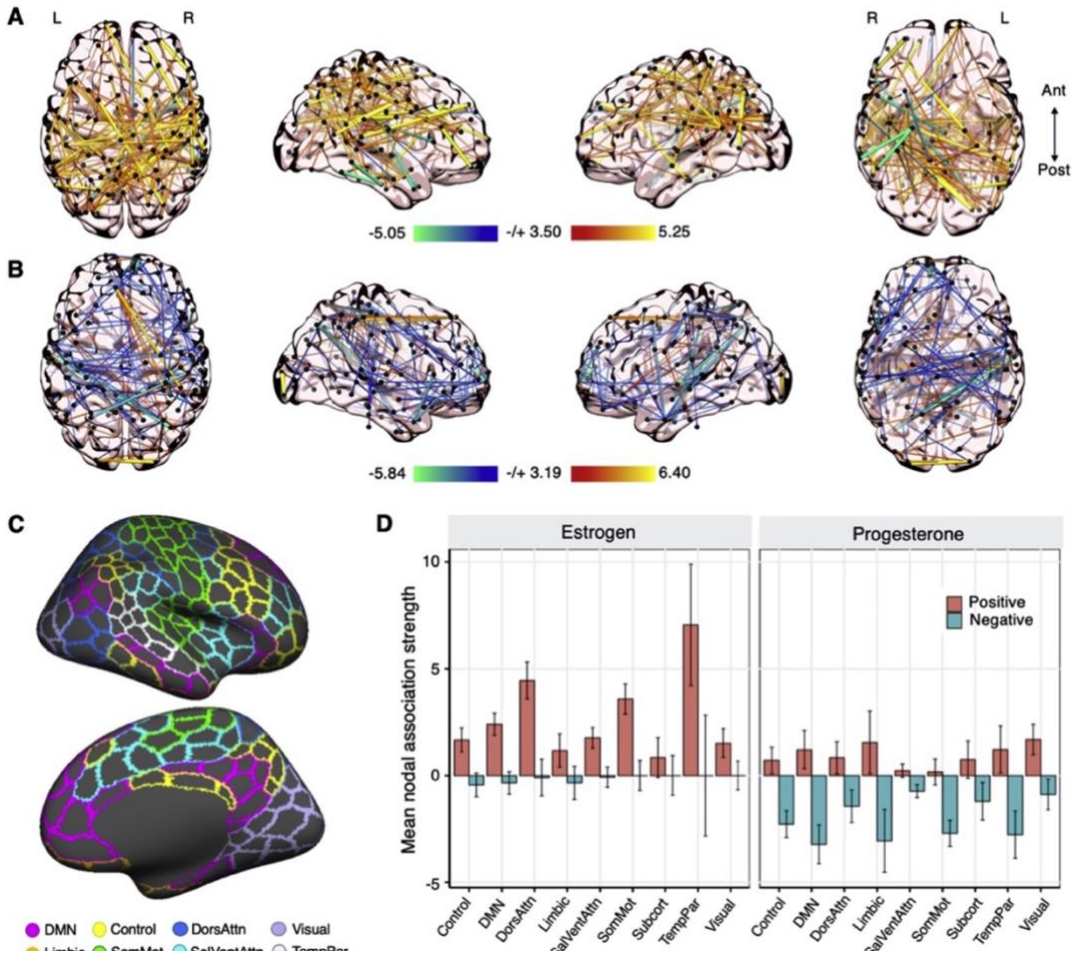

Figure 3.4. Whole-brain functional connectivity at rest is associated with intrinsic fluctuations in estradiol and progesterone (Study 1) **(A)** Time-synchronous (i.e. day-by-day) associations between estradiol and coherence. Hotter colors indicate increased coherence with higher concentrations of estradiol; cool colors indicate the reverse. Results are empirically-thresholded via 10,000 iterations of nonparametric permutation testing ($p < .001$). Nodes without significant edges are omitted for clarity. **(B)** Time-synchronous associations between progesterone and coherence. **(C)** Cortical parcellations were defined by the 400-node Schaefer atlas (shown here). An additional 15 subcortical nodes were defined from the Harvard-Oxford atlas. **(D)** Mean nodal association strengths by network and hormone. Error bars give 95% confidence intervals. 'Positive' refers to the average magnitude of positive associations (e.g. stronger coherence with higher estradiol); 'Negative' refers to the average magnitude of inverse associations (e.g. weaker coherence with higher estradiol). Abbreviations: DMN, Default Mode Network; DorsAttn, Dorsal Attention Network; SalVentAttn, Salience/Ventral Attention Network; SomMot, SomatoMotor Network; TempPar, Temporal Parietal Network.

that the Default Mode, Frontoparietal Control, and Dorsal Attention Networks would be most sensitive to hormone fluctuations across the cycle.

In Study 1, we observed robust increases in coherence as a function of increasing estradiol across the brain (**Fig. 3.4A**). When summarizing the average magnitude of association per network (as defined by our parcellation; **Fig. 3.4C**), components of the Temporal Parietal Network had the strongest positive associations with estradiol on average, as well as the most variance (**Fig. 3.4D**). With the exception of Subcortical nodes, all networks demonstrated some level of significantly positive association strength on average (95% CIs not intersecting zero). We observed a paucity of edges showing inverse associations (connectivity decreasing while estradiol increased), with no networks demonstrating significantly negative association strengths on average (**Fig. 3.4D)**. These findings suggest that edgewise functional connectivity is primarily characterized by increased coupling as estradiol rises over the course of the cycle.

Progesterone, by contrast, yielded a widespread pattern of inverse association across the brain, such that connectivity decreased as progesterone rose (**Fig. 3.4B**). Most networks (with the exception of the Salience / Ventral Attention and SomatoMotor Networks) still yielded some degree of significantly positive association over time; however, the general strength of negative associations was larger in magnitude and significantly nonzero across all networks (**Fig. 3.4D**). Together, the direction of these observed relationships offers a macroscale analogue to cellular-level animal models of estradiol and progesterone function, consistent with proliferative (increased connectivity) and reductive (decreased

connectivity) effects, respectively. Re-analysis with global signal regression included during preprocessing yielded a similar pattern of results (**Appendix A Fig. 5**), suggesting that the relationships observed in Study 1 are *not* due to arbitrary changes in global signal over time (e.g., due to physiological variability over the cycle).

Given the predominantly positive associations between connectivity and estradiol, we further assessed the dependence of these effects on the estradiol surge that occurs during ovulation. Removal of the ovulation window erased significant associations across the brain almost entirely (**Appendix A Fig. 6A**), indicating that the hallmark rise of estradiol during ovulation may be a key modulator of functional coupling over a reproductive cycle. We then tested the reliability of these associations when estradiol fluctuations were unopposed by progesterone (Study 2): this revealed similarly ubiquitous increases in connectivity coincident with estradiol fluctuations (**Appendix A Fig. 7**). As before, removal of the three highest estradiol days during the mid-cycle peak (akin to the ovulatory window from Study 1) greatly reduced whole-brain associations (**Appendix A Fig. 6B**). Thus, whole-brain functional connectivity appears highly sensitive to estradiol regardless of reproductive status.

Time-lagged associations between estradiol and whole-brain functional connectivity

We then employed time-lagged methods from dynamical systems analysis to further elucidate the degree to which intrinsic functional connectivity is sensitive to fluctuations in estradiol: specifically, vector autoregression (VAR), which supports

more *directed* temporal inference than standard regression models. As described previously, we report results from second-order VAR models: thus, in order to assess connectivity or hormonal states on a given day of the experiment, we consider their values on both the previous day (hereafter referred to as 'lag 1') and two days prior (hereafter referred to as 'lag 2'). Ultimately, if brain variance over time is attributable to previous states of estradiol, this suggests that temporal dynamics in connectivity may be *driven* (in part) by fluctuations in this hormone.

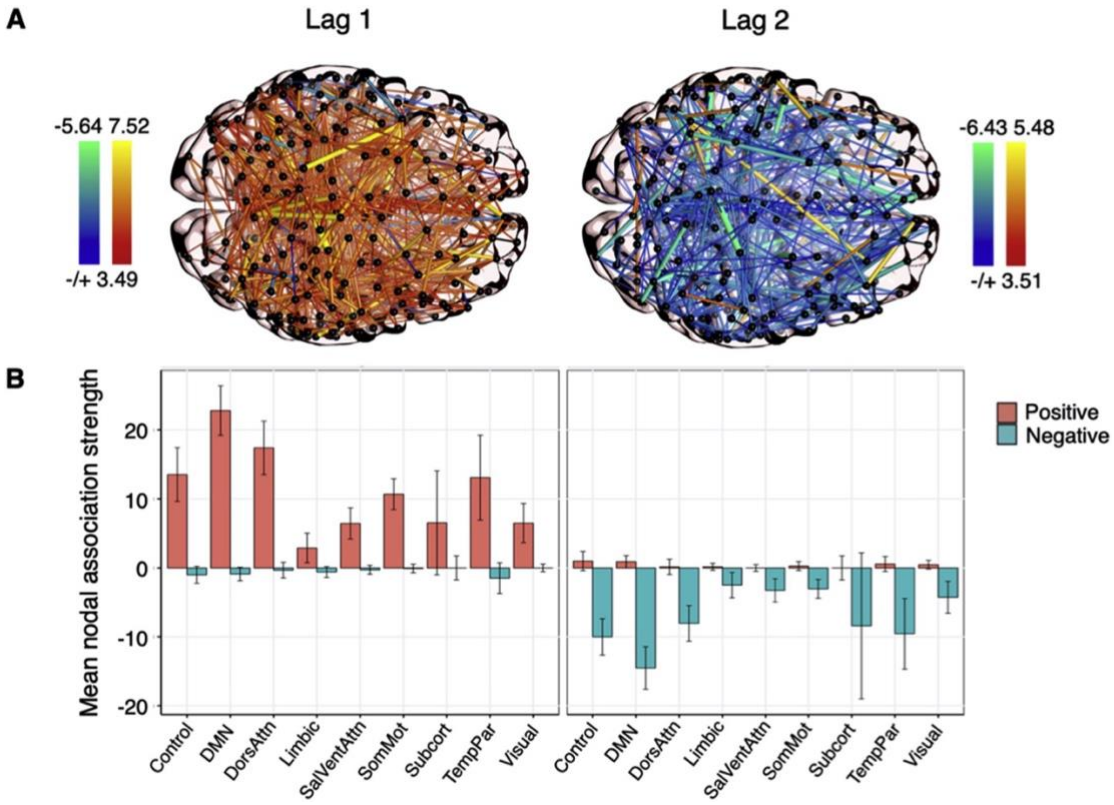

Figure 3.5. Whole-brain functional connectivity is linearly dependent on previous states of estradiol (Study 1). (**A**) Time-lagged associations between coherence and estradiol at lag 1 (left) and lag 2 (right), derived from edgewise vector autoregression models. Hotter colors indicate a predicted increase in coherence given previous concentrations of estradiol; cool colors indicate the reverse. Results are empirically-thresholded via 10,000 iterations of nonparametric permutation testing ($p < .001$). Nodes without significant edges are omitted for clarity. (**B**) Mean nodal association strengths by network and time lag. Error bars give 95% confidence intervals. 'Positive' refers to the average magnitude of positive associations (stronger coherence when prior states of estradiol were high); 'Negative' refers to the average magnitude of inverse associations (weaker coherence when prior states of estradiol were high).

When assessing edgewise connectivity states, a powerful disparity emerged between the brain's autoregressive effects and the effects of estradiol in Study 1. We observed vast, whole-brain associations with prior hormonal states, both at lag 1 and lag 2 (**Fig. 3.5A**). Perhaps most immediately striking, the sign of these brain-hormone associations inverts between lags, such that it is predominantly positive at lag 1 and predominantly negative at lag 2—this holds for all networks when considering their nodal association strengths (**Fig. 3.5B**). We interpret this as a potential regulatory dance between brain states and hormones over the course of the cycle, with estradiol perhaps playing a role in maintaining both steady states (when estradiol is low) and transiently-high dynamics (when estradiol rises). No such pattern emerged in the brain's autoregressive effects, with sparse, low-magnitude, and predominantly negative associations at lag 1 and lag 2 (**Appendix A Fig. 8**). The observed associations between estradiol and edgewise connectivity were partially unidirectional. Previous states of coherence were associated with estradiol across a number of edges, intersecting all brain networks. This emerged at both lag 1 and lag 2; however, unlike the lagged effects of estradiol on coherence, association strengths were predominantly negative and low-magnitude (on average) at both lags (**Appendix A Fig. 9**). Moreover—and importantly—*none* of the edges that informed the temporal evolution of estradiol were also significantly preceded *by* estradiol at either lag (i.e., there was no evidence of mutual modulation at any network edge).

We again tested the reliability of these effects in the replication sample. The autoregressive trends in edgewise coherence remained sparse and low-magnitude

on average; however, unlike the original sample, nearly all networks demonstrated significantly positive associations at lag 1, and lag 2 was dominated by negative associations (**Appendix A Fig. 10**). Previous states of coherence also informed changes in estradiol over time, but this, too, differed from the original sample at the network level. While coherence at lag 1 was generally associated with decreases in estradiol across most networks, several networks (including the Control, Default Mode, and Dorsal Attention Networks) were associated with increases on average at lag 2 (**Appendix A Fig. 11**). Finally, and importantly, we observed highly robust associations between lagged states of estradiol and coherence, with widespread positive associations at lag 1 and predominantly negative associations at lag 2 (**Appendix A Fig. 12**). Curiously, in contrast to the naturally-cycling data, 'non-cognitive' networks such as the SomatoMotor and Visual Networks demonstrated by far the strongest-magnitude associations on average—particularly at lag 1. It is possible that estradiol's effects are magnified when unopposed by the inhibitory nature of progesterone, a topic to be addressed in future investigations.

Time-lagged associations between estradiol and functional network topologies

Given the findings above, we applied the same time-lagged framework to *topological states* of brain networks in order to better capture the directionality and extent of brain-hormone interactions at the mesoscopic level. These states were quantified using common graph theory metrics: namely, the *participation coefficient* (an estimate of *between-network* integration) and *global efficiency* (an estimate of

within-network integration). We focus on significant network-level effects below, but a full documentation of our findings is available in the **Appendix A**.

Estradiol and between-network participation

As expected, estradiol demonstrated significant autoregressive trends across all models in Study 1. However, between-network integration was only tenuously associated with previous states of estradiol: in several intrinsic networks, overall model fit (variance accounted for, R^2, and root mean-squared error, *RMSE*) was at best marginal compared to empirical null distributions of these statistics, and we therefore urge caution in interpreting these results. For example, in the Dorsal Attention Network (DAN; **Fig. 3.6A-B**; **Table 3.2**), estradiol was significantly associated with between-network participation both at lag 1 (b = -0.56, SE = 0.25, t = -2.27, p = .035) and at lag 2 (b = 0.53, SE = 0.24, t = 2.16, p = .042). Overall fit for

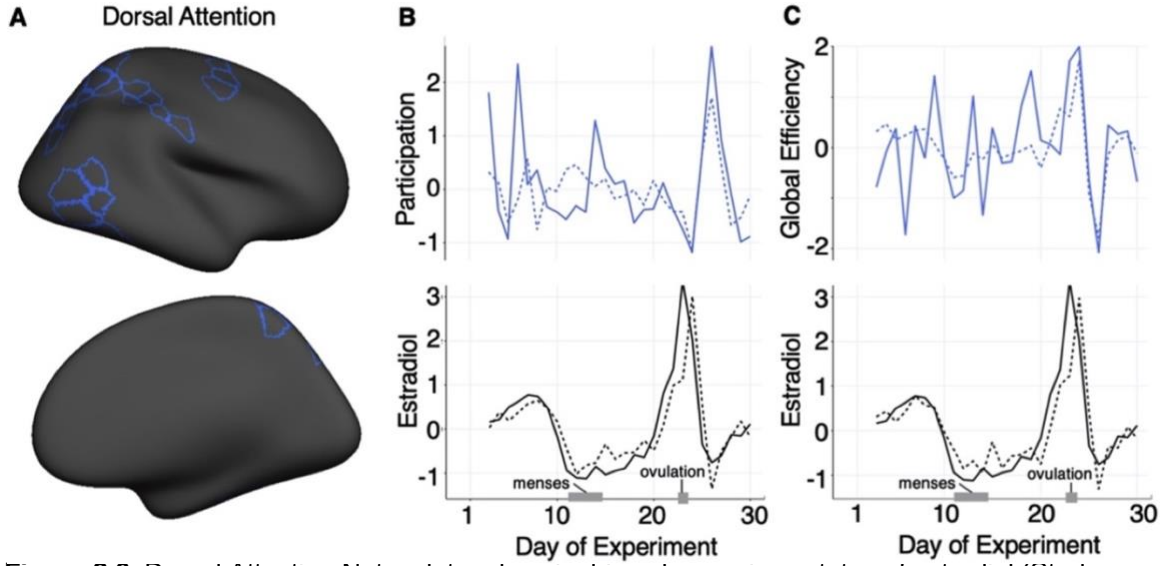

Figure 3.6. Dorsal Attention Network topology is driven by previous states of estradiol (Study 1). Observed data (solid lines) vs. VAR model fits (dotted lines) for between network participation (**B**, middle) and within-network efficiency (**C**, right) in the Dorsal Attention Network (**A**, left). Timeseries for each network statistic are depicted above in (**B,C**) and estradiol for each VAR is plotted below. Data are in standardized units and begin at experiment day three, given the second-order VAR (lag of two days).

DAN participation, however, rested at the classical frequentist threshold for significance relative to empirical nulls (R^2 = 0.32, p = .049; *RMSE* = 0.79, p = .050). We observed a similar pattern of results for the Default Mode Network (DMN) and Limbic Network, where lagged states of estradiol were significantly associated with cross-network participation, but model fit as a whole was low (see **Appendix A Table 1**).

Table 3.2. VAR model fit: Between-network participation (Study 1).

Network	Outcome	Predictor	Estimate	*SE*	*T* (*p*)
		Constant	0.08	0.16	0.49 (.099)
		DAN_{t-1}	0.15	0.18	0.84 (.405)
	Participation	**$Estradiol_{t-1}$**	**-0.56**	**0.25**	**-2.27 (.035)**
		DAN_{t-2}	-0.29	0.17	-1.71 (.093)
		$Estradiol_{t-2}$	**0.53**	**0.24**	**2.16 (.042)**
			R^2 = 0.32 (*p* = .049); *RMSE* = 0.79 (*p* = .050)		
Dorsal Attention					
		Constant	6.88×10^{-5}	0.12	0.001 (.998)
		DAN_{t-1}	0.06	0.14	0.47 (.627)
	Estradiol	**$Estradiol_{t-1}$**	**1.12**	**0.18**	**6.12 (< .0001)**
		DAN_{t-2}	0.03	0.13	0.24 (.806)
		$Estradiol_{t-2}$	**-0.48**	**0.18**	**-2.65 (.007)**
			R^2 = 0.67 (*p* = .0001); *RMSE* = 0.59 (*p* = .0009)		

Note. *p*-values empirically-derived via 10,000 iterations of nonparametric permutation testing.

Importantly, we failed to replicate these effects in Study 2 under hormonal suppression (**Appendix A Table 2**). The autoregressive trends in estradiol were generally blunted, with lag 2 now offering no predictive value. Previous states of DAN participation also informed the temporal evolution of estradiol (whereas there was no reciprocity in lagged effects in Study 1); however, this only emerged at lag 1 (b = -0.09, *SE* = 0.04, t = -2.08, p = .044). The Limbic and Subcortical Networks additionally demonstrated significant autoregressive trends at lag 1, but neither showed significant associations with estradiol. In sum, the marginal model fits, along

with failures to replicate in Study 2, requires further investigation in future work before robust conclusions can be drawn for between-network participation.

Estradiol and global efficiency

In contrast to between-network integration, estradiol was more strongly associated with within-network integration, both in terms of lagged parameter estimates and overall fit. Here, the Default Mode Network provided the best-fitting model in Study 1 (R^2 = 0.50, p = .003; *RMSE* = 0.70, p = .022; **Fig. 3.7A-B**). As before, estradiol demonstrated significant autoregressive effects at lag 1 (b = 1.15, *SE* = 0.19, t = 6.15, p < .0001) and lag 2 (b = -0.48, *SE* = 0.19, t = -2.50, p = .012). When assessing dynamics in DMN efficiency, previous states of estradiol remained significant both at lag 1 (b = 0.98, *SE* = 0.23, t = 3.37, p = .0003) and at lag 2 (b = -0.93, *SE* = 0.23, t = -4.00, p = .002). Critically, these effects were purely directional: prior states of Default Mode efficiency were not associated with estradiol, nor did

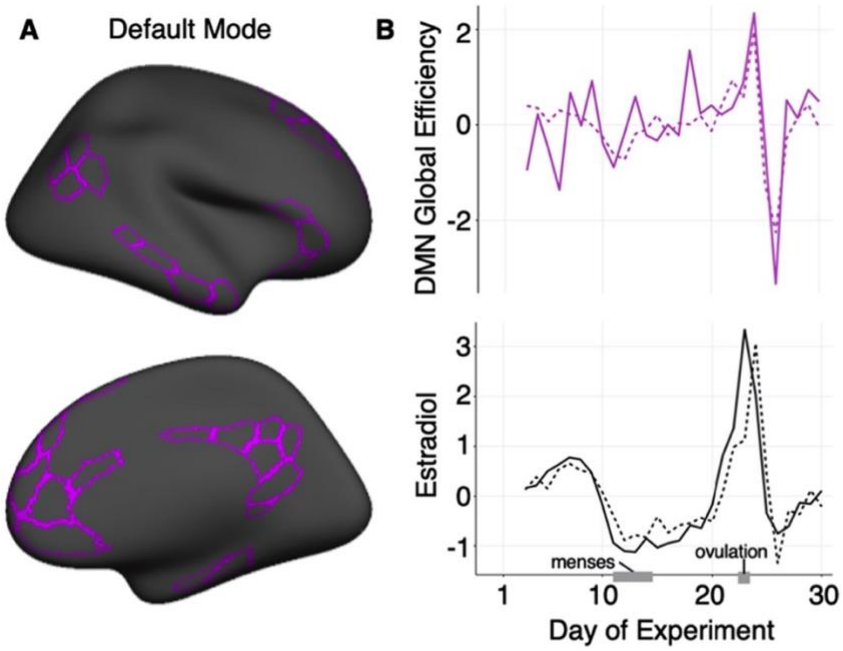

Figure 3.7. Default Mode Network topology is driven by previous states of estradiol (Study 1). Observed data (solid lines) vs. VAR model fits (dotted lines) for within-network efficiency (**B**, right) in the Default Mode Network (**A**, left). The efficiency timeseries is depicted above in (**B**) and estradiol is plotted below. Data are in standardized units and begin at experiment day three, given the second-order VAR (lag of two days).

they have significant autoregressive effects, suggesting that variance in topological network states (perhaps within-network integration, in particular) is primarily accounted for by estradiol—not the other way around (**Table 3.3**).

Table 3.3 VAR model fit: Global efficiency (Study 1).

Network	Outcome	Predictor	Estimate	*SE*	*T* (*p*)
Default Mode	Efficiency	Constant	0.04	0.15	0.28 (.279)
		DMN_{t-1}	-0.04	0.16	-0.27 (.764)
		$Estradiol_{t-1}$	**0.98**	**0.23**	**3.37 (.0003)**
		DMN_{t-2}	-0.02	0.16	-0.11 (.907)
		$Estradiol_{t-2}$	**-0.93**	**0.23**	**-4.00 (.002)**
			R^2 = 0.50 (*p* = .003); *RMSE* = 0.70 (*p* = .022)		
	Estradiol	Constant	0.01	0.12	0.09 (.729)
		DMN_{t-1}	-0.12	0.13	-0.95 (.339)
		$Estradiol_{t-1}$	**1.15**	**0.19**	**6.15 (< .0001)**
		DMN_{t-2}	-0.01	0.13	-0.08 (.930)
		$Estradiol_{t-2}$	**-0.48**	**0.19**	**-2.50 (.012)**
			R^2 = 0.67 (*p* < .0001); *RMSE* = 0.58 (*p* = .0004)		
Dorsal Attention	Efficiency	Constant	0.01	0.16	0.08 (.783)
		DAN_{t-1}	-0.11	0.18	-0.60 (.562)
		$Estradiol_{t-1}$	**0.84**	**0.25**	**3.35 (.002)**
		DAN_{t-2}	-0.10	0.18	-0.58 (.571)
		$Estradiol_{t-2}$	**-0.67**	**0.16**	**-2.57 (.017)**
			R^2 = 0.37 (*p* = .022); *RMSE* = 0.77 (*p* = .023)		
	Estradiol	Constant	0.01	0.12	0.06 (.808)
		DAN_{t-1}	-0.17	0.13	-1.29 (.207)
		$Estradiol_{t-1}$	**1.17**	**0.19**	**6.30 (< .0001)**
		DAN_{t-2}	-0.02	0.13	-0.16 (.875)
		$Estradiol_{t-2}$	**-0.48**	**0.19**	**-2.49 (.011)**
			R^2 = 0.68 (*p* < .0001); *RMSE* = 0.57 (*p* = .0004)		

Note. *p*-values empirically-derived via 10,000 iterations of nonparametric permutation testing.

We observed a similar pattern of results in the Dorsal Attention Network (R^2 = 0.37, p = .022; *RMSE* = 0.77, p = .023; **Fig. 3.6C, Table 3.3**). Estradiol again demonstrated significant autoregressive trends at lag 1 (b = 1.17, *SE* = 0.19, t = 6.30, p < .0001) and lag 2 (b = -0.48, *SE* = 0.19, t = -2.49, p = .011), as well as significant lagged associations with DAN efficiency both at lag 1 (b = 0.84, *SE* = 0.25, t = 3.35, p = .002) and at lag 2 (b = -0.67, *SE* = 0.26, t = -2.57, p = .017). As

before, Dorsal Attention efficiency had no significant effects on estradiol, nor were there significant autoregressive effects of the network on itself.

The Control and Temporal Parietal networks also yielded partial support for time-dependent modulation of efficiency by estradiol (Control R^2 = 0.34, p = .039; Temporal Parietal R^2 = 0.36, p = .026). The time-lagged effects of estradiol followed the trends observed above; however, the overall model fit (with respect to prediction error) was not significantly better than their empirical nulls (Control *RMSE* = 0.83, p = .133; Temporal Parietal *RMSE* = 0.79, p = .057). Estradiol did not explain a significant proportion of variance in efficiency for any other networks in Study 1 (**Appendix A Table 3**).

In contrast to between-network participation, within-network efficiency yielded stronger evidence for replication in Study 2. The DMN again demonstrated the strongest model fit (R^2 = 0.38, p = .019; *RMSE* = 0.74, p = .011), with estradiol informing fluctuations in DMN efficiency both at lag 1 (b = 2.48, *SE* = 0.75, t = 3.29, p = .003) and lag 2 (b = -2.69, *SE* = 0.91, t = -2.94, p = .009). We also observed a significant autoregressive effect of DMN efficiency at lag 2 (b **=** -0.45, *SE* = 0.19, t = -2.41, p = .027), but not at lag 1. In the DAN, significant model fit was achieved with respect to prediction error (*RMSE* = 0.79, p = .045), but variance accounted for was marginal relative to empirical nulls (R^2 = 0.32, p = .052). Accordingly, estradiol was significantly associated with DAN efficiency at lag 1 (b = 1.88, *SE* = 0.79, t = 2.37, p = .026) but not at lag 2. Finally, previous states of estradiol (both lags 1 and 2) significantly informed efficiency in the Control, Salience / Ventral Attention,

SomatoMotor, and Subcortical Networks; however, aside from the SomatoMotor Network (R^2 = 0.34, p = .039; *RMSE* = 0.76, p = .018), overall fit in these models was nonsignificant (**Appendix A Table 4**). Thus, while we observed trends largely consistent with Study 1 (with respect to DMN and DAN efficiency), there may be additional network-level effects in a neuroendocrine system unopposed by progesterone, warranting future investigation.

D. Discussion

In this dense-sampling, deep-phenotyping project, a naturally-cycling female underwent resting state fMRI and venipuncture for 30 consecutive days, capturing the dynamic endocrine changes that unfold over the course of a complete menstrual cycle. Time-synchronous analyses illustrate estradiol's widespread associations with cortical network dynamics, spanning all but one of the networks in our parcellation. Time-lagged vector autoregressive models tested the temporal directionality of these effects, suggesting that intrinsic network dynamics may be partially driven by recent states of estradiol, particularly with respect to within-network connectivity: global efficiency in the Default Mode and Dorsal Attention Networks exhibited the strongest associations with fluctuations in estradiol, replicated between Studies 1 and 2. In contrast to estradiol's proliferative effects, progesterone was primarily associated with reduced coherence across the whole brain. Findings from a replication dataset further establish estradiol's impact on large-scale cortical dynamics. Critically, removal of high estradiol days in both studies reduced associations across the brain, suggesting that the hallmark rise and fall of estradiol surrounding the ovulatory

window may be a key modulator of functional coupling during the reproductive cycle (**Appendix A Fig. 6**). Together, these results reveal the rhythmic nature in which brain networks reorganize across the human menstrual cycle.

The network neuroscience community has begun to probe functional networks over the timescale of weeks, months, and years to understand the extent to which brain networks vary between individuals or within an individual over time (Poldrack et al., 2015; Finn et al., 2015; Gordon et al., 2017; Betzel et al., 2017; Horien et al., 2019; Seitzman et al. 2019). These studies indicate that functional networks are dominated by common organizational principles and stable individual features, especially in frontoparietal control regions (Finn et al., 2015; Gordon et al., 2017; Gratton et al., 2018a; Horien et al., 2019). An overlooked feature of these regions is that they are populated with estrogen and progesterone receptors and are exquisitely sensitive to major changes in sex hormone concentrations (Berman et al., 1997; Jacobs and D'Esposito, 2011; Hampson and Morley, 2013; Shanmugan and Epperson, 2014; Jacobs et al., 2016a,b). Our findings demonstrate significant effects of estradiol on functional network nodes belonging to the DMN, DAN, and FCN that overlap with ER-rich regions of the brain, including medial/dorsal PFC (Wang et al., 2010; Yeo et al., 2011). This study merges the network neuroscience and endocrinology disciplines by demonstrating that higher-order processing systems are modulated by day-to-day changes in sex hormones over the timescale of one month.

Sex hormones regulate brain organization across species

Animal studies offer unambiguous evidence that sex steroid hormones shape the synaptic organization of the brain, particularly in regions that support higher order cognitive functions (Woolley and McEwen, 1993; Frick et al., 2015; Hara et al., 2015; Galea et al., 2017; Frick et al., 2018). In rodents, estradiol increases fast-spiking interneuron excitability in deep cortical layers (Clemens et al., 2019). In nonhuman primates, whose reproductive cycle length is similar to humans, estradiol increases the number of synapses in PFC (Hara et al., 2015). Recently, this body of work has begun to uncover the functional significance of sinusoidal *changes* in estradiol. For example, estradiol's ability to promote PFC spinogenesis in ovariectomized animals occurs *only if* the hormone add-back regimen mirrors the cyclic pattern of estradiol release typical of the macaque menstrual cycle (Hao et al., 2006; Ohm et al., 2012). Pairing estradiol with cyclic administration of progesterone blunts this increase in spine density (Ohm et al., 2012). In the hippocampus, progesterone has a similar inhibitory effect on dendritic spines, blocking the proliferative effects of estradiol 6 hours after administration (Woolley and McEwen, 1993). Together, the preclinical literature suggests that progesterone antagonizes the largely proliferative effects of estradiol (for review, see Brinton et al., 2008). We observed a similar relationship, albeit at a different spatiotemporal resolution, with estradiol demonstrating positive associations with coherence across numerous cortical networks and progesterone having an opposite, negative association on average. In sum, animal studies have identified estradiol's influence on regional brain organization at the microscopic scale. Here, we show that estradiol and progesterone may have analogous effects evident at the mesoscopic scale of whole-

brain connectivity, measured by spectral coherence and macroscopic features of network topology.

Resting state network characteristics differ by cycle stage

Group-based and sparser-sampling neuroimaging studies provide further support that cycle stage and sex hormones impact resting state networks (Petersen et al., 2014; Lisofsky et al., 2015; De Bondt et al., 2015; Syan et al., 2017; Weis et al., 2019). For instance, Petersen and colleagues (2014) demonstrated that women sampled in the follicular stage had greater connectivity within default mode and execute control networks compared to those sampled in the luteal stage. Lisofsky and colleagues (2015) studied women four times across their menstrual cycles, observing significant increases in connectivity between the hippocampus and superior parietal lobule during the late follicular phase. However, recent work by Weis and colleagues (2019) provides compelling yet contrasting evidence for sex hormones' relationship with resting-state functional connectivity: studying women three times across the cycle, their group observed heightened connectivity between a region of the left frontal cortex and the DMN during menstruation when estradiol levels are lowest. Inconsistencies between studies could be due to a number of factors such as differences in cycle staging methods, divergent functional connectivity estimation methods, or unaccounted for intra/inter-individual variability (Beltz and Moser, 2019). Our results suggest that failure to properly capture the complete ovulatory window, when estradiol levels rapidly rise, could lead to skewed estimates of stability within functional brain networks across the menstrual cycle (Hjelmervik et al., 2014). As such, dense-sampling studies provide a novel solution

to capturing pivotal moments experienced across a complete human menstrual cycle. Arélin and colleagues (2015) sampled an individual every 2-3 days across four cycles and found that progesterone was associated with increased connectivity between the hippocampus, dorsolateral PFC and sensorimotor cortex, providing compelling evidence that inter-regional connectivity varies over the cycle. This particular dense-sampling approach allowed the authors to examine brain-hormone relationships while accounting for intra-individual cycle variation.

Estradiol is capable of inducing rapid, non-genomic effects and slower, genomic effects on the central nervous system. For example, spine density on hippocampal neurons varies by ~30% over the rodent estrous cycle. *In-vivo* MRI evidence in mice demonstrates that these hormone-mediated changes can occur rapidly, with differences detectable within a 24-hour period. To capture time-synchronous (rapid) and time-lagged (delayed) effects of sex steroid hormones, we expanded upon Arélin and colleagues' approach by sampling an individual every 24 hours for 30 consecutive days. Our results illuminate how time-synchronous correlations and time-lagged computational approaches reveal unique aspects of where and how hormones exert their effect on the brain's intrinsic networks. Time-synchronous analyses illustrated contemporaneous, zero-lag associations between estradiol, progesterone, and whole-brain connectivity. The introduction of lagged states in VAR allowed us to examine the temporal directionality of those relationships and suggest that recent fluctuations in estradiol (within two days) inform current brain states—this raises the interesting possibility that estradiol may

play a partial role in driving changes in connectivity, particularly in the DMN and DAN.

Neurobiological interpretations of hormonal effects and future studies

The following considerations could enhance the interpretation of these data. First, our investigation deeply sampled a single woman, limiting our ability to generalize these findings to other individuals. To enrich our understanding of the relationship between sex hormones and brain function, this dense-sampling approach should be extended to a diverse sample of women. Doing so will allow us to examine the consistency of our results with respect to inter-individual differences in network organization over the menstrual cycle. Additionally, examining network organization during a state of complete hormone suppression would serve as a valuable comparison given that certain oral hormonal contraceptives suppress the production of both ovarian hormones. If dynamic changes in estradiol are *facilitating* increases in resting-state connectivity, we expect hormonally-suppressed individuals to show less dynamic modulation of functional brain networks over time. Given the widespread use of oral hormonal contraceptives (100 million users worldwide), it is critical to determine whether sweeping changes to an individual's endocrine state impacts brain states and whether this, in turn, has any bearing on cognition.

Second, in freely-cycling individuals, sex hormones function as proportionally-coupled *nonlinear* oscillators (Boker et al., 2014). Within-person cycle variability is almost as large as between-person cycle variability, which hints that there are highly complex hormonal interactions within this regulatory system (Fehring et al., 2006;

Boker et al., 2014). The VAR models we have explored reveal *linear* dependencies between brain states and hormones, but other methods (e.g., coupled latent differential equations) may offer more biophysical validity (Boker et al., 2014). However, the current sample size precludes robust estimation of such a model.

Third, while permutation tests have been used as empirical null models for VAR (Hyvärinen et al., 2010) and its statistical relatives (e.g. Granger causality; Barnett & Seth, 2014), the practice of temporally-scrambling a timeseries will drastically alter its autocorrelative structure and potentially skew observed dependencies over time. Phase-shifting, surrogate data tests such as the amplitude adjusted Fourier transform (AAFT) may offer more robust null distributions. However, AAFT also makes strong distributional assumptions about the original timeseries (Gaussian normality) that, unfortunately, are not met by these data. Additionally, the small sample size over a single cycle precludes the ability to derive robust surrogate realizations of the timeseries. While AAFT is arguably an *ideal* procedure for analyses such as those reported here, these data simply cannot meet the assumptions required for valid surrogate testing and thus is a major limitation within the current study. Future investigations involving larger samples of women over several cycles that allow implementation of such models will be critical.

Fourth, while coherence is theoretically robust to timing differences in the hemodynamic response function, hormones can affect the vascular system (Krause et al., 2006). Therefore, changes in coherence may be due to vascular artifacts that affect the hemodynamic response in fMRI, rather than being *neurally*-relevant. Future investigations exploring the assumptions of hemodynamics in relation to sex

steroid hormone concentrations will add clarity as to how the vascular system's response to hormones might influence large-scale brain function.

Fifth, these findings contribute to an emerging body of work on estradiol's ability to enhance the efficiency of PFC-based cortical circuits. In cycling women performing a working memory task, PFC activity is exaggerated under low estradiol conditions and reduced under high estradiol conditions (Jacobs and D'Esposito, 2011). The same pattern is observed decades later in life: as estradiol production decreases over the menopausal transition, working memory-related PFC activity becomes more exaggerated, despite no difference in working memory performance (Jacobs et al., 2016a). Here, we show that day-to-day changes in estradiol enhance the global efficiency of functional networks, with pronounced effects in networks (DMN and FCN) that encompass major regions of the PFC (Yeo et al., 2011; Schaefer et al., 2018). Together, these findings suggest that estradiol generates a neurally efficient PFC response at rest and while engaging in a cognitive task. Estradiol's action may occur by enhancing dopamine synthesis and release (Creutz and Kritzer, 2002). The PFC is innervated by midbrain dopaminergic neurons that form the mesocortical dopamine track (Kritzer and Creutz, 2008). Dopamine signaling enhances the signal-to-noise ratio of PFC pyramidal neurons (Williams and Goldman-Rakic, 1995) and drives cortical efficiency (Cai and Arnsten, 1997; Granon et al., 2000; Gibbs and D'Esposito, 2005; Vijayraghavan et al., 2007). In turn, estradiol enhances dopamine release and modifies the basal firing rate of dopaminergic neurons (Thompson and Moss, 1994; Pasqualini et al., 1995; Becker, 1990), a possible neurobiological mechanism by which alterations in estradiol could

impact cortical efficiency. Future multimodal neuroimaging studies in humans can clarify the link between estradiol's ability to stimulate dopamine release and the hormone's ability to drive cortical efficiency within PFC circuits.

Sixth, we observed surprisingly few autoregressive effects in brain measures across our time-lagged models. This was despite relatively strong day-to-day similarity in whole-brain patterns of connectivity (**Fig. S3**), and clear evidence for autocorrelation when assessing the brain data in an independent, univariate fashion. Thus, the incorporation of sex hormones into a time-lagged modeling framework attributed more temporal variability in the brain to fluctuations in hormone concentrations. Nevertheless, an ongoing debate within the network neuroscience community surrounds test-retest reliability in resting-state functional connectivity analyses. Some studies state that large amounts of data (>20 minutes) are necessary for test-retest reliability (Noble et al., 2017; Gratton et al., 2018a), while others argue that reliability can be derived from shorter (5-15 minutes) scans (Van Dijk et al., 2010; Birn et al., 2014). We are limited in our ability to assess whether the ostensibly weak autoregressive trends suggested by our time-lagged models would be replicated under longer scanning durations and hope future work addresses this issue.

Finally, we chose to apply a well-established group-based atlas (Schaefer et al., 2018) to improve generalizability to other individuals, as a key goal of our investigation was to demonstrate how sex steroid hormones explain variability in intrinsic network topologies based on regional definitions shown to be reliable across thousands of individuals (Yeo et al., 2011; Schaefer et al., 2018). Yet, group-based

atlases can lead to potential loss in individual-level specificity, and recent work has demonstrated that fixed atlases may not capture underlying reconfigurations in the parcellations themselves within an individual (Bijsterbosch et al., 2019, Salehi et al., 2020a, Salehi et al., 2020b). Therefore, future work using individual-derived functional networks will be necessary to determine whether spatial reconfigurations in *parcellations* emerge as a function of the menstrual cycle, over and above the influence of state or trait features. Relatedly, variation in analytic pipelines of brain imaging data can lead to divergent conclusions even within the same dataset (Botvinik-Nezer et al., 2020); for complete transparency, we are committed to making all neuroimaging data and code publicly available so that other investigators can assess these brain-hormone associations using their preferred methods.

Estradiol modulates global efficiency in estrogen-receptor rich brain regions

Using dense-sampling approaches to probe brain-hormone interactions could reveal organizational principles of the functional connectome previously unknown, transforming our understanding of how hormones influence brain states. Human studies implicate sex steroid hormones in the regulation of brain structure and function, particularly within ER-rich regions like the PFC and hippocampus (Berman et al., 1997; Girard et al., 2017; Hampson and Morley, 2013; Jacobs et al., 2015, 2016a,b; Jacobs and D'Esposito, 2011; Shanmugan and Epperson, 2014, Zeydan et al., 2019), and yet, the neuroendocrine basis of the brain's network organization remains understudied. Here, we used a network neuroscience approach to investigate how hormones modulate the topological integration of functional

networks across the brain, showing that estradiol is associated with increased coherence across broad swaths of cortex that extend beyond regions with established ER expression. At the network level, estradiol enhances the efficiency of most functional networks (with robust effects in DAN and DMN) and, to a lesser extent, modulates between-network participation (although critically, this finding failed to replicate in Study 2). Moving forward, a complete mapping of ER/PR expression in the human brain will be essential for our understanding and interpretation of brain-hormone interactions. Furthermore, this dense-sampling approach could be applied to brain imaging studies of other major neuroendocrine transitions, such as pubertal development and reproductive aging (e.g. menopause).

Implications of hormonally regulated network dynamics for cognition

An overarching goal of network neuroscience is to understand how coordinated activity within and between functional brain networks supports cognition. Increased global efficiency is thought to optimize a cognitive workspace (Bullmore and Bassett, 2011), while between-network connectivity may be integral for integrating top-down signals from multiple higher-order control hubs (Gratton et al., 2018b). The dynamic reconfiguration of functional brain networks is implicated in performance across cognitive domains, including motor learning (Bassett et al., 2011; Mattar et al., 2018), cognitive control (Seeley et al., 2007) and memory (Fornito et al., 2012). Our results suggest that the within-network connectivity of these large-scale networks is temporally-dependent on hormone fluctuations across the human menstrual cycle, particularly in states of high estradiol (e.g. ovulation).

Future studies should consider whether these network changes confer advantages to domain-general or domain-specific cognitive performance. Accordingly, future planned analyses from this dataset will incorporate task-based fMRI to determine whether the brain's network architecture is similarly-variable across the cycle when engaging in a cognitive task, or in the dynamic reconfiguration that occurs when transitioning from rest to task.

Implications of hormonally regulated network dynamics for clinical diagnoses

Clinical network neuroscience seeks to understand how large-scale brain networks differ between healthy and patient populations (Fox and Greicius, 2010; Hallquist and Hillary, 2018). Disruptions in functional brain networks are implicated in a number of neurodegenerative and neuropsychiatric disorders: intrinsic connectivity abnormalities in the DMN are evident in major depressive disorder (Greicius et al., 2007) and Alzheimer's disease (Buckner et al., 2009). Notably, these conditions have a sex-skewed disease prevalence: women are at twice the risk for depression and make up two-thirds of the Alzheimer's disease patient population (Nebel et al., 2018). Here, we show that estradiol modulates efficiency within the DMN and DAN, with pronounced rises in estradiol significantly preceding increases in within-network coherence. A long history of clinical evidence implicates sex hormones in the development of mood disorders (Plotsky et al., 1998; Young and Korszun, 2002; Rubinow and Schmidt, 2006). For example, the incidence of major depression increases with pubertal onset in females (Angold and Costello, 2006), chronic use of hormonal contraceptives (Young et al., 2007), the postpartum period (Bloch et al.,

2000), and perimenopause (Schmidt and Rubinow, 2009). Moving forward, a network neuroscience approach might have greater success at identifying the large-scale network disturbances that underlie, or predict, the emergence of disease symptomology by incorporating sex-dependent variables (such as endocrine status) into clinical models. This may be particularly true during periods of profound neuroendocrine change (e.g. puberty, pregnancy, menopause, and use of hormone-based medications, reviewed in Taylor et al., 2019) given that these hormonal transitions are associated with a heightened risk for mood disorders.

4

Neuroanatomical changes observed over the course of a human pregnancy

Adapted from the following manuscript: **Pritschet, L.,** Taylor, C.M., Cossio, D., Santander, T., Grotzinger, H., Faskowitz, J., Handwerker, D., Layher, E., Chrastil, E.R., Jacobs, E.G. Neuroanatomical changes observed over the course of a human pregnancy. *Under review.*

Authorship Contributions: The overall study was conceived by L.P., C.M.T., E.R.C., and E.G.J.; L.P., C.M.T., D.C., T.S., E.L., E.R.C., and E.G.J. performed the experiments; data analysis strategy was conceived by L.P., C.M.T., D.C., T.S., J.F., D.A.H., E.R.C. and E.G.J., then implemented by L.P. (GMV, CT), C.M.T. (MTL), and D.C. (Diffusion); L.P., C.M.T., H.G., D.C., E.R.C, and E.G.J. wrote the manuscript; T.S., J.F., D.A.H., and E.L. edited the manuscript.

A. Introduction

Each year, ~140 million women around the globe experience one of the most transformative events of their lifetime—pregnancy (WHO, 2022). Over an approximately 40-week gestational window the maternal body undergoes profound physiological adaptations to support the development of the fetus, including increases in plasma volume, metabolic rate, oxygen consumption, and immune regulation (Thornburg et al., 2015). These rapid adaptations are initiated by hundred- to thousand-fold increases in hormone production, including estrogen and progesterone. These neuromodulatory hormones also drive significant

reorganization of the central nervous system. New mechanistic insights from animal models converge on pregnancy as a period of remarkable neuroplasticity (Puri et al., 2023; Celik et al., 2022; Barrière et al., 2021; Haim et al., 2017; Brunton & Russell et al., 2008). In humans, reductions in gray matter volume (GMV) have been observed postpartum (Hoekzema et al., 2017, 2022; Martínez-García, et al., 2021a), particularly in regions central to theory-of-mind processing (Hoekzema et al., 2017). These GMV changes persist at six years postpartum (Martínez-García et al., 2021b) and are traceable decades later (De Lange et al., 2019; Orchard et al., 2020, 2023), underscoring the permanence of this major remodeling event. Yet, the changes that occur within the maternal brain during gestation itself are virtually unknown.

Here, we conducted the first precision imaging study of pregnancy in which a healthy 38-year-old primiparous woman underwent 26 MRI scans and venipuncture beginning 3 weeks pre-conception through two years postpartum. We observed widespread reductions in GMV and cortical thickness (CT) occurring in step with the dramatic rise in sex hormone production across gestation. Next, high-resolution imaging and segmentation of the medial temporal lobe suggest specific volumetric reductions within parahippocampal cortex. In contrast to widespread decreases in GMV, correlational tractography analyses revealed non-linear increases in white matter quantitative anisotropy (QA) throughout the brain —indicating greater tract integrity— as gestational week progressed. Together, these findings are the first to reveal the highly dynamic changes that unfold in the human brain across pregnancy, raising the possibility that the adult brain undergoes extensive remodeling well into adulthood.

B. Methods

Participant

Our participant (author E.R.C.) was a healthy 38-year-old primiparous woman who underwent in-vitro fertilization (IVF) to achieve pregnancy. Previous studies reported no observable differences in neural changes pre- to post-pregnancy between women who conceived naturally versus women who conceived via IVF (Hoekzema et al., 2017), and doing so provides a controlled way of monitoring pregnancy status. The participant nursed through one-year postpartum, and had no history of neuropsychiatric diagnosis, endocrine disorders, prior head trauma or history of smoking. The participant gave written informed consent and the study was approved by the University of California, Irvine Human Subjects Committee.

Study Design

The participant underwent 26 magnetic resonance imaging (MRI) scanning sessions from 3 weeks prior to conception through two years postpartum (162 weeks), during which high-resolution anatomical and diffusion spectrum imaging scans of the brain were acquired. Scans were distributed throughout this period, including pre-pregnancy (4 scans), first trimester (4 scans), second trimester (6 scans), third trimester (5 scans), and postpartum (7 scans) (**Fig. 4.1B**). The first 6 sessions took place at the UCSB Brain Imaging Center (BIC), the final 20 sessions took place at the UCI Facility for Imaging and Brain Research (FIBRE). The MRI protocol, scanner (Siemens 3T Prisma), and software (version MR E11) were identical across sites. To ensure the robustness of the findings, after the final study session the subject

completed two additional back-to-back validation scans at UCSB and UCI within a 12-hour window to assess reliability between scanners. Intraclass correlation coefficients (two-way, random effects, absolute agreement, single rater) reveal 'excellent' test-retest reliability between scanners, including: ROI-level GMV (*ICC* = 0.97, *95% CI*: 0.80–0.99); ROI-level CT (*ICC* = 0.96, *95% CI*: 0.90–0.98); MTL subfield volume (*ICC* = 0.99, *95% CI:* 0.97–0.99); and ROI-level QA (*ICC* = 0.94, *95% CI:* 0.91–0.97). Further, when examining the relationship between gestation week, cortical and subcortical GMV among UCI-only gestational sessions, consistent findings were observed (**Appendix B Fig. 5**), indicating that site differences are highly unlikely to have contributed meaningfully to the observed effects.

Endocrine Procedures

The participant underwent a blood draw (n = 19, **Fig. 4.1B**) prior to MRI scanning. Sex steroid concentrations were determined via ultra-sensitive liquid chromatography–mass spectrometry (LC-MS) at the Brigham and Women's Hospital Research Assay Core (BRAC). Assay sensitivities, dynamic range, and intra-assay coefficients of variation were as follows: estradiol: 1.0 pg/ml, 1–500 pg/ml, <5% relative standard deviation (RSD); progesterone: 0.05 ng/ml, 0.05–10 ng/ml, 9.33% RSD. Serological samples were not acquired in five sessions due to scheduling conflicts with UC Irvine's Center for Clinical Research.

MRI Acquisition

Magnetic resonance imaging (MRI) scanning sessions at the University of California, Santa Barbara and Irvine were conducted on 3T Prisma scanners equipped with 64-channel phased-array head/neck coil (of which 50 coils are used for axial brain imaging). High-resolution anatomical scans were acquired using a T1-weighted (T1w) magnetization prepared rapid gradient echo (MPRAGE) sequence (TR = 2500 ms, TE = 2.31 ms, T1 = 934 ms, flip angle = 7°, 0.8 mm thickness) followed by a gradient echo fieldmap (TR = 758 ms; TE1 = 4.92 ms; TE2 = 7.38 ms; flip angle = 60°). A T2-weighted (T2w) turbo spin echo (TSE) scan was also acquired with an oblique coronal orientation positioned orthogonally to the main axis of the hippocampus (TR/TE = 9860/50 ms, flip angle = 122°, 0.4 × 0.4 mm^2 in-plane resolution, 2 mm slice thickness, 38 interleaved slices with no gap, total acquisition time = 5:42 min). The DSI protocol sampled the entire brain with the following parameters: single phase, TR = 4300 ms, echo time = 100.2 ms, 139 directions, b-max = 4990, FoV = 259 x 259 mm, 78 slices, 1.7986 x 1.7986 x 1.8 mm voxel resolution. These images were linearly registered to the whole-brain T1w MPRAGE image. A custom foam headcase was used to provide extra padding around the head and neck, as well as to minimize head motion. A custom-built sound-absorbing foam girdle was placed around the participant's waist to attenuate sound near the fetus during second and third trimester scanning.

Image Processing

Cortical Volume and Thickness

Cortical thickness and gray matter volume were measured with Advanced Normalization Tools version 2.1.0 (ANTs) (Avants et al., 2011). First, a custom subject-specific template (SST) (*antsMultivariateTemplateConstruction2*) and tissue priors (*antsCookTemplatePriors*) were built based on the subject's two pre-conception whole-brain T1-weighted scans to examine neuroanatomical changes relative to the subject's pre-pregnancy baseline. Labels from the OASIS population template, provided by ANTs, were used as priors for this step. For each session, the structural image was processed and registered to the SST using the ANTs cortical thickness pipeline (*antsCorticalThickness*). This begins with an N4 bias field correction for field inhomogeneity, then brain extraction using a hybrid registration/segmentation method (see Tustison et al., 2014). Tissue segmentation was performed using Atropos (Avants et al., 2011) to create tissue masks of cerebrospinal fluid (CSF), gray matter, white matter, and deep gray matter. Atropos allows prior knowledge to guide the segmentation algorithm, and we used labels from our SST as priors to minimize warping and remain in native subject space. Cortical thickness measurements were then estimated using the DiReCT algorithm (Das et al., 2009), which estimates the gray/white matter interface and the gray matter/CSF interface and computes a diffeomorphic mapping between the two interactions, from which thickness is derived. Each gray matter tissue mask was normalized to the template and multiplied to a Jacobian image that was computed via affine and non-linear transforms. Summary, regional-level estimates of CT, GMV, and CSF for each scan were obtained by taking the first eigenvariate (akin to a

'weighted mean', Friston et al., 2006) across all voxels within each parcel of the Schaefer 400-region atlas (Schaefer et al., 2018). We then averaged ROIs across networks, which were defined by the 17-network Schaefer scheme (Yeo et al., 2011; Schaefer et al., 2018). Global measures of CT, GMV, and CSF were computed for each session by summing across all voxels within the respective output image. Our findings held when using an SST derived from all 26 MRIs (pre- through postpartum), as well as when estimating the mean (vs. weighted mean) of all voxels within each parcel. The ANTs CT pipeline is highly validated with good test-retest reproducibility and improved ability to predict variables such as age and gender from region-wise CT measurements compared to surface-based FreeSurfer (Tustison et al., 2014). However, to reproduce our findings across software packages, we also ran the T1w data through the longitudinal FreeSurfer cortical thickness pipeline (Dale et al., 1999), which corroborated our findings using both the Schaefer 400-cortical atlas (**Appendix B Table 1**, **Appendix Fig. 3**) and the popular Desikan-Killiany cortical atlas (Desikan et al., 2004, see **Appendix B Fig. 5**); lateral ventricle volume estimates were derived from this output. A complete reporting of findings can be found in the **Appendix B**.

Mean framewise displacement (FWD) estimates from gestation sessions with a 10-minute resting state scan (n = 17) were used to indirectly assess whether motion increased throughout pregnancy. Average FWD (millimeters) was extremely minimal across the entire experiment (*M* = 0.13, *SD* = 0.02, *range* = 0.09–0.17) and varied only slightly by pregnancy stage (pre: *M* = 0.11, *SD* = 0.004; first: *M* = 0.11, *SD* = 0.01; second: *M* = 0.14, *SD* = 0.02; third: *M* = 0.16, *SD* = 0.007; post: *M* =

0.13, *SD* = 0.01). While mean FWD did correspond with gestation week ($r = 0.90$, $p < .001$), controlling for this did not alter our main findings (e.g., total GMV and gestation, partial correlation: $r = -0.64$, $p = 0.004$) owing to the fact that motion differences between stages were minuscule (**Appendix B Fig. 6A**).

As a further test of the robustness of the dataset, I ran quality control (QC) assessments on all T1w images using the IQMs pipeline from *MRIQC* (Esteban et al., 2017). Assessments of interest included 1) coefficient of joint variation (CJV), 2) signal-to-noise ratio for gray matter (SNR), and 3) contrast-to-noise ratios (CNR). All QC metrics fell within expected standard ranges (**Appendix B Fig. 6B–D**). Although correlations existed between gestation week and QC measures (CJV, $r = 0.70$, $p < .001$; SNR and CNR, $r = -0.83$, $p < .001$), including these variables in the regression models did not alter our main findings. Gestation remained tied to decreases in GMV, especially within regions belonging to attention and somatosensory networks. When looking across all *MRIQC* outputs, discrepancies were noted in session seven (gestation week nine, first trimester). Removing this day from the analyses only strengthened observed relationships between cortical volume and gestation; however for completeness, data from this day is included in the main findings.

Hippocampal Segmentation

T1- and T2-weighted images (n = 25) were submitted to the automatic segmentation of hippocampal subfields package (ASHS) (Yushkevich et al., 2015) for bilateral parcellation of seven MTL subregions: CA1, CA2/3, dentate gyrus (DG), subiculum (SUB), perirhinal cortex (PRC), entorhinal cortex (ERC), and parahippocampal

cortex (PHC). The ASHS segmentation pipeline automatically segmented the hippocampus in the T2w MRI scans using a segmented population atlas, the Princeton Young Adult 3T ASHS Atlas template (n = 24, mean age 22.5 years; Aly and Turk-Browne, 2016). A rigid-body transformation aligned each T2w image to the respective T1w scan for each day. Using ANTs deformable registration, the T1w was registered to the population atlas. The resulting deformation fields were used to resample the data into the space of the left and right template MTL regions of interest (ROI). Within each template ROI, each of the T2w scans of the atlas package was registered to that day's T2w scan. The manual atlas segmentations were then mapped into the space of the T2w scan, with segmentation of the T2w scan computed using joint label fusion (Wang et al., 2012). Finally, the corrective learning classifiers contained in ASHS were applied to the consensus segmentation produced by joint label fusion. The output of this step is a corrected segmentation of the T2w scan. Further description of the ASHS protocol can be found in (Yushkevich et al., 2015). T2w scans and segmentations were first visually examined using ITK-SNAP (Yushkevich et al., 2006) for quality assurance and then subjected to manual editing in native space using ITK-SNAP (v.3.8.0-b; author CMT). One bilateral segmentation (Scan 15, third trimester) was discarded due to erroneous scan orientation. The anterior extent of the segmented labels was anchored 4 mm (2 slices) anterior to the appearance of the limen insulae, and the posterior extent was anchored to the disappearance of hippocampal gray matter from the trigone of the lateral ventricle. Boundaries between perirhinal, entorhinal, and parahippocampal cortices were established in keeping with the Olsen-Amaral-Palombo (OAP)

segmentation protocol (Palombo et al., 2013). In instances where automatic segmentation did not clearly correspond to the underlying neuroanatomy, such as when a certain label was missing several gray matter voxels, manual retouching allowed for individual voxels to be added or removed. All results are reported using the manually retouched subregion volumes to ensure the most faithful representation of the underlying neuroanatomy. Scans were randomized and segmentation was performed in a random order, blind to pregnancy stage. To assess intra-rater reliability for the present analyses, two days underwent manual editing a second time. The generalized Dice similarity coefficient (Crum et al., 2006) across subregions was 0.87 and the Intraclass Correlation Coefficient was 0.97, suggesting robust reliability in segmentation.

White Matter Microstructure

Diffusion scans were preprocessed using the automation software QSIprep version 0.15.3 (Cieslak et al., 2022) and run primarily with the default parameters, with the exceptions '–output resolution 1.8', '–dwi denoise window 5',–force-spatial-normalization', '–hmc model 3dSHORE', '–hmc-transform Rigid', and '–shoreline iters 2'. Twenty-one sessions were preprocessed and analyzed, with the remaining five scans excluded due to missing data or the corresponding field map for distortion correction. T1-weighted (T1w) images were corrected for intensity non-uniformity (*N4BiasFieldCorrection*) and skull-stripped (*antsBrainExtraction*). The images underwent spatial normalization and registration to the ICBM 152 Nonlinear Asymmetrical Template. Finally, brain tissue segmentation of CSF, GM, and WM

was performed on each brain-extracted T1w using FMRIB's Automated Segmentation Tool (FAST). Preprocessing of diffusion images began by implementing MP-PCA denoising with a 5-voxel window using MRtrix3's *dwidenoise* function. B1 field inhomogeneity was corrected using *dwibiascorrect* from MRtrix3 with the N4 algorithm. Motion was corrected using the *SHORELine* method. Susceptibility distortion correction was based on GRE field maps. Preprocessed Nifti scans were prepared for tractography using DSI Studio version Chen-2022-07-31 (Yeh et al., 2016). Diffusion images were converted to Source Code files using the DSI studio command line *'--action=src'* and a custom script to convert all images. The diffusion data were reconstructed in MNI space using q-space diffeomorphic reconstruction (Yeh et al., 2011) with a diffusion sampling of 1.25 and output resolution of 1.8mm isotropic. The following output metrics were specified to be included in the output FIB file: quantitative anisotropy (QA) and mean diffusivity (MD). The quality and integrity of reconstructed images were assessed using `*QC1: SRC Files Quality Control*`. First, consistency of image dimension, resolution, DWI count, shell count was checked for each image. Second, each image was assessed for the "neighboring DWI Correlation" which calculates the correlation coefficient of low-b DWI volumes that have similar gradient direction. Lower correlation values may indicate issues with the diffusion signal due to artifacts or head motion. Finally, DSI studio performed an outlier check, labelling images as a "low quality outlier" if the correlation coefficient was greater than 3 standard deviations from the absolute mean. None of our scans were flagged as outliers. The reconstructed subject files were aggregated into one connectometry database per metric.

Statistical Analysis

All statistical analyses were conducted in R (version 3.4.4). To isolate how brain structure changes during pregnancy, the following analyses included sessions from baseline through 36 weeks gestation unless otherwise stated.

Gray Matter Volume & Cortical Thickness

We first computed Pearson's product-moment correlation matrices between the following variables (n = 19 pregnancy scans): gestation week, estradiol, progesterone, total GMV, and the 17 network-level average GMV values. We then ran a multivariate regression analysis predicting ROI-level GMV changes by gestation week. To *identify* which regions were changing at a rate different from the global decrease, we then re-ran the analyses to include total GMV in the regression model. This was extended at the network level, where we ran partial correlations accounting for total GMV. These analyses were then run for cortical thickness. Percent change at the network level was computed by subtracting the final pregnancy value (36 weeks pregnant) from the first pre-pregnancy baseline, then dividing that difference by said first pre-pregnancy baseline value. All analyses underwent multiple comparisons testing (FDR-corrected at $q < 0.05$). Ventricle volume and CSF displayed non-linear patterns across the experiment; therefore, we used generalized additive models (GAM; cubic spline basis), a method of non-parametric regression analysis (R package: *mgcv*), to explore the relationship between ventricles, CSF, and gestation week. For each variable, the GAM model outperformed a linear model fit, as determined by a Chi-squared test. To note, for

this analysis, we included all 26 sessions to capture the sharp decline of these measures into postpartum.

Hippocampal Segmentation

To evaluate a linear relationship between time and medial temporal lobe (MTL) subregion volume change, we conducted Pearson's product-moment correlations between gestation week and individual bilateral MTL subregion volumes (average of left and right, n = 7 subfields; N = 17 MTL scans). We had no strong a priori hypothesis that structure–hormone relationships would differ by hemisphere; thus, volumes are reported averaged across hemispheres. As a control, we also computed relative MTL subregion volumes expressed as a percentage of total intracranial volume (sum of whole brain gray, white, and cerebrospinal fluid volumes) calculated by ASHS. This allowed us to correct for the changes in total intracranial volume, which was linearly correlated with gestation week (r = -.723, p < .0001). Relationships were considered significant only if they met FDR correction with q < 0.05. Finally, we conducted a linear regression to evaluate the relationship between endogenous sex hormones (estrogen and progesterone) and volumes of regions that changed significantly across pregnancy.

Diffusion - White Matter Microstructure

DSI Studio's correlational tractography (Yeh et al., 2016) was used to analyze the relationship between white matter structure and gestational week (n = 15). A truncated model was run to examine the relationship between white matter and sex

steroid hormones (n = 10) for the subset of diffusion scans with paired endocrine data. A non-parametric Spearman correlation was used to derive the correlation between gestational week and endocrine factors and our metrics of interest (QA and MD; see **Appendix B Tables 7–8**, **Appendix Fig. 4** for MD results) because the data were not normally distributed. Statistical inference was reached using connectometry, a permutation-based approach that tests the strength of coherent associations found between the local connectome and our variables of interest. It provides higher reliability and replicability by correcting for multiple comparisons. This technique provides a high-resolution characterization of local axonal orientation. The correlational tractography was run with the following parameters: T-score threshold of 2.5, 4 pruning iterations, and a length threshold of 25 voxel distance. To estimate the false discovery rate (FDR), a total of 4000 randomized permutations were applied to obtain the null distribution of the track length. Reported regions were selected based on FDR cutoff (FDR < 0.2, suggested by DSI Studio), and contained at least 10 tracts. For visualization of global QA at each gestational stage, QA values were extracted using DSI Studio's whole brain fiber tracking algorithm and tractometry (Yeh et al., 2016). Finally, we used generalized additive models (cubic spline basis) to explore the non-linearity of QA from pre- through postpartum (N = 21 scans; see GMV analysis).

C. Results

Endocrine Assessments

Serological evaluations captured canonical hormone fluctuations characteristic of the prenatal, perinatal, and postnatal periods (**Fig. 4.1A–C**). Serum hormone concentrations increased significantly over the course of pregnancy and dropped precipitously postpartum (pre-conception: estradiol (E) = 3.42 pg/mL, progesterone (P) = 0.84 ng/mL; 3 weeks prior to parturition: E = 12,400 pg/mL, P = 103 ng/mL; 3 months after parturition: E = 11.50 pg/mL, P = 0.04 ng/mL).

Cortical Volume & Thickness

To begin, we quantified the neuroanatomical changes that unfold during gestation itself (baseline–36 weeks pregnant; 19 scans). Changes in GMV were near-ubiquitous across the cortical mantle (**Fig. 4.1D**), with strong negative associations between gestational week and total GMV (r = -0.90, p < .001, *total change* = -3.5%). Most large-scale brain networks exhibited decreases in GMV (**Fig. 4.1E, Appendix B Table 1**); indeed, 80% of the 400 regions of interest (ROIs) demonstrated negative relationships with GMV throughout gestation (**Fig. 4.1D**, **Appendix B Table 2**). Together, these results provide evidence of a global decrease in cortical volume across pregnancy. A handful of sensory and attention subnetworks were particularly sensitive to gestation, such as the Control (B), Salience/Ventral Attention (A), Dorsal Attention (B), Default (A), and Somatomotor (A,B) Networks; each significantly covarying with gestation week even after accounting for total GMV change. Regions driving these network-level changes

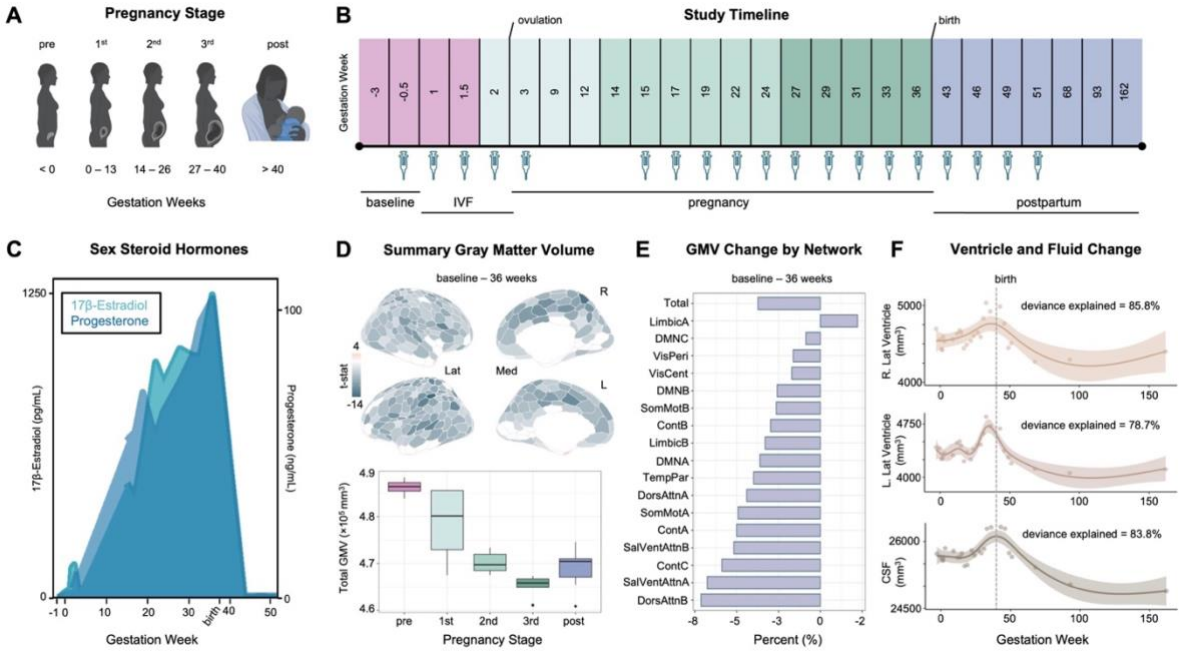

Figure 4.1. Precision imaging reveals neuroanatomical changes throughout gestation. **A)** Standard medical demarcations for pregnancy stages (e.g., trimesters) by gestation week. **B)** A healthy 38-year-old primiparous woman underwent 26 scanning sessions from 3 weeks preconception through two years postpartum. Scans were distributed throughout preconception (4 scans), first trimester (4 scans), second trimester (6 scans), third trimester (5 scans), and postpartum (7 scans); colors indicate pregnancy stage. The participant underwent in-vitro fertilization (IVF) to achieve pregnancy, allowing for precise mapping of ovulation, conception, and gestation week. Serological assessments to evaluate steroid hormones were available for 19 sessions (see *Methods*). **C)** Sex steroid hormones increased significantly over the course of pregnancy and dropped precipitously postpartum, as is characteristic of the pre- and postnatal periods. **D)** Multivariate regression analyses reveal largely negative relationships between gestation week and regional GMV (top), with only a minority of regions unaffected or increasing over the gestational window. All associations presented here were corrected for multiple comparisons (FDR at $q < 0.05$). Summarizing GMV across the entire study (baseline – 162 weeks) suggests slight recovery in the postpartum period (bottom). **E)** Average network change was calculated by estimating GMV change from baseline – 36 weeks gestation. Attention and Control Networks appeared most affected. **F)** Left and right lateral ventricle and cerebrospinal fluid volumes displayed non-linear increases across gestation, with a notable rise in the second and third trimester before dropping sharply postpartum. Shaded regions represent a 95% confidence interval; dashed line indicates parturition. *Abbreviations*: IVF = in-vitro fertilization; Lat = lateral; Med = medial; t-stat = test statistic; GMV = gray matter volume; DMN = Default Mode Networks; VisPeri = Visual Peripheral Network; SomMot = Somatomotor Networks; VisCent = Visual Central Network; Cont = Control Networks; TempPar = Temporal Parietal Network; DorsAttn = Dorsal Attention Networks; SalVentAttn = Salience / Ventral Attention Networks; CSF = cerebrospinal fluid

include the inferior parietal lobe, post central gyri, insulae, prefrontal cortex, posterior cingulate, and somatosensory cortex (**Fig. 4.2**, **Appendix B Table 2**). These regions and associated brain networks appear to decrease in volume at a faster rate than

the rest of the brain throughout pregnancy. GMV reductions were also significantly correlated with the participant's sex hormone concentrations. (**Appendix B Table 1**). A highly similar pattern of results was observed when examining pregnancy-related cortical thickness changes (**Appendix B Fig. 1** and **Tables 3–4**). In contrast, GMV within regions of the Default Mode (C), Limbic (A,B), and Visual Peripheral Networks buck the global trend by slightly increasing (e.g., temporal poles), remaining constant (e.g., orbitofrontal cortex), or reducing at a much slower rate (e.g., extrastriate) than total GMV (**Fig. 4.1E, Appendix B Table 1–4**). Cortical thickness changes in these regions exhibit similar patterns (**Appendix B Table 3–4**).

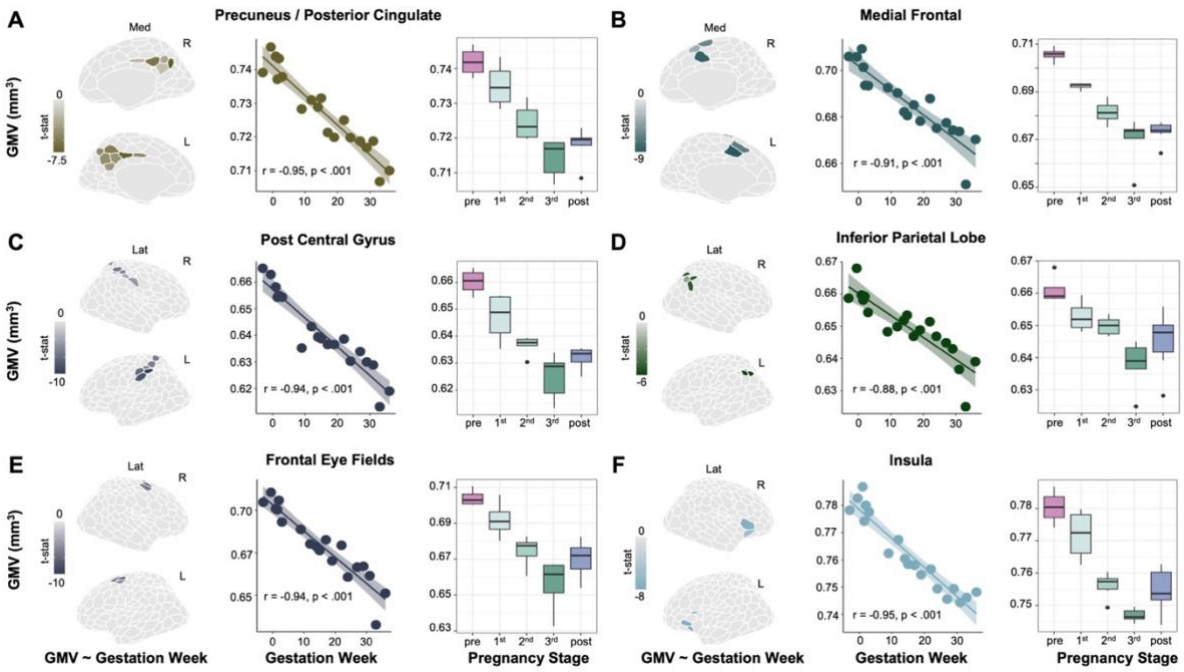

Subcortical Volume

Consistent with the broader cortical reductions in GMV, high-resolution medial temporal lobe segmentations revealed decreased parahippocampal cortex (PHC) volume (r = -0.79, FDR-corrected at $q < 0.05$) across gestation (**Fig. 4.3B**). Results remained significant after proportional volume correction for total GMV. Notably, there was no significant change in other hippocampal and medial temporal cortical subregions, or in gross hippocampal volume (**Appendix B Fig. 3** and **Table 6**).

White matter microstructure

In contrast to decreasing global GMV, correlational tractography of white matter—which tests for linear trends in the data— revealed increasing microstructural integrity (quantitative anisotropy, QA) across the whole brain during gestation, concomitant with the rise in 17ß-estradiol and progesterone (*FDRs* < .001) (**Fig. 4.3C, Appendix B Fig. 4**). Tracts displaying robust correlations with gestational week include the cingulum bundle, middle and superior longitudinal fasciculus, corpus callosum, and arcuate fasciculus (**Fig. 4.3D**, see **Appendix B Table 6** for complete list). Next, we widened the aperture to capture changes extending into the postpartum period (baseline–2 years postpartum; 26 scans),

Figure 4.2. Pronounced GMV changes across gestation. A–F) Six representative regions that decline in volume at a rate greater than the global decrease. For each panel, we display results of a multivariate regression revealing significant associations between clustered ROI GMV and gestation week (left), Pearson's product-moment correlations between the average GMV of the ROIs and gestation week (middle), and summary ROI GMV by pregnancy stage across the whole study (right). All statistical tests were corrected for multiple comparisons (FDR at $q < 0.05$). ROI subregions are color-coded by network affiliation (see **Appendix B Fig. 2**). N.b., shown here are raw data values (see **Appendix B** for more).

revealing non-linear patterns for several brain measures. Global QA for white matter increased throughout the first and second trimester before returning to baseline levels in the postpartum period (*whole brain QA, F* = 6.791*, p* < .002*, deviance explained* = 71.9%) (**Fig. 4.3E**). Similarly, we observed non-linear patterns of lateral ventricle expansion *(left, F* = 7.70*, p* < .001*, deviance explained* = 78.7%; *right, F* = 11.99*, p* < .001*, deviance explained* = 85.8%) and increased cerebrospinal fluid (CSF; *F* = 13.32*, p* < .001*, deviance explained* = 83.8%), rising in the second and

third trimester before dropping sharply in postpartum (**Fig. 4.1F**). After linearly decreasing during gestation, GMV and CT appear to partially rebound postpartum.

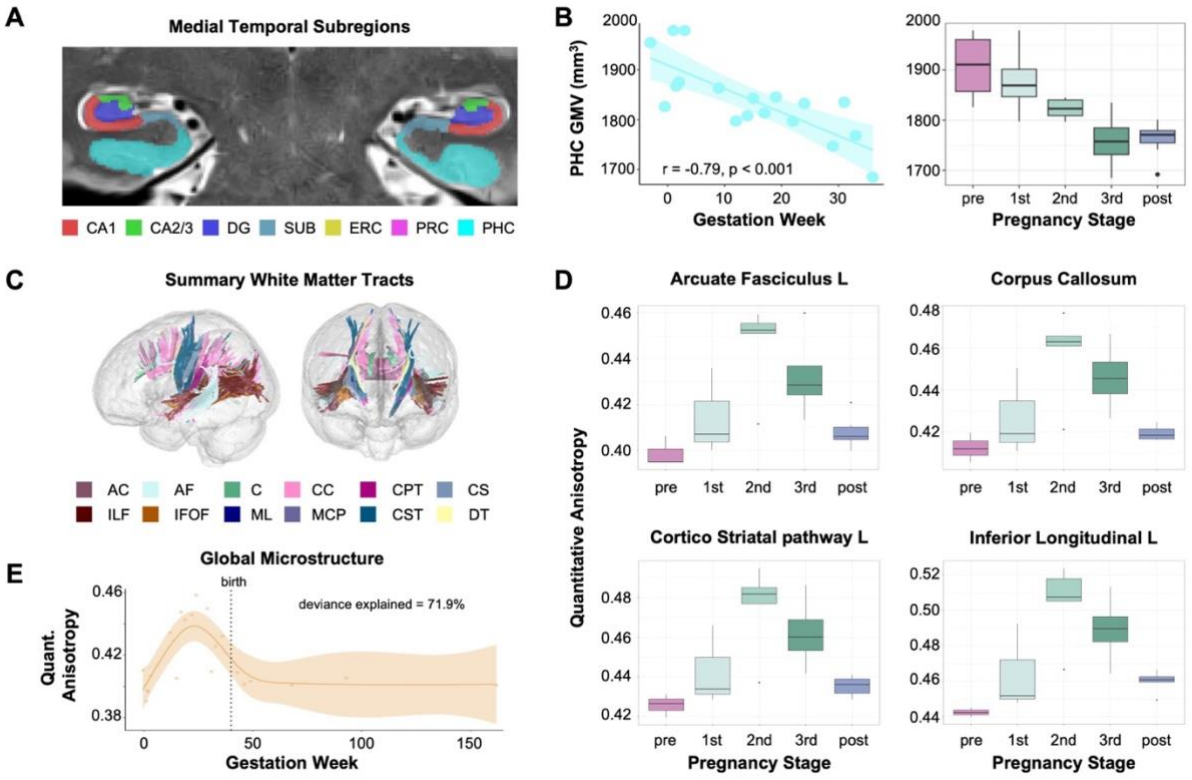

Figure 4.3. Hippocampal subfields and white matter microstructure across gestation. A) Sample image of medial temporal lobe segmentation determined via manual editing of the output of the Automatic Segmentation of Hippocampal Subfields (ASHS) software package. The participant's hippocampus and surrounding cortex were segmented into seven bilateral subregions. **B)** Parahippocampal cortex (PHC) volume was negatively associated with gestation week (left) and did not return to baseline postpartum (right). **C)** White matter tracts demonstrate increasing quantitative anisotropy in relation to gestation week as determined by correlational tractography analysis. **D)** Summary of quantitative anisotropy (QA) values by pregnancy stage for representative ROIs identified as significantly associated with gestation week. Tractometry was used to extract quantitative anisotropy values. **E)** Whole brain QA displayed non-linear patterns of growth across gestation. Shaded region represents the 95% confidence interval. Abbreviations: AC= Anterior Commissure; PHC = parahippocampal cortex; GMV = gray matter volume; AF = arcuate fasciculus; CC = corpus callosum; ILF = inferior longitudinal fasciculus; CS = corticostriatal tracts; CST = corticospinal tracts; CPT = Corticopontine tracts; IFOF = inferior frontal occipital fasciculus; ML = medial lemniscus; MCP = middle cerebellar peduncle; DT = dentothalamic tract; QA = quantitative anisotropy

D. Discussion

Emerging findings across taxa establish pregnancy as a remarkable period of synaptic plasticity, underscoring the brain's ability to undergo neuroanatomical changes beyond adolescence (Dulac et al., 2014; Carmona et al., 2019; Hoekzema et al., 2017, 2022; Martínez-García, et al., 2021a; Pawluski et al., 2022). Investigations that compare women pre- and postpartum provide the strongest evidence to date that the human brain undergoes such neural changes (Martínez-García 2021b, Orchard et al., 2023), and our results are largely consistent with the findings from those designs. But what about pregnancy itself? Over what time-course do anatomical changes in the maternal brain manifest? Are they tied to the substantial increase in sex hormone production? Here, we begin to address these outstanding questions. This paper and corresponding open-access dataset offer neuroscientists the first atlas of the human brain across gestation.

Our findings suggest that the gestational period is characterized by sweeping decreases in gray matter volume, cortical thinning, and enhanced white matter microstructural integrity that unfold week by week. Some of these changes persist at two years postpartum (e.g., global reductions in GMV, CT), while others, including markers of white matter integrity, appear to be transient. Ventricle expansion and contraction parallel these cortical changes. These patterns, paired with increased CSF volume, could reflect increased water retention and subsequent compression of cortical tissue. However, regional variation in GMV, CT, and QA changes hint at cellular underpinnings, such as alterations in glia or neuron number, synaptic

density, and myelination. Future studies of the relationship between fluid dynamics and volumetric changes will help clarify the factors that drive global neural changes during pregnancy; such insights have broad implications for maternal health (e.g., neurological effects tied to pre-eclampsia or edema).

Dynamic neural changes occurred *within* the pregnancy window itself, a nuance not captured by studies limited to pre- versus post-pregnancy comparisons. For example, we observed large increases in white matter microstructural integrity (QA) throughout the first and second trimester of pregnancy, but these measures fully returned to baseline values by the first postpartum scan. This pattern may explain why previous studies report no pregnancy-related differences in white matter tractography (Hoekzema, 2022). Other measures, such as GMV and CT, decreased throughout gestation and displayed only a modest rebound postpartum. Together, these non-linear patterns suggest that only quantifying pre- and postpartum brain structure may overlook the full dynamic range of changes that unfold within the gestational window — and underrepresent the brain's metamorphosis during pregnancy. Further, although global brain changes were the norm, some regions displayed notable stability (e.g., the majority of medial temporal lobe and extrastriate cortex), which merits further study. Similar precision imaging studies have captured dynamic brain reorganization across other neuroendocrine transitions, such as the menstrual cycle (see review: Pritschet et al., 2021), underscoring the powerful role sex steroid hormones play in shaping the mammalian brain (Taxier et al., 2020). Endocrine changes across pregnancy dwarf those that occur across the menstrual

cycle, which highlights the critical need to map the brain's response to this unique hormonal milieu.

The neuroanatomical changes that unfold during matrescence have broad implications for understanding individual differences in parental behavior (Dulac et al., 2014; Hoekzema et al., 2017; Kohl et al., 2018), vulnerability to mental health disorders (Pawluski et al., 2017; Barba-Müller et al., 2019) and patterns of brain aging (de Lange et al., 2019; Barth & de Lange, 2020; Orchard et al., 2020, 2023). Decreases in GMV may reflect "fine-tuning" of the brain by neuromodulatory hormones in preparation for parenthood (Pawluski et al., 2022). For example, GMV reduction is pronounced in areas of the brain important for social cognition and the magnitude of these changes correspond with increased parental attachment behaviors (Hoekzema et al., 2017). Similarly, we observed the greatest GMV change in regions within attention, sensory, and default mode networks (see also: Paternina-Die et al., 2023). Quantifying the rate of change within these circuits could be key for understanding the behavioral adaptions that emerge during and after pregnancy, such as honing the brain's visual and auditory responses to infant cues and elicitation of maternal behavior.

This precision imaging study mapped neuroanatomical changes across pregnancy in a single individual. These findings provide critical rationale for conducting further dense-sampling studies of demographically enriched cohorts to determine the universality and idiosyncrasy of these adaptations and their role in maternal health. For example, this approach could determine whether the pace of pregnancy-induced neuroanatomical changes drives divergent brain health

outcomes in women, as may be the case during other rapid periods of brain development (Tooley et al. 2021). One in five women experiences postpartum depression (Wang et al., 2021), and while the first FDA-approved treatment is now available (Deligiannidis et al., 2023), early detection remains elusive. Precision imaging studies could offer clues about an individual's risk for or resilience to postpartum depression prior to symptom onset. Neuroscientists and clinicians also lack tools to facilitate detection and treatment of neurological disorders that co-occur, worsen, or remit with pregnancy, such as epilepsy, headaches, multiple sclerosis, and intracranial hypertension (Shehata et al., 2004). This new area of study—precision mapping of the maternal brain—lays the groundwork for a greater understanding of the subtle and sweeping structural, functional, behavioral, and clinical changes that unfold across gestation. Such pursuits will advance our basic understanding of the human brain and its remarkable ability to undergo protracted plasticity in adulthood.

5

The impact of endocrine aging on large-scale functional brain networks in healthy, midlife women

A. Introduction

A major challenge in neuroscience is to understand what happens to the brain as it ages. As such, over the last quarter century, a staggering number of human brain imaging studies have probed the neural basis of age-related cognitive decline. These studies generally enroll adults over the age of 65, a historical precedent rooted in the average retirement age of U.S. wage-earners (Jacobs and Goldstein, 2018). A consequence of this research tradition is that it overlooks one of the most significant neuroendocrine changes in a woman's life — the transition to menopause — a time in which many women report changes in memory and attention (e.g., "menopause fog"; Greendale et al., 2011).

Reproductive (i.e., endocrine) aging, defined as the change in sex hormone production that occurs with age, is a major contributor to the physiological changes that take place during middle age in both men and women. For men, age-related changes in sex hormone production occurs at a gradual linear rate, with a protracted decline beginning in the mid-30s and continuing throughout life (Fabbri et al., 2016).

In contrast, women undergo a more complex hormonal transition at midlife, one that is marked by high fluctuations in steroid hormone production during the perimenopausal phase and culminating in ovarian senescence at the end of menopause—median age of complete reproductive senescence being 52.4 years (Gold et al., 2001; Harlow et al., 2012). The menopausal transition results in a substantial decline in sex steroid hormone production— up to 90% for both estradiol and progesterone—a dramatic endocrine change that impacts multiple biological systems including the nervous system (Morrison et al., 2006; Brinton et al., 2015).

Sex hormones are critical neuromodulators, influencing the brain at all levels, from microscopic intracellular and synaptic events (Taxier et al., 2020) to macroscopic structural (Zsido et al., 2019) and functional connectivity (Pritschet et al., 2021). Two regions critical for higher-order cognition, the prefrontal cortex (PFC) and medial temporal lobes (MTL), contain abundant populations of sex hormone receptors and are major sites of sex hormone action. In nonhuman primates, estrogen receptor-α (ERα) is present in ~50% of PFC pyramidal neurons, and greater ERα expression is associated with better working memory performance (Wang et al., 2010). The *suppression* of sex hormones via surgical menopause decreases spine density in PFC neurons (Hao et al., 2006) and impairs working memory (Rapp et al., 2003). In rodent hippocampal CA1 neurons, surgical menopause leads to a 30% loss in dendritic spine density, which is reversed following estradiol replacement (Dumitriu et al., 2010). Similarly, in nonhuman primates surgical menopause reduces hippocampal spine density and impairs recognition memory (Hara et al., 2012) and in humans, early surgical menopause is

tied to thinner entorhinal cortex volume compared to age-matched controls (Zeydan et al., 2019). A handful of human studies have directly examined the effect of hormone replacement therapy (HRT) on brain morphology in menopausal women, revealing that hippocampal volume increases in response to certain HRT regimens (Albert et al., 2017).

These macrostructural changes evident in the hippocampus in response to hormone supplementation may produce cognitive benefits (for a review, see Daniel et al., 2015). For example, Maki et al., (2011) found that women who began HRT in perimenopause had enhanced hippocampal activity during a verbal recognition task and better verbal memory performance relative to nonusers. When initiated early in the menopausal transition, hormone replacement also appears to enhance cognitive-control related dorsolateral PFC activity and improve task-switching performance in women (Girard et al., 2017). Thus, converging evidence strongly suggests that ovarian hormone depletion leads to morphological and functional changes in memory and attention circuitry.

Growing evidence from animal studies indicates that estradiol and progesterone play neuroprotective roles in the brain and support the structure and function of brain regions vulnerable to neurodegeneration (Mosconi et al., 2018; Beltz and Moser, 2020). In the context of cognitive aging, female reproductive aging

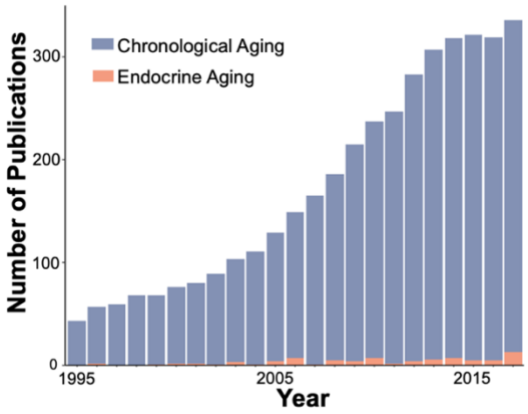

Figure 5.1. The number of brain imaging publications considering the effects of endocrine aging (orange) is dwarfed by the number of chronological aging studies (blue). Figure adapted from Taylor et al., 2019.

represents a critical yet highly understudied factor (**Fig. 5.1**) that is likely essential for understanding sex-specific trajectories of cognitive decline and sex differences in dementia risk (Rahman et al., 2020; Taylor et al., 2019). A striking feature of ER–rich regions is that they overlap with neural circuits vulnerable to age-related decline and encompass regions (e.g., entorhinal and perirhinal cortex, PFC, posterior cingulate cortex) that harbor accumulating neuropathology in the progression to AD (Brinton et al., 2015). Further, ~70% of women experience hot flashes and night sweats along with other neurological symptoms (e.g., mood disruption, insomnia, cognitive complaints) during menopause (Brinton et al., 2015), and the frequency of these symptoms paired with declining in sex hormones is hypothesized to increase the risk of Alzheimer's disease (AD) (Rahman et al., 2020). However, to date, we lack a clear understanding of how sex hormones regulate the functional and structural architecture of higher-order cognitive and AD-sensitive circuits in the human brain.

Our current understanding of how female endocrine aging impacts the brain stems from studies identifying fairly coarse regional differences in brain activity or morphology as a function of women's menopausal status (Jacobs and Goldstein, 2018). The degree to which menopause relates to neurophysiological changes in brain connectivity represents a significant knowledge gap that has yet to be adequately examined. Here, I combined techniques from network neuroscience and neuroendocrinology to determine how aspects of endocrine aging (i.e., menopause stage and symptoms) alter the topology of intrinsic functional brain networks. Based on our team's previous work (see Studies 1 and 2), I predicted that ovarian decline

will preferentially and negatively impact the functional topology of the Default Mode (DMN), Frontal Control (FCN), and Dorsal Attention Networks (DAN).

B. Methods

Participants

We recruited 99 midlife women (ages 43–60) from the greater Santa Barbara community to participate in the 'Midlife Hormones and Cognition Study'. Exclusionary criteria included no history of hormone-replacement therapy, no current use of hormonal contraceptives, no MRI contraindications, and no major medical disorders. After quality control assessments, 14 women were excluded due to 1) incomplete or low-quality data, 2) confounding medication intake on the day of testing (e.g., prednisone), or 3) exceedingly high levels of estradiol (>300 pg/mL), likely due to the testing day not falling within the early-to-mid follicular phase of the participant's cycle. The latter exclusion did not significantly impact the results. The final subject population (N=85) was enriched to include women at distinct stages of reproductive aging: premenopausal (N=32), perimenopausal (N=28), and postmenopausal (N=25) women. While the analyses here focus on endocrine aging in women, the larger parent study also included age-matched male subjects (N=38).

No group-level differences were observed in body mass index (BMI), years of education, or verbal intelligence (American National Adult Reading Test; Grober et al., 1991). As expected, there were significant chronological age differences by group ($F(2, 82)$ = 52.33, p < .001), with advancing endocrine age related to older chronological age (p < .05) (**Table 5.1**).

Study Procedure

Subjects completed one 4-hour test session at the University of California, Santa Barbara (UCSB) (**Fig. 5.2A**). Women who were still menstruating were tested in the early follicular phase (day 2–5) of their menstrual cycle, pursuant to subject report. Each subject underwent a time-locked 2-hour MRI scanning session consisting of structural and functional sequences, followed by a blood draw to assess hypothalamic–pituitary–gonadal axis (HPG) hormones. Endocrine samples were collected, at minimum, after two hours of no food or drink consumption (excluding water) and standard caffeine intake was requested on the experiment day. A detailed medical history was acquired to assess diagnoses of chronic diseases, medications, lifetime and current substance use, and reproductive history (e.g., age at menarche, history and duration of hormonal birth control use, parity, fertility treatments, breastfeeding, reproductive surgeries).

Additional assessments were collected on the day of testing, including mood and health/lifestyle factors that might impact or mediate the effect of endocrine aging on the brain and subsequent cognitive performance, such as perceived stress (Cohen et al., 1983), sleep quality (Buysse et al., 1989), and vasomotor symptoms. A composite 'symptom score' was computed by summing participants' self-reported frequency of menopause-related symptoms over the last 14 days, including vaginal dryness, irritability, hot flashes, and night sweats. The composite symptom frequency did not significant differ by group (**Fig. 5.2F, Table 5.1**). Pearson's product-moment correlation matrices were computed between sex hormones (estradiol, progesterone, FSH), menopausal symptoms (night sweats, hot flashes,

irritability, vaginal dryness), and state-dependent measures (perceived stress, sleep quality). Vasomotor symptoms, in particular, were significantly associated with HPG-axis hormones: FSH was positively correlated with night sweats (r = 0.28, p = .03) and hot flashes (r = 0.39, p < .001), while estradiol demonstrated a negative relationship with frequency of hot flashes (r = -0.31, p = .01). As expected, individual menopausal symptoms were correlated to each other (p < .05) (**Fig. 5.2B**).

Endocrine Assessments

A licensed phlebotomist inserted a saline-lock intravenous line into the dominant or non-dominant hand or forearm to evaluate hypothalamic-pituitary-gonadal axis hormones, including serum levels of gonadal hormones (17β-estradiol, progesterone and testosterone) and the pituitary gonadotropins luteinizing hormone (LH) and follicle stimulating hormone (FSH). One 10cc mL blood sample was collected in a vacutainer SST (BD Diagnostic Systems) from each participant. The sample clotted at room temperature for 45 min until centrifugation (2000 × g for 10 minutes) and were then aliquoted into three 1 ml microtubes. Serum samples were stored at -20°C until assayed.

Serum concentrations were determined via liquid chromatography-mass spectrometry (for all steroid hormones) and immunoassay (for all gonadotropins) at the Brigham and Women's Hospital Research Assay Core. Assay sensitivities, dynamic range, and intra-assay coefficients of variation were as follows, respectively: estradiol, 1 pg/mL, 1-500 pg/mL, < 5% relative standard deviation (RSD); progesterone, 0.05 ng/mL, 0.05-10 ng/mL, 9.33% RSD; FSH and LH levels

were determined via chemiluminescent assay (Beckman Coulter). The assay sensitivity, dynamic range, and the intra-assay coefficient of variation were as follows: FSH, 0.2 mIU/mL, 0.2-200 mIU/mL, 3.1-4.3%; LH, 0.2 mIU/mL, 0.2-250 mIU/mL, 4.3-6.4%.

Menopausal Staging

The timing of the menopausal transition, between the first clinical appearance of decreased ovarian function (i.e. shorter inter-menstrual time periods) to menstrual irregularity and final amenorrhea, is variable. Midlife women were sampled at various states of ovarian decline (**Fig. 5.2C–E**): some women were in menopause with permanent amenorrhea, low estradiol levels and elevated gonadotropins; some exhibit signs of follicular failure (elevated FSH and oligo-amenorrhea); and some show normal cycling patterns. Reproductive histories and hormonal evaluations determined women's reproductive stage categorization, following the Stages of Reproductive Aging Workshop-10 criteria (Harlow et al., 2012). Principal staging criteria were based on menstrual cycle characteristics, with supportive criteria provided by FSH levels. Women fell within the late reproductive stage ('premenopause'), menopausal transition ('perimenopause'), or early postmenopause ('postmenopause').

MRI

Each participant completed an MRI scan on a Siemens 3T Prisma scanner equipped with a 64-channel phased-array head coil at the UCSB Brain Imaging Center. High-

resolution anatomical scans are acquired using a T1-weighted magnetization prepared rapid gradient echo (MPRAGE) sequence with 0.8mm^3 thickness, followed by a gradient echo fieldmap (TR = 785 ms, TE1 = 4.92ms, TE2 = 7.38ms, flip angle = 60°). Participants completed an 8-min resting-state fMRI scan using a T2*-weighted echo-planar imaging (EPI) sequence sensitive to the blood oxygenation level-dependent (BOLD) contrast (72 oblique slices, TR = 2000ms, TE = 37ms, voxel size = 2 mm^3, flip angle = 52°). Note that physiological recordings were not collected during scanning.

fMRI preprocessing

Initial preprocessing was performed using the Statistical Parametric Mapping 12 software (SPM12, Wellcome Trust Centre for Neuroimaging, London) in Matlab. Functional data were realigned and unwarped to correct for head motion and geometric deformations due to motion and magnetic field inhomogeneities. Registration and normalization were performed using Advanced Normalization Tools (version 2.3.5) (Tustison et al., 2014). The mean motion-corrected image was first registered to the high-resolution anatomical scan, then all functional images were registered to the mean motion-corrected image. All images were normalized to standard MNI space for between-subject comparison. A 4 mm full-width at half-maximum (FWHM) isotropic Gaussian kernel was subsequently applied to smooth the functional data. Further preparation for resting-state functional connectivity was implemented using in-house Matlab scripts. Global signal scaling (median = 1,000) was applied to account for fluctuations in signal intensity across space and time, and

voxelwise timeseries were linearly detrended. Residual BOLD signal from each voxel was extracted after removing the effects of head motion and five physiological noise components (CSF + white matter signal). Motion was modeled based on the Friston-24 approach, using a Volterra expansion of translational/rotational motion parameters, accounting for autoregressive and nonlinear effects of head motion on the BOLD signal (Friston et al., 1996). Our use of coherence allows for the estimation of frequency-specific covariances in spectral components below the range contaminated by physiological noise.

Functional connectivity estimation

Functional network nodes were defined based on a 400-region cortical parcellation (Schaefer et al., 2018) (**Fig. 5.3A**). To note, subcortical connectivity was not assessed here. For each participant, a summary timecourse was extracted per node by taking the first eigenvariate across functional volumes (Friston et al., 2006). These regional timeseries were then decomposed into several frequency bands using a maximal overlap discrete wavelet transform. Low-frequency fluctuations in wavelets 3-6 (~0.01-0.17 Hz) were selected for subsequent connectivity analyses (Patel & Bullmore, 2016). We estimated the *spectral* association between regional timeseries using magnitude-squared coherence: this yielded a 400 × 400 functional association matrix for each subject (**Fig. 5.3B**), whose elements indicated the strength of functional connectivity between all pairs of nodes (FDR-thresholded at $q < .05$). Coherence offers several advantages over alternative methods for assessing connectivity: 1) estimation of *frequency-specific* covariances, 2) *simple*

interpretability (values are normalized to the [0,1] interval), and 3) *robustness to temporal variability in hemodynamics* between brain regions, which can otherwise introduce time-lag confounds to connectivity estimates via Pearson correlation.

With respect to brain states, we modeled factors related to macroscale network topologies. Specifically, we computed measures of *within-network* integration (global efficiency, quantifying the ostensible ease of information transfer across nodes inside a given network) and *between-network* integration (the participation coefficient; i.e. the average extent to which network nodes are communicating with other networks over time). These were derived using the relevant functions for weighted graphs in the Brain Connectivity toolbox (Rubinov & Sporns, 2010). For global efficiencies, the 400 x 400 matrices were subdivided into smaller network-specific matrices as defined by our parcellation, yielding estimates of integration *only* among within-network nodes. Estimation of participation coefficients took the full (400 x 400) FDR-thresholded coherence matrices along with a vector of network IDs, quantifying the extent to which each node was connected to other nodes outside of its own network; summary, mean participation coefficients were then obtained for each network across its constituent nodes.

Statistical analysis

The following statistical analyses were conducted in R (version 3.4.4).

One-way Analysis of Variance (ANOVA) models were used to examine mean differences in sex hormones and network metrics between pre, peri, and postmenopausal groups. Multivariate regression analysis was used to predict

network topologies (global efficiency, network participation) by 1) sex hormones, 2) menopause status, symptomology, and the interaction between the two independent variables, and 3) chronological age, menopause status, and the interaction between the two independent variables. Lastly, we computed Pearson's product-moment correlations to examine linear relationships between endocrine factors (e.g., symptoms, hormones), chronological age, and network metrics (e.g., global efficiencies and network participation)

Dummy coding for menopause status (treated as discrete variable) in regression analyses was done automatically in R, with pre-menopausal women serving as the reference group. All significant associations reported below survived multiple comparisons correction (FDR-correction, $q < .05$).

C. Results

Endocrine Assessments

Analysis of sex steroid hormone and gonadotropin concentrations confirmed the expected hormonal profiles across the menopausal transition (**Table 5.1, Fig. 2C-E**). Significant group differences were observed for estradiol, $F(2, 82) = 13.67$, $p < .001$, with significantly lower concentrations in the postmenopausal group compared to premenopausal ($p < .001$) and perimenopausal ($p < .001$) women. A similar pattern was observed for progesterone, $F(2,82) = 5.64$, $p = .005$, with significantly lower concentrations in postmenopausal versus premenopausal women ($p = .005$). The

opposite pattern was observed for FSH, $F(2,82) = 60.06$, $p < .001$, which increased as a function of advancing menopause status (post > peri > pre, $p < .05$).

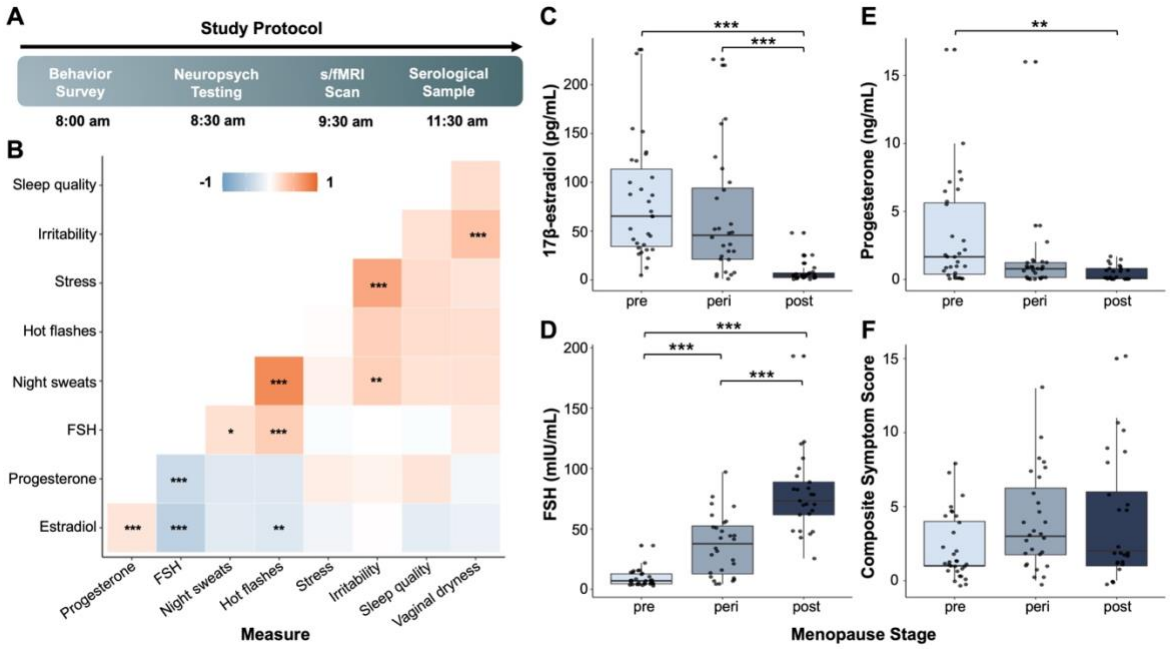

Figure 5.2. Midlife women at various states of ovarian decline were recruited to participate in our study. **A)** Subjects completed one 4-hour test session, involving a 2-hour MRI session followed by a blood draw to assess ovarian hormone concentrations. **B)** A correlation matrix was computed to assess relationships between sex hormones, state-dependent measures, and menopausal symptoms. Cooler colors indicate negative correlations, warm colors indicate positive correlations. **C-E**) Average sex hormone concentrations differ by menopause stage, with decreasing ovarian hormones and increasing gonadotropins as a function of advancing endocrine age **F)** Composite symptom scores were computed by tallying the frequency of common vasomotor and neurological symptoms (e.g., night sweats, hot flashes, irritability, and vaginal dryness) over the last two weeks. Displayed here by menopause stage. Error bars indicate ± SEM. Asterisks indicate significant correlations after FDR-corrected at q < 0.05, p ≤ 0.05, **p ≤ 0.01, ***p ≤ 0.001. *Abbreviations:* FSH, Follicle Stimulating Hormone.

Table 5.1. Breakdown of participant characteristics and sex hormones by menopause stage

Measure	Pre mean (SD)	Peri mean (SD)	Post mean (SD)	*F value*
N	32	28	25	--
Age	47.2 (2.3)	51.0 (2.1)	53.9 (2.9)	52.33***
Education (Years)	16.8 (1.8)	16.6 (2.0)	16.9 (2.2)	0.10
Verbal IQ	126.0 (5.8)	126.0 (5.1)	125.0 (7.3)	0.31
Body Mass Index	25.6 (4.4)	24.7 (3.6)	25.9 (5.8)	0.52
% Caucasian	87	100	84	--
Estradiol (pg/mL)	80.0 (58.6)	64.9 (63.8)	8.2 (10.7)	14.40***
Progesterone (ng/mL)	3.1 (3.9)	1.4 (3.0)	0.5 (0.5)	5.77**
FSH (mIU/mL)	9.1 (6.9)	36.7 (25.2)	78.6 (33.8)	59.02***
Menopausal symptoms	2.2 (2.3)	4.0 (3.3)	4.0 (4.1)	2.91

*p ≤ 0.05, **p ≤ 0.01, ***p ≤ 0.001

Functional network topologies, sex hormones, and menopause status

We first sought to examine the relationship between network connectivity and sex hormones across all 85 participants via linear regression. Weak negative relationships were observed between estradiol and Limbic Network B global efficiency (R^2 = .08, $F(1,83)$ = 7.29, p = .008) and network participation (R^2 = .06, $F(1,83)$ = 5.52, p = .02). Similar negative relationships were observed between estradiol and network participation among Control Networks B (R^2 = .06, $F(1,83)$ = 5.11, p = .03) and C (R^2 = .06, $F(1,83)$ = 5.29, p = .02). No other relationships with hormones were observed.

The sensitivity of Limbic Network B was extended when examining topology by menopausal stage (R^2 = .18, $F(2,82)$ = 5.29, p < .001). Here, postmenopausal women demonstrated *slightly* higher global efficiency compared to pre and perimenopausal groups. Taking these results together, estradiol may be an important driver of these group-level differences given the inherently lower estradiol concentrations among postmenopausal women. However, it is important to note that regions belonging to the Limbic B network all fall within orbitofrontal cortex, an area of the brain sensitive to extraneous noise (e.g., signal dropout, distortion from magnetic field inhomogeneities due to proximity of sinuses; Cordes et al., 2000). As such, these results must be interpreted with caution. No other group differences were observed (**Fig. 5.3A-C, Appendix C**).

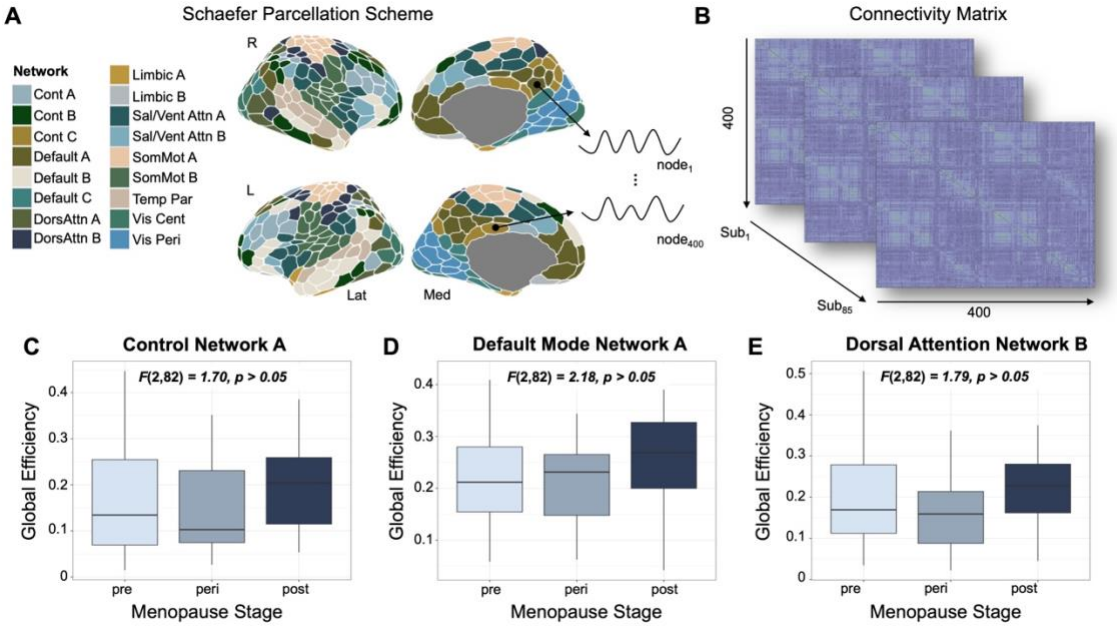

Figure 5.3. In this study, we determined how aspects of endocrine aging alter the topology of intrinsic functional brain networks. **A)** Functional network nodes were defined based on the Schaefer 400-region cortical parcellation and averaged across networks defined by the 17-network Yeo/Schaefer scheme (Yeo et al., 2011, Schaefer et al., 2018). **B)** A summary timecourse was extracted per node, yielding a 400 × 400 coherence matrix between all nodes for each subjects. **C-E)** No differences in global efficiency within the predicted association networks were observed between the three menopausal groups. Error bars indicate ± SEM. *Abbreviations:* DMN = Default Mode Networks; VisPeri = Visual Peripheral Network; SomMot = Somatomotor Networks; VisCent = Visual Central Network; Cont = Control Networks; TempPar = Temporal Parietal Network; DorsAttn = Dorsal Attention Networks; SalVentAttn = Salience / Ventral Attention Networks.

Interactions between menopause status and symptoms

We then asked whether the frequency of menopause symptoms — a hallmark of the menopausal transition — would play a role in shaping functional network topologies.

Within-network connectivity

Among postmenopausal women, frequent symptoms were associated with decreased within-network connectivity among several higher-order brain networks. Among Control (A/B), Default Mode (A), and Salience/Ventral Attention (A/B) Networks, multiple regression analysis revealed a significant main effect of

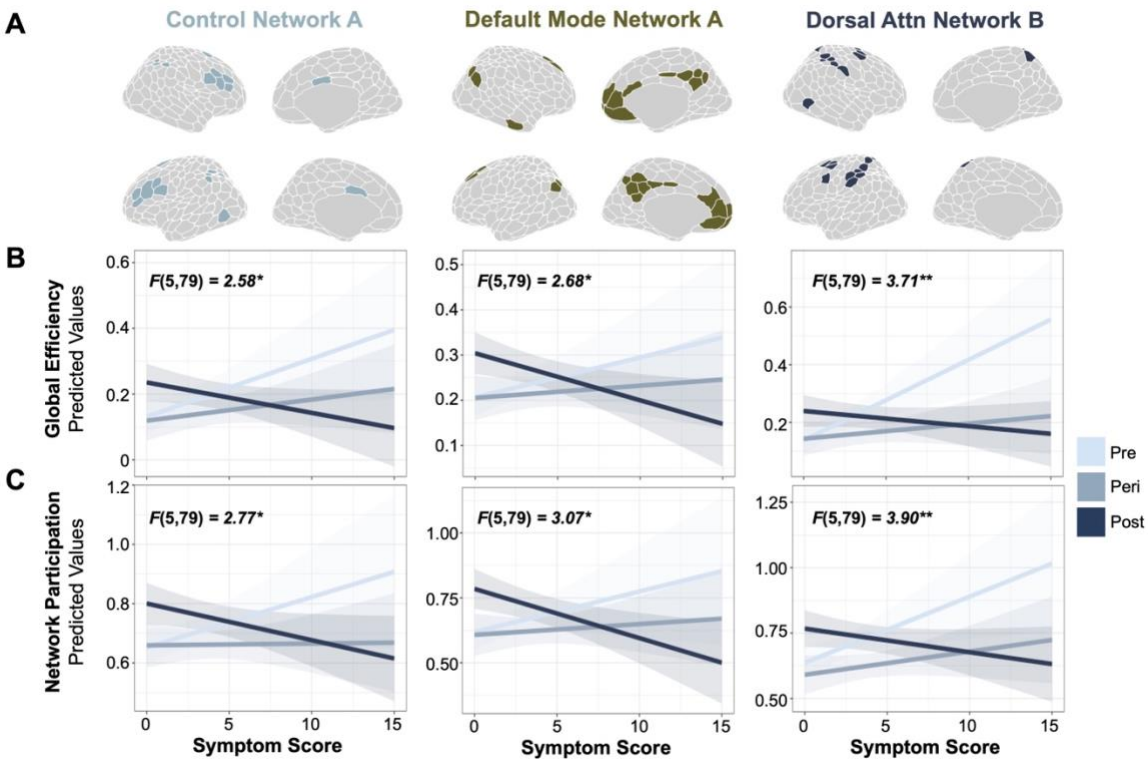

Figure 5.4. Interactions between menopause status and symptoms in predicting global efficiencies of large-scale networks. **A)** A spatial map of large-scale networks sensitive to endocrine aging. **B)** Among postmenopausal women, frequent symptoms were associated with decreased within-network connectivity among Control, Default, and Attention Subnetworks. **C)** A highly similar pattern emerged when examining network participation in relation to endocrine aging factors. This appeared to be a widespread pattern, as the majority of networks were implicated. See **Appendix** for a complete report; select networks shown here for consistency with global efficiency results.

postmenopausal status on global efficiency, indicating that individuals with advanced endocrine age had slightly higher within-network connectivity. However, these effects were attenuated by a significant negative interaction between symptomology and post-menopause status, suggesting that the impact of frequency symptomology on network connectivity may be dependent on where women are at in the transition period (see **Table 5.2, Fig. 5.4B**, and **Appendix C** for full reporting of model estimates).

Table 5.2. Within-network connectivity predicted by menopause group and symptom frequency

Network	Term	Estimate	Std. Error	T-statistic
Control Network A *F(5,79)* = 2.58, *p* = 0.03, R^2 = 0.14	**Intercept**	**0.12**	**0.03**	**4.70*** **
	Symptom Score	**0.02**	**0.01**	**2.44***
	Meno Status: Peri	-0.001	0.04	-0.04
	Meno Status: Post	**0.11**	**0.04**	**3.00***
	Symptoms × Peri	-0.01	0.01	-1.34
	Symptoms × Post	**-0.03**	**0.01**	**-3.05****
Default Mode Network A *F(5,79)* = 2.68, *p* = 0.02, R^2 = 0.14	**Intercept**	**0.20**	**0.02**	**9.60*** **
	Symptom Score	0.01	0.01	1.50
	Meno Status: Peri	0.003	0.03	0.12
	Meno Status: Post	**0.10**	**0.03**	**3.29****
	Symptoms × Peri	-0.007	0.01	-0.88
	Symptoms × Post	**-0.02**	**0.01**	**-2.61***
Dorsal Attention Network B *F(5,79)* = 3.71, *p* = 0.005, R^2 = 0.19	**Intercept**	**0.13**	**0.03**	**5.14*** **
	Symptom Score	**0.03**	**0.01**	**3.75****
	Meno Status: Peri	0.01	0.04	0.38
	Meno Status: Post	**0.11**	**0.04**	**2.98***
	Symptoms × Peri	**-0.02**	**0.01**	**-2.52***
	Symptoms × Post	**-0.04**	**0.01**	**-3.77****

FDR-corrected at q < 0.05; *p ≤ 0.05, **p ≤ 0.01, ***p ≤ 0.001

A handful of networks showed heightened sensitivity to these interactions. For Dorsal Attention Network B, multiple regression analyses also revealed a significant main effect of symptomology (*b* = .03, *SE* = .008, *p* = .002) and postmenopausal status (*b* = .11, *SE* = .04, *p* = .01) on global efficiency, indicating that individuals with frequent symptoms and advanced endocrine age had higher within-network connectivity. Again, these effects were attenuated by a significant negative interaction between symptomology and peri/postmenopausal status (peri: *b* = -.02, *SE* = .01, *p* = .04; post: *b* = -.04, *SE* = .01, *p* = .001), suggesting that connectivity among this network may be reduced earlier in the menopausal transition depending on symptom frequency. The same pattern of results was observed for Limbic Network A global efficiency. Importantly, within-network connectivity among sensory

networks (e.g., Somatomotor and Visual), displayed no relationships with endocrine aging.

Between-network connectivity

A highly similar pattern of findings was observed for network participation, wherein postmenopausal stage and symptom frequency interactions consistently emerged to predict a decrease in network participation among most all 17 networks. The most sensitive networks appeared to be Control, Default, Limbic, and Attention subnetworks (see **Fig. 5.4C**). These widespread relationships highlight the potential for a global shift in communication between nodes across the cortex as a function of increasing symptomology and endocrine age. See **Appendix C** for a complete reporting of results.

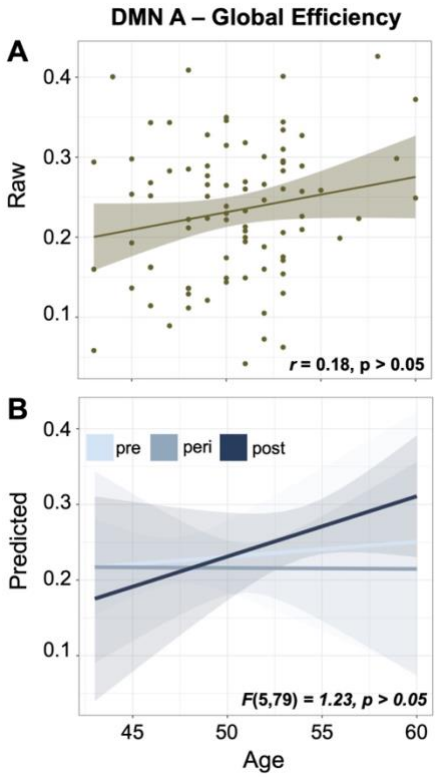

Figure 5.5. Despite differences across menopausal groups, chronological age shows no relationship with network metrics at the individual level (**A**) or when incorporated into a regression model with menopause status (**B**). Shown here is DMN A, but this applies to all networks.

<u>Functional network topologies and chronological age</u>

Despite significant differences between groups, chronological age did not seem to play a role in the relationship between endocrine aging and functional connectivity. No significant relationships were observed between age and network topologies when looking

independently (**Fig. 5.5A**) or when including age in the regression models (**Fig. 5.5B**), all $p > .05$. To note, chronological age was not controlled for in symptomology × menopause regression models due to the high collinearity between chronological and endocrine age.

D. Discussion

Most women will spend 1/3rd of their lives in the post-reproductive years, yet cognitive neuroscientists largely overlook how the depletion of sex steroid hormones during menopause shapes the brain (Taylor et al., 2019). As a result, a major gap in the brain imaging literature is understanding how the brain's intrinsic functional networks change throughout menopause when sex hormone production declines precipitously. Here, we leveraged techniques from network neuroscience to begin filling this gap, revealing that the frequency of menopausal symptoms likely exacerbates intrinsic brain network connectivity decline in post-menopausal women, especially among association networks (e.g., DMN, Control, Attention, Limbic).

When examining network topology in relation to menopausal group or sex hormones alone, few significant relationships emerged. This is perhaps unsurprising, considering the highly variable nature of individuals' response to ovarian hormone decline in midlife (Avis et al., 2015). Some women are barely impacted by hormonal withdrawal, while others struggle with frequent and severe vasomotor and neurological symptoms over the course of months to years (Freeman et al., 2011; Avis et al., 2015; Brinton et al., 2015; Maki and Thurston, 2020). These symptoms, especially hot flashes, negatively impact known regulators of brain function,

including sleep quality (de Zambotti et al., 2014), blood pressure (Jackson et al., 2016), and memory function (Maki et al., 2020). In our own midlife sample, night sweats and vaginal dryness were associated with increased irritability.

An emerging literature has provided evidence to suggest that vasomotor symptoms may be key determinants of menopause-induced brain changes, over and above endogenous hormone levels and/or broad menopause categorizations (Maki and Thurston, 2020). In one recent study, the frequency and severity of physiologic hot flashes were shown to be associated with *increased* DMN connectivity among a sample of predominantly postmenopausal women (Thurston et al., 2015). This relationship was strongest when hot flashes occurred during the night, interrupting sleep. Hot flashes have also been linked to increased brain activity during a verbal working memory task (Maki et al., 2020). In both studies, the findings were independent of serum hormone concentrations. In this study, I incorporated menopausal symptomology (i.e., night sweats, hot flashes, vaginal dryness, irritability) as a variable of interest in models predicting brain connectivity to better capture meaningful differences in an individual's experience with menopause. Once accounting for these major aspects of endocrine aging concurrently, interesting relationships began to emerge. To note, a similar pattern of results held when only incorporating the frequency of night sweats and hot flashes, suggesting that vasomotor symptoms may have the biggest impact on brain dynamics.

When looking across the entire sample of women, the frequency of symptoms was associated with increased connectivity. However, this was only apparent with respect to Dorsal Attention Network B, Limbic Network A, Somatomotor Network A,

and Control Network A. Between-network connectivity among Attention, Limbic, Somatomotor, Visual, and Limbic (A) networks displayed similar positive relationships with symptoms. Dorsal Attention Network B, which is comprised of regions implicated in somatic sensation (i.e., postcentral gyrus) appeared to be the most sensitive. Interestingly, symptomology alone was not tied to DMN connectivity in this sample; rather, these findings suggest that a wider range of large-scale brain networks may be sensitive to these neurological and vasomotor symptoms. A number of factors could be driving the differences between these findings and the previous study, including 1) differences in how we define connectivity — seed-based versus the atlas-based approach I used here, 2) how we measured symptomology — skin conductance monitoring versus self-report, 3) sample size differences (18 vs. 85), and/or 4) the hormonal profiles of the participants — here, the sample was made up of women at various stages of endocrine decline, including pre and perimenopausal women. Regardless, future work with larger cohorts of women, paired with objective measures of symptom severity and frequency, will be necessary to establish how menopausal symptomology — present in 70% of women — shapes intrinsic brain network connectivity.

Once accounting for symptom frequency in the models, *main* effects of menopause status emerged. Postmenopausal women conferred slightly greater network connectivity compared to pre and perimenopausal groups. For network participation, this seemed to be a global effect; for global efficiency, this was only observed in a handful of higher-order networks. This pattern may reflect a compensatory response rather than a heightened advantage due to decreased

presence of sex hormones. Evidence for a ‘compensatory’ response throughout menopause has been shown in previous investigations by Emily Jacobs and colleagues (see review: Jacobs and Goldstein, 2018). For example, their team found that postmenopausal women showed greater dorsolateral PFC and hippocampal activity compared to premenopausal women during a verbal working memory task, going on to reveal that the magnitude of activity and the strength of functional connectivity in these regions was associated with task performance (Jacobs et al., 2016a). One hypothesis is that the postmenopausal brain may have to expend more energy to properly integrate and segregate with other regions compared to pre and perimenopausal states. This idea is strengthened with the knowledge that decreased DMN connectivity, for example, has been associated with improved memory performance (Daselaar et al., 2004).

However, this slight increase in connectivity was attenuated once considering interactions between menopause stage and symptomology — interestingly, only among postmenopausal women. These findings may be reflective of the ‘double hit’ hypothesis put forth in the aging literature (see Morrison and Baxter, 2012), wherein the loss of neuroprotective hormones after menopause, compounded by frequent menopause-related symptoms, may be drivers of decreases in both within- and between network connectivity. This presents the possibility that a compensatory response is no longer viable when frequent and/or severe neurological symptoms are present. However, more work is needed to support this idea, clarifying why there may be increased functional connectivity in postmenopausal and whether this has

any bearing on cognitive outcomes. In the future, I will examine the relationship between endocrine aging and task-based fMRI in this same sample of women.

Implications for endocrine modulation of large-scale brain networks

The application of network science techniques to the study of the brain has allowed neuroscientists to move beyond examining individual regions in isolation, instead granting us the ability to understand how functional networks distributed across broad swaths of cortex support cognition (Bullmore and Bassett, 2011). Intrinsic functional connectivity of large-scale brain networks changes as a function of chronological age (Andrews-Hanna et al., 2007), differs by sex (Scheinost et al., 2015), and disease states (Buckner et al., 2009; Seeley et al., 2009). A central feature of healthy brain network connectivity is the presence of a set of highly interconnected hubs that support information flow between regions (Bullmore and Bassett, 2011). Due to high metabolic demands, these hubs are also the most vulnerable to degeneration. Indeed, clinical neuroscience studies have revealed consistent patterns of brain network disruption in neurological disorders (Stam, 2014). Hub nodes within the DMN (e.g. posterior cingulate cortex, precuneus), as well as highly-connected brain regions in temporal, parietal, and frontal association areas, are dysregulated in AD (Minoshima et al., 1997; Greicius et al., 2004; Palmqvist et al., 2017;). High spatial overlap exists between these DMN hubs and amyloid beta deposition (Pascoal et al., 2019) and several studies suggest that disruptions in DMN connectivity may be an early neural marker of AD pathophysiology before clinical symptoms emerge (Buckner et al., 2009). What physiological properties make these hubs so prone to damage?

Endocrine status also plays an integral role in maintaining and shaping properties of large-scale brain networks, particularly the DMN (Pritschet et al., 2021). In this study, I demonstrated that features of menopause — a key endocrine transition state that involves hormones going offline — are linked to decreasing global efficiency and network participation in the DMN, as well as other major higher-order circuits (e.g., Frontal Control Network; Dorsal and Ventral Attention Networks). As such, endocrine aging, over and above chronological aging, may uniquely impact functional properties of the brain in midlife, placing these hub nodes in a vulnerable state and providing a sex-specific pathway contributing to women's increased risk for AD decades prior to disease onset.

Limitations and considerations

It is important to note the limitations of this study. For one, although statistically significant, the effects are relatively subtle, explaining a small amount of variance. This may be due to the heterogenous nature of a cross-sectional design, exacerbated by the low sample size at the group-level (Marek et al., 2022) and short scanning duration (Noble et al., 2017). Although our study sample was tightly controlled with respect to reproductive and medical exclusionary criteria, confounding factors (e.g., undiagnosed medical conditions, lifestyle, and environment) can still permeate. Future studies with larger sample sizes and improved temporal resolution will be necessary to establish state- and trait-level features of the functional connectome that emerge during the menopausal transition.

Another key limitation in this study is our inability to quantify how the menopausal transition *changes* the brain; given the cross-sectional nature, we can only identify differences between the stages. Changes in sex hormones, over and above absolute concentrations, are key drivers of brain state alterations and place the brain in a vulnerable state among a subset of women (Schiller et al., 2016). Future work using longitudinal and dense-sampling designs will be key to establishing how the rate and trajectory of change in brain structure and function may dictate cognitive, behavior, and health outcomes among midlife women in post-reproductive years. Increasing the frequency of within-person measurements can also provide better opportunities to identify neural biomarkers that can lead to individualized inferences, detection, and treatment of psychiatric and neurologic conditions that emerge during hormonal transition periods (e.g., major depression). Further, deeply characterizing this midlife period may help us identify at-risk individuals in the earliest stages of neurodegeneration and may suggest new lines of preventative treatment (e.g., hormone therapy) for AD and cognitive decline in peri and early postmenopausal years. The women in this study were ostensibly healthy, as determined by strict medical and reproductive exclusionary criteria. Future studies should prioritize the recruitment of enriched sample of individuals with varied genotypes, lifestyle factors, environment exposures, and health conditions in pursuit of more ecologically valid models of disease risk as a function of endocrine aging.

Finally, the findings presented here are based upon a single imaging modality, resting-state fMRI. However, the menopause transition is a neurological

transition state that involves global shifts in biological features inherently tied to basic principles of fMRI, such as glucose metabolism, hemodynamics, and microstructure (Brinton et al., 2015). Considering widespread differences in network participation were observed across the whole brain as a function of menopausal status, it is highly likely that global shifts among other latent variables are driving this effect. Future planned analyses include taking a multi-modal approach (e.g., combining structural, functional, and diffusion MRI) to better understand the impact of endocrine aging on various brain dynamics. This may shed new light on these intrinsic brain network connectivity findings, in turn improving our interpretation of what happens during this midlife period. For instance, vasomotor symptoms have recently been linked to heightened white matter hyperintensities (Thurston et al., 2023). Therefore, it is imperative that we examine whether structure–function relationships start to decouple in midlife, and whether this is accelerated by menopausal status or symptomology. My findings suggest that major aspects of endocrine aging interact to impact the brain's functional architecture among midlife women.

Endocrine aging from a lifespan perspective

How does a woman's lifespan reproductive history shape brain aging trajectories? Why, how, and over what time course? Focusing exclusively on factors related to menopause may not provide us with a complete understanding of the endocrine basis of brain aging and subsequent AD risk. For example, does age of initiation or duration of oral contraceptive use alter age-related changes in brain morphology?

Do common medications that suppress sex hormone levels (e.g. Lupron for endometriosis) have enduring effects on brain structure, function, and cognition? Although we collected extensive reproductive histories in this study, we do not have the statistical power to assess the relationships between lifespan endocrine events and brain function. Population-level consortium studies, such as UkBiobank, have the statistical power to ask these questions and have begun shedding light on some of these unanswered questions (Taylor et al., 2021). For one, it was recently revealed that the number of pregnancies can be traceable in brain structure and function decades later (de Lange et al., 2019, Orchard et al., 2020). Establishing these relationships at the population level can then help guide tightly controlled follow up studies.

6

Conclusions

Despite 20 years of evidence from rodent, nonhuman primate, and human studies demonstrating the tightly coupled relationship between our endocrine and nervous systems (Hara et al., 2015; Frick et al., 2018; McEwen, 2018; Beltz and Moser, 2019), the field of cognitive neuroscience has largely overlooked how endocrine factors shape the brain (Taylor et al., 2021). The dynamic endocrine changes that unfold over the menstrual cycle, during gestation, and across the menopause transition are natural features of half of the world's population. This collective body of work provides further evidence that basic neuroendocrine events significantly shape brain morphology and function over previously unexplored windows of time.

Applying dense-sampling to reveal endocrine modulation of the nervous system

The unique strength of these precision imaging studies derives from their ability to capture, with high spatial and temporal resolution, the brain's response to a central feature of the mammalian endocrine system: hormonal rhythmicity (Pritschet et al., 2021).

In Study 1, we observed robust increases in coherence across the brain as a function of increasing estradiol across the menstrual cycle. In contrast to estradiol's

proliferative effects, progesterone was primarily associated with reduced coherence across the whole brain. When used time-lagged methods from dynamical systems analysis to test the temporal directionality of these associations, we found that estradiol most strongly enhances within-network integration in the DMN and DAN. These results were replicated in the follow-up study (where progesterone, but not estradiol, was selectively suppressed), further strengthening the notion that estradiol drives changes in network connectivity. In fact, across both studies, estradiol often predicted brain states better than previous states of the brain itself.

However, questions remained regarding how hormones shape large-scale functional brain network reorganization: which nodes are driving this network reorganization and how do they reorganize? Our team has since worked to further our understanding of the brain's response to the menstrual cycle at the mesoscopic level. In collaborator with Joshua Mueller and Jean Carlson, we applied methods from complex systems analysis—dynamic community detection (DCD)—to identify periods of time when functionally coupled regions began to shift the network communities with which they were affiliated: so-called network 'flexibility'. Despite a large degree of network stability over the menstrual cycle, a striking reorganization event occurred within the DMN, coincident with the peaks in serum estradiol (Mueller et al., 2020). During the 3-day ovulatory window, the DMN core split into two smaller groups, leading to the transient formation of a new functional community. This was one of only two large-scale reorganization events—the other occurring during the luteal phase's secondary peak in estradiol, which involved an overlapping set of nodes located predominantly within the PFC (Mueller et al., 2021).

While DCD expanded upon our earlier finding by highlighting cycle-dependent alterations in DMN organization, unique effects emerged when comparing naturally-cycling (Study 1) and oral contraceptive (Study 2) conditions. Our original investigation revealed that estradiol's ability to drive global efficiency within the DMN was invariant to condition (i.e. evident under naturally cycling conditions and when progesterone was selectively suppressed). In contrast, a closer look with DCD revealed increased DMN network flexibility only during ovulation: networks were largely stable under the oral contraceptive regimen, with no major reorganizations despite the fact that fluctuations in estradiol were on par with those observed under naturally cycling conditions. It is possible that hormone-driven changes in subnetwork organization are specific to conditions in which gonadotropins and ovarian hormones exert coordinated action in the brain, as occurs across the menstrual cycle.

In addition to sex hormone–driven changes in the functional connectome, the 28andMe dataset was also leveraged by team member Caitlin Taylor to reveal hormone-related changes in morphology over short timescales (Taylor et al., 2020). Using high-resolution hippocampal subfield imaging, she discovered that endogenous hormone fluctuations and exogenous hormone manipulations alter medial temporal lobe morphology. Across the menstrual cycle, intrinsic fluctuations in progesterone were associated with volumetric changes in CA2/3, entorhinal, perirhinal, and parahippocampal cortex. Chronic progesterone suppression abolished these cycle-dependent effects. These results suggest progesterone has

the ability to dynamically shape medial temporal lobe morphology over rapid timescales.

The work presented in **Study 2** offers us the first atlas of the human brain across gestation. Notably, the *fetal* brain has received considerable attention over the past decade, with scientists generating increasingly intricate MRI-based maps of fetal brain development as early as ~20 weeks' gestation (Thomason, 2020). A comparable understanding of the maternal brain is lacking. Our novel findings reveal that the gestational period is characterized by sweeping reductions in gray matter volume, widespread cortical thinning, and enhanced white matter microstructural integrity that unfold week by week. Ventricle enlargement and contraction parallels these cortical changes. Critically, dynamic neural changes occur *within* the pregnancy window itself, a nuance not captured by studies limited to pre- versus post-pregnancy comparisons. For example, white matter microstructural integrity increases throughout the first and second trimester, before returning to baseline values by the first postpartum scan. Other measures, such as GMV and cortical thickness, decrease throughout gestation and display a modest rebound postpartum. Interestingly, the only subcortical region to show sensitivity to pregnancy was the PHC — an area of the brain we also demonstrated to be influenced by hormone fluctuations in 28andMe (Taylor et al., 2020). Together, these non-linear patterns underscore the utility of precision imaging to capture the full dynamic range of changes that unfold within the gestational window — and more fully represent the brain's remarkable metamorphosis during pregnancy.

The neuroanatomical changes that unfold during matrescence have broad implications for understanding individual differences in parental behavior, vulnerability to mental health disorders, and brain aging patterns. Precision mapping of the maternal brain lays the groundwork for a greater understanding of the subtle and sweeping structural, functional, behavioral, and clinical changes that unfold across gestation. Such pursuits will advance our basic understanding of the human brain and its remarkable ability to undergo protracted plasticity well into adulthood.

The wax and wane of brain networks over the lifespan

The studies shown here provide evidence that endocrine status is linked to the reorganization of the structural and functional connectome in humans, revealing a consistent set of networks that appear to be the most sensitive to changing hormonal milieus, especially the Default Mode Network. After the onset of puberty, hub nodes of the DMN display sex-specific perfusion trajectories, with females displaying increases in cerebral blood flow compared to males (Satterthwaite et al., 2014). Across the menstrual cycle, our team demonstrated that functional connectivity is altered in response to fluctuations in sex hormones (Pritschet et al., 2020; Mueller et al., 2021). Further, our group and others show that pregnancy leads to reductions in gray matter volume in regions overlapping with the DMN (Hoekzema et al., 2017). Lastly, postmenopausal HRT increases DMN resting-state blood flow (Maki and Resnick, 2000), and the findings in Study 3 suggest that DMN connectivity is influenced by features of the menopausal transition. Interestingly, hubs within these networks overlap with ER-rich brain regions, including the posterior cingulate

and prefrontal cortex. What might it mean for cognition, behavior, and health if these major networks undergo reorganization — continuous wax and waning — over the lifespan. Are there benefits? And perhaps more importantly, are there any consequences? This likely depends on the individual.

Throughout the life course, major hormonal transition periods (e.g., puberty, pregnancy, initiation of oral contraceptive use, and perimenopause) coincide with an increased risk for depression (Rubinow and Schmidt, 2016), especially among susceptible women. Are 'susceptible women' the ones showing the greatest network reorganization in response to hormone fluctuations? If so, does this place them in a vulnerable state in post-reproductive years? The DMN is particularly vulnerable to AD progression, demonstrating distinct abnormalities in functional connectivity compared to healthy controls (Buckner et al., 2009). Notably, DMN connectivity is also altered in MDD (Scalabrini et al., 2020), a known risk factor for AD (Herbert and Lucassen, 2016). Given that women are disproportionately affected by both AD and MDD, and that the DMN is a highly endocrine-modulated network, it is imperative that we think about these diseases and disorders with a women's health lens.

Further, modeling dynamic *changes* in these tightly-coupled systems (e.g. brain networks, ovarian hormones) in the healthy brain could help us better predict the likely consequences of their disruption in the disordered brain. Doing so could afford us unique insight as to why hormonally-driven disorders (e.g., postpartum depression) emerge in some individuals but not others. However, given the wide array of direct and indirect influences sex hormones have on the brain, we must

transition to multi-modal (e.g., PET, MRI) and multi-level (e.g., structure, function, blood flow, receptor maps) designs.

Future work

Current studies exploring the impact of endocrine aging on the brain are often underpowered, model reproductive factors in isolation, and focus largely on pre vs. postmenopausal comparisons (Jacobs and Goldstein, 2018; Taylor et al., 2019). As such, it remains unclear how collective factors of endocrine aging—age at menopause, surgical versus spontaneous menopause, use of hormone therapy, polygenic risk factors—mediate the relationship between menopause and disease risk and cognitive decline in post-reproductive years. Beyond menopause itself, how do past neuroendocrine events shape current ones? In Study 2, we revealed that brain structure does not return to a baseline, pre-pregnancy state. What might this mean for brain aging, especially if one undergoes pregnancy several times? The same pressing question exists when thinking about the impact of oral hormonal contraceptives. What happens to the brain in midlife after decades of hormonal suppression? Taking away or modifying sex hormones — neuromodulatory and neuroprotective inputs across the brain — is likely to have a widespread effect. The answers to these questions are not straightforward, nor easy to address. However, only by deeply characterizing the normative effects of sex hormones' influence on the human brain can we begin to understand the drivers of dysfunction. For example, applying dense-sampling methods to the menopausal transition would allow us to observe how an individual's brain—especially DMN architecture—

responds to a changing hormonal milieu decades before disease onset and may yield important clues about what constitutes normative reproductive aging versus a prodromal period of heightened disease risk.

The training I have received in graduate school has provided me the vast skill set necessary to kickstart these future studies. Future plans include conducting a longitudinal menopause study combining multimodal brain imaging, extensive reproductive histories, serological assessments, genotyping, and higher-order cognitive paradigms to establish the full extent to which menopause changes the brain. This approach will greatly improve our ability to later build a comprehensive neuroendocrine model of AD risk. Lastly, it is imperative that future studies like the one proposed above are representative of all demographics to ensure that women of all racial, ethnic, and socioeconomic backgrounds are benefiting from our scientific efforts equally. Characterizing how menopause shapes the brain in one homogenous group of white women does not get us that much closer to our ultimate goal of understanding menopause — this is a priority of mine in all future investigations.

References

1. Albert, K., Hiscox, J., Boyd, B., Dumas, J., Taylor, W., & Newhouse, P. (2017). Estrogen enhances hippocampal gray-matter volume in young and older postmenopausal women: a prospective dose-response study. *Neurobiology of aging*, *56*, 1-6.

2. Almey, A., Milner, T. A., & Brake, W. G. (2015). Estrogen receptors in the central nervous system and their implication for dopamine-dependent cognition in females. *Hormones and behavior*, *74*, 125-138.

3. Aly, M., & Turk-Browne, N. B. (2016). Attention stabilizes representations in the human hippocampus. *Cerebral Cortex*, *26*(2), 783-796.

4. Amin, Z., Canli, T., & Epperson, C. N. (2005). Effect of estrogen-serotonin interactions on mood and cognition. *Behavioral and cognitive neuroscience reviews*, *4*(1), 43-58.

5. Andrews-Hanna, J. R., Snyder, A. Z., Vincent, J. L., Lustig, C., Head, D., Raichle, M. E., & Buckner, R. L. (2007). Disruption of large-scale brain systems in advanced aging. *Neuron*, *56*(5), 924-935.

6. Angold A, Costello EJ. Puberty and depression. Child Adolesc Psychiatr Clin N Am. 2006; 15(4):919—937

7. Arélin K, Mueller K, Barth C, Rekkas PV, Kratzsch J, Burmann I, Villringer A, Sacher J. Progesterone mediates brain functional connectivity changes during the menstrual cycle-a pilot resting state MRI study. Front Neurosci. 2015; 9:44.

8. Avants, B. B., Tustison, N. J., Song, G., Cook, P. A., Klein, A., & Gee, J. C. (2011). A reproducible evaluation of ANTs similarity metric performance in brain image registration. Neuroimage, 54(3), 2033-2044.

9. Avis, N. E., Crawford, S. L., Greendale, G., Bromberger, J. T., Everson-Rose, S. A., Gold, E. B., ... & Study of Women's Health Across the Nation. (2015). Duration of menopausal vasomotor symptoms over the menopause transition. *JAMA internal medicine*, *175*(4), 531-539

10. Barba-Müller, E., Craddock, S., Carmona, S., & Hoekzema, E. (2019). Brain plasticity in pregnancy and the postpartum period: links to maternal caregiving and mental health. *Archives of women's mental health*, *22*, 289-299.

11. Barnett L, Seth AK. The MVGC multivariate Granger causality toolbox: A new approach to Granger-causal inference. Journal of Neuroscience Methods. 2014; 223:50–68.

12. Barrière, D. A., Ella, A., Szeremeta, F., Adriaensen, H., Même, W., Chaillou, E., Migaud, M., Même, S., Lévy, F., & Keller, M. (2021). Brain orchestration of pregnancy and maternal behavior in mice: A longitudinal morphometric study. *NeuroImage*, *230*, 117776.

13. Barth, C., & de Lange, A.-M. G. (2020). Towards an understanding of women's brain aging: The immunology of pregnancy and menopause. *Frontiers in Neuroendocrinology*, *58*, 100850.

14. Bassett DS, Wymbs NF, Porter MA, Mucha PJ, Carlson JM, Grafton ST. Dynamic reconfiguration of human brain networks during learning. Proc Natl Acad Sci USA. 2011; 108(18):7641–7646.

15. Bassett, D. S., & Gazzaniga, M. S. (2011). Understanding complexity in the human brain. *Trends in cognitive sciences*, *15*(5), 200-209.

16. Becker JB. Estrogen rapidly potentiates amphetamine-induced striatal dopamine release and rotational behavior during microdialysis. Neurosci Lett. 1990; 118(2):169–171.

17. Becker, J. B. (1990). Estrogen rapidly potentiates amphetamine-induced striatal dopamine release and rotational behavior during microdialysis. *Neuroscience letters*, *118*(2), 169-171.

18. Been, L. E., Sheppard, P. A., Galea, L. A., & Glasper, E. R. (2022). Hormones and neuroplasticity: A lifetime of adaptive responses. *Neuroscience & Biobehavioral Reviews*, *132*, 679-690

19. Beery, A.K., Zucker, I., 2011. Sex bias in neuroscience and biomedical research. Neurosci. Biobehav. Rev. 35, 565–572.

20. Beltz, A. M., & Moser, J. S. (2020). Ovarian hormones: a long overlooked but critical contributor to cognitive brain structures and function. *Annals of the New York Academy of Sciences*, *1464*(1), 156-180.

21. Berman KF, Schmidt PJ, Rubinow DR, Danaceau MA, Van Horn JD, Esposito G, Ostrem JL, Weinberger DR. Modulation of cognition-specific cortical activity by gonadal steroids: a positron-emission tomography study in women. Proc Natl Acad Sci USA. 1997; 94(16):8836–8841.

22. Betzel, R. F., Bertolero, M. A., Gordon, E. M., Gratton, C., Dosenbach, N. U., & Bassett, D. S. (2019). The community structure of functional brain networks exhibits scale-specific patterns of inter-and intra-subject variability. *Neuroimage*, *202*, 115990.

23. Bijsterbosch JD, Beckmann CF, Woolrich MW, Smith SM, Harrison SJ. The relationship between spatial configuration and functional connectivity of brain regions revisited.

24. Birn RM, Molloy EK, Patriat R, Parker T, Meier TB, Kirk GR, Nair VA, Meyerand ME, Prabhakaran V. The effect of scan length on the reliability of resting-state fMRI connectivity estimates. Neuroimage. 2013 12; 83:550–558.

25. Bloch M, Schmidt PJ, Danaceau M, Murphy J, Nieman L, Rubinow DR. Effects of gonadal steroids in women with a history of postpartum depression. Am J Psychiatry. 2000; 157(6):924–930

26. Boker SM, Neale MC, Klump KL. In: Molenaar PC, Lerner R, Newll K, editors. A differential equations model for the ovarian hormone cycle. New York: Guilford Press; 2014. p. 369–391.

27. Botvinik-Nezer, R., Holzmeister, F., Camerer, C. F., Dreber, A., Huber, J., Johannesson, M., ... & Rieck, J. R. (2020). Variability in the analysis of a single neuroimaging dataset by many teams. *Nature*, *582*(7810), 84-88.

28. Brinton RD, Thompson RF, Foy MR, Baudry M, Wang J, Finch CE, Morgan TE, Pike CJ, Mack WJ, Stanczyk FZ, Nilsen J. Progesterone receptors: form and function in brain. Front Neuroendocrinol. 2008; 29(2):313–339

29. Brinton, R. D., Yao, J., Yin, F., Mack, W. J., & Cadenas, E. (2015). Perimenopause as a neurological transition state. *Nature reviews endocrinology*, *11*(7), 393-405

30. Brunton, P. J., & Russell, J. A. (2008). The expectant brain: Adapting for motherhood. *Nature Reviews Neuroscience*, *9*(1), 11–25.

31. Buckner RL, Sepulcre J, Talukdar T, Krienen FM, Liu H, Hedden T, Andrews-Hanna JR, Sperling RA, Johnson KA. Cortical hubs revealed by intrinsic functional connectivity: mapping, assessment of stability, and relation to Alzheimer's disease. J Neurosci. 2009; 29(6):1860–1873

32. Buckner, R. L., Sepulcre, J., Talukdar, T., Krienen, F. M., Liu, H., Hedden, T., ... & Johnson, K. A. (2009). Cortical hubs revealed by intrinsic functional connectivity: mapping, assessment of stability, and relation to Alzheimer's disease. *Journal of neuroscience*, *29*(6), 1860-1873.

33. Bullmore ET, Bassett DS. Brain graphs: graphical models of the human brain connectome. Annu Rev Clin Psychol. 2011; 7:113–140.

34. Buysse DJ, Reynolds CF, Monk TH, Berman SR, Kupfer DJ. The Pittsburgh Sleep Quality Index: a new instrument for psychiatric practice and research. Psychiatry Res. 1989; 28(2):193–213.

35. Cai JX, Arnsten AF. Dose-dependent effects of the dopamine D1 receptor agonists A77636 or SKF81297 on spatial working memory in aged monkeys. J Pharmacol Exp Ther. 1997; 283(1):183–189.

36. Carmona, S., Martínez-García, M., Paternina-Die, M., Barba-Müller, E., Wierenga, L. M., Alemán-Gómez, Y., ... & Hoekzema, E. (2019). Pregnancy and adolescence entail similar neuroanatomical adaptations: a comparative analysis of cerebral morphometric changes. *Human brain mapping*, *40*(7), 2143-2152.

37. Celik, A., Somer, M., Kukreja, B., Wu, T., & Kalish, B. T. (2022). The Genomic Architecture of Pregnancy-Associated Plasticity in the Maternal Mouse Hippocampus. *Eneuro*, *9*(5).

38. Cieslak, M., Cook, P. A., He, X., Yeh, F. C., Dhollander, T., Adebimpe, A., ... & Satterthwaite, T. D. (2021). QSIPrep: an integrative platform for preprocessing and reconstructing diffusion MRI data. *Nature methods*, *18*(7), 775-778.

39. Clayton, J. A., & Collins, F. S. (2014). Policy: NIH to balance sex in cell and animal studies. *Nature*, *509*(7500), 282-283.

40. Clemens AM, Lenschow C, Beed P, Li L, Sammons R, Naumann RK, Wang H, Schmitz D, Brecht M. Estrus-cycle regulation of cortical inhibition. Curr Biol. 2019; 29(4):605–615.

41. Cohen JR, Gallen CL, Jacobs EG, Lee TG, D'Esposito M. Quantifying the reconfiguration of intrinsic networks during working memory. PLOS ONE. 2014; 9(9):1–8.

42. Cohen S, Kamarck T, Mermelstein R. A global measure of perceived stress. J Health Soc Behav. 1983; 24(4):385–396.

43. Cordes, D., Turski, P. A., & Sorenson, J. A. (2000). Compensation of susceptibility-induced signal loss in echo-planar imaging for functional applications. *Magnetic Resonance Imaging*, *18*(9), 1055-1068.

44. Creutz LM, Kritzer MF. Estrogen receptor-beta immunoreactivity in the midbrain of adult rats: regional, subregional, and cellular localization in the A10, A9, and A8 dopamine cell groups. J Comp Neurol. 2002; 446(3):288–300.

45. Crum, W. R., Camara, O., & Hill, D. L. (2006). Generalized overlap measures for evaluation and validation in medical image analysis. *IEEE transactions on medical imaging*, *25*(11), 1451-1461.

46. Dale, A. M., Fischl, B., & Sereno, M. I. (1999). Cortical surface-based analysis: I. Segmentation and surface reconstruction. Neuroimage, 9(2), 179-194.

47. Daniel, J. M., Witty, C. F., & Rodgers, S. P. (2015). Long-term consequences of estrogens administered in midlife on female cognitive aging. *Hormones and behavior*, *74*, 77-85.

48. Das, S. R., Avants, B. B., Grossman, M., & Gee, J. C. (2009). Registration based cortical thickness measurement. Neuroimage, 45(3), 867-879.

49. Daselaar, S. M., Prince, S. E., & Cabeza, R. (2004). When less means more: deactivations during encoding that predict subsequent memory. *Neuroimage*, *23*(3), 921-927.

50. De Bondt T, Smeets D, Pullens P, Van Hecke W, Jacquemyn Y, Parizel PM. Stability of resting state networks in the female brain during hormonal changes and their relation to premenstrual symptoms. Brain Res. 2015; 1624:275–285.

51. de Lange, A.-M. G., Kaufmann, T., van der Meer, D., Maglanoc, L. A., Alnæs, D., Moberget, T., Douaud, G., Andreassen, O. A., & Westlye, L. T. (2019). Population-based neuroimaging reveals traces of childbirth in the maternal brain. *Proceedings of the National Academy of Sciences*, *116*(44), 22341–22346.

52. de Zambotti, M., Colrain, I. M., Javitz, H. S., & Baker, F. C. (2014). Magnitude of the impact of hot flashes on sleep in perimenopausal women. *Fertility and Sterility*, *102*(6), 1708-1715.

53. Deligiannidis, K. M., Meltzer-Brody, S., Maximos, B., Peeper, E. Q., Freeman, M., Lasser, R., ... & Doherty, J. (2023). Zuranolone for the Treatment of Postpartum Depression. *American Journal of Psychiatry*, appi-ajp.

54. Desikan, R. S., Ségonne, F., Fischl, B., Quinn, B. T., Dickerson, B. C., Blacker, D., ... & Killiany, R. J. (2006). An automated labeling system for

subdividing the human cerebral cortex on MRI scans into gyral based regions of interest. Neuroimage, 31(3), 968-980.

55. Dulac, C., O'Connell, L. A., & Wu, Z. (2014). Neural control of maternal and paternal behaviors. *Science*, *345*(6198), 765–770. ELife. 2019; 8.

56. Dumitriu, D., Rapp, P. R., McEwen, B. S., & Morrison, J. H. (2010). Estrogen and the aging brain: an elixir for the weary cortical network. *Annals of the New York Academy of Sciences*, *1204*(1), 104-112.

57. Epperson, C. N., Amin, Z., Ruparel, K., Gur, R., & Loughead, J. (2012). Interactive effects of estrogen and serotonin on brain activation during working memory and affective processing in menopausal women. *Psychoneuroendocrinology*, *37*(3), 372-382.

58. Esteban, O., Birman, D., Schaer, M., Koyejo, O. O., Poldrack, R. A., & Gorgolewski, K. J. (2017). MRIQC: Advancing the automatic prediction of image quality in MRI from unseen sites. PloS one, 12(9), e0184661.

59. Fabbri, E., An, Y., Gonzalez-Freire, M., Zoli, M., Maggio, M., Studenski, S. A., ... & Ferrucci, L. (2016). Bioavailable testosterone linearly declines over a wide age spectrum in men and women from the Baltimore Longitudinal Study of Aging. *Journals of Gerontology Series A: Biomedical Sciences and Medical Sciences*, *71*(9), 1202-1209.

60. Fehring RJ, Schneider M, Raviele K. Variability in the phases of the menstrual cycle. J Obstet Gynecol Neonatal Nurs. 2006; 35(3):376–384.

61. Finn ES, Shen X, Scheinost D, Rosenberg MD, Huang J, Chun MM, Papademetris X, Constable RT. Functional connectome fingerprinting: Identifying individuals using patterns of brain connectivity. Nat Neurosci. 2015; 18(11):1664–1671.

62. Fornito A, Harrison BJ, Zalesky A, Simons JS. Competitive and cooperative dynamics of large-scale brain functional networks supporting recollection. Proc Natl Acad Sci USA. 2012; 109(31):12788–12793.

63. Fortress, A. M., & Frick, K. M. (2014). Epigenetic regulation of estrogen-dependent memory. *Frontiers in neuroendocrinology*, *35*(4), 530-549.

64. Fox MD, Greicius M. Clinical applications of resting state functional connectivity. Front Syst Neurosci. 2010; 4:19.

65. Freeman, E. W., Sammel, M. D., Lin, H., Liu, Z., & Gracia, C. R. (2011). Duration of menopausal hot flushes and associated risk factors. *Obstetrics and gynecology*, *117*(5), 1095.

66. Frick KM, Kim J, Koss WA. Estradiol and hippocampal memory in female and male rodents. Curr Opin Behav Sci. 2018; 23:65–74.

67. Frick KM, Kim J, Tuscher JJ, Fortress AM. Sex steroid hormones matter for learning and memory: Estrogenic regulation of hippocampal function in male and female rodents. Learn Mem. 2015; 22(9):472–493.

68. Frick, K. M. (Ed.). (2019). *Estrogens and memory: basic research and clinical implications*. Oxford University Press.

69. Frick, K. M., & Kim, J. (2018). Mechanisms underlying the rapid effects of estradiol and progesterone on hippocampal memory consolidation in female rodents. *Hormones and behavior*, *104*, 100-110.

70. Friston KJ, Rotshtein P, Geng JJ, Sterzer P, Henson RN. A critique of functional localisers. Neuroimage. 2006; 30(4):1077–1087.

71. Friston KJ, Williams S, Howard R, Frackowiak RS, Turner R. Movement-related effects in fMRI time-series. Magn Reson Med. 1996; 35(3):346–355.

72. Friston, K. J., Rotshtein, P., Geng, J. J., Sterzer, P., & Henson, R. N. (2006). A critique of functional localisers. Neuroimage, 30(4), 1077-1087.

73. Galea LAM, Frick KM, Hampson E, Sohrabji F, Choleris E. Why estrogens matter for behavior and brain health. Neurosci Biobehav Rev. 2017; 76:363–379.

74. Galea, L. A., Frick, K. M., Hampson, E., Sohrabji, F., & Choleris, E. (2017). Why estrogens matter for behavior and brain health. *Neuroscience & Biobehavioral Reviews*, *76*, 363-379.

75. Galea, L. A., Leuner, B., & Slattery, D. A. (2014). Hippocampal plasticity during the peripartum period: influence of sex steroids, stress and ageing. *Journal of neuroendocrinology*, *26*(10), 641-648.

76. Galea, L. A., Perrot-Sinal, T. S., Kavaliers, M., & Ossenkopp, K. P. (1999). Relations of hippocampal volume and dentate gyrus width to gonadal hormone levels in male and female meadow voles. *Brain research*, *821*(2), 383-391.

77. Gibbs SEB, D'Esposito M. Individual capacity differences predict working memory performance and prefrontal activity following dopamine receptor stimulation. Cogn Affect Behav Neurosci. 2005; 5(2):212–221.

78. Girard R, Metereau E, Thomas J, Pugeat M, Qu C, Dreher JC. Hormone therapy at early post-menopause increases cognitive control-related prefrontal activity. Sci Rep. 2017; 7:44917.

79. Girard, R., Météreau, E., Thomas, J., Pugeat, M., Qu, C., & Dreher, J. C. (2017). Hormone therapy at early post-menopause increases cognitive control-related prefrontal activity. *Scientific reports*, *7*(1), 44917.

80. Gold, E. B., Bromberger, J., Crawford, S., Samuels, S., Greendale, G. A., Harlow, S. D., & Skurnick, J. (2001). Factors associated with age at natural menopause in a multiethnic sample of midlife women. *American journal of epidemiology*, *153*(9), 865-874.

81. Gordon, E. M., Laumann, T. O., Gilmore, A. W., Newbold, D. J., Greene, D. J., Berg, J. J., ... & Dosenbach, N. U. (2017). Precision functional mapping of individual human brains. *Neuron*, *95*(4), 791-807.

82. Gould, E., Woolley, C. S., Frankfurt, M., & McEwen, B. S. (1990). Gonadal steroids regulate dendritic spine density in hippocampal pyramidal cells in adulthood. *Journal of Neuroscience*, *10*(4), 1286-1291.

83. Granon S, Passetti F, Thomas KL, Dalley JW, Everitt BJ, Robbins TW. Enhanced and impaired attentional performance after infusion of D1 dopaminergic receptor agents into rat prefrontal cortex. J Neurosci. 2000; 20(3):1208–1215.

84. Gratton C, Laumann TO, Nielsen AN, Greene DJ, Gordon EM, Gilmore AW, Nelson SM, Coalson RS, Snyder AZ, Schlaggar BL, Dosenbach NUF, Petersen SE. Functional brain networks are dominated by stable group and individual factors, not cognitive or daily variation. Neuron. 2018a; 98(2):439–452.

85. Gratton C, Sun H, Petersen SE. Control networks and hubs. Psychophysiology. 2018b; 55(3).

86. Gratton, C., & Braga, R. M. (2021). Editorial overview: Deep imaging of the individual brain: past, practice, and promise. *Current Opinion in Behavioral Sciences*, *40*, iii-vi.

87. Greendale, G. A., Derby, C. A., & Maki, P. M. (2011). Perimenopause and cognition. *Obstetrics and Gynecology Clinics*, *38*(3), 519-535.

88. Greicius MD, Flores BH, Menon V, Glover GH, Solvason HB, Kenna H, Reiss AL, Schatzberg AF. Resting-state functional connectivity in major depression: Abnormally increased contributions from subgenual cingulate cortex and thalamus. Biol Psychiatry. 2007; 62(5):429–437.

89. Greicius, M. D., Srivastava, G., Reiss, A. L., & Menon, V. (2004). Default-mode network activity distinguishes Alzheimer's disease from healthy aging: evidence from functional MRI. *Proceedings of the National Academy of Sciences*, *101*(13), 4637-4642.

90. Grober, E., Sliwinsk, M., & Korey, S. R. (1991). Development and validation of a model for estimating premorbid verbal intelligence in the elderly. *Journal of clinical and experimental neuropsychology*, *13*(6), 933-949.

91. Haim, A., Julian, D., Albin-Brooks, C., Brothers, H. M., Lenz, K. M., & Leuner, B. (2017). A survey of neuroimmune changes in pregnant and postpartum female rats. Brain, behavior, and immunity, 59, 67-78.

92. Hallquist MN, Hillary FG. Graph theory approaches to functional network organization in brain disorders: A critique for a brave new small-world. Netw Neurosci. 2019; 3(1):1–26.

93. Hampson E, Levy-Cooperman N, Korman JM. Estradiol and mental rotation: Relation to dimensionality, difficulty, or angular disparity? Horm Behav. 2014; 65(3):238–248.

94. Hampson E, Morley EE. Estradiol concentrations and working memory performance in women of reproductive age. Psychoneuroendocrinology. 2013; 38(12):2897–2904.

95. Hao J, Rapp PR, Leffler AE, Leffler SR, Janssen WGM, Lou W, McKay H, Roberts JA, Wearne SL, Hof PR, Morrison JH. Estrogen alters spine number and morphology in prefrontal cortex of aged female rhesus monkeys. J Neurosci. 2006; 26(9):2571–2578.

96. Hara Y, Waters EM, McEwen BS, Morrison JH. Estrogen effects on cognitive and synaptic health over the lifecourse. Physiol Rev. 2015; 95(3):785–807.

97. Hara, Y., Park, C. S., Janssen, W. G., Roberts, M. T., Morrison, J. H., & Rapp, P. R. (2012). Synaptic correlates of memory and menopause in the hippocampal dentate gyrus in rhesus monkeys. *Neurobiology of aging*, *33*(2), 421-e17.

98. Harlow, S. D., Gass, M., Hall, J. E., Lobo, R., Maki, P., Rebar, R. W., ... & STRAW+ 10 Collaborative Group. (2012). Executive summary of the Stages

of Reproductive Aging Workshop+ 10: addressing the unfinished agenda of staging reproductive aging. *Climacteric*, *15*(2), 105-114.

99. Herbert, J., & Lucassen, P. J. (2016). Depression as a risk factor for Alzheimer's disease: Genes, steroids, cytokines and neurogenesis–What do we need to know?. *Frontiers in neuroendocrinology*, *41*, 153-171.

100. Hjelmervik H, Hausmann M, Osnes B, Westerhausen R, Specht K. Resting states are resting traits—An FMRI study of sex differences and menstrual cycle effects in resting state cognitive control networks. PLOS ONE. 2014; 9(7):e103492.

101. Hoekzema, E., Barba-Müller, E., Pozzobon, C., Picado, M., Lucco, F., García-García, D., Soliva, J. C., Tobeña, A., Desco, M., Crone, E. A., Ballesteros, A., Carmona, S., & Vilarroya, O. (2017). Pregnancy leads to long-lasting changes in human brain structure. *Nature Neuroscience*, *20*(2), 287–296.

102. Hoekzema, E., van Steenbergen, H., Straathof, M., Beekmans, A., Freund, I. M., Pouwels, P. J. W., & Crone, E. A. (2022). Mapping the effects of pregnancy on resting state brain activity, white matter microstructure, neural metabolite concentrations and grey matter architecture. *Nature Communications*, *13*(1), 6931.

103. Horien C, Shen X, Scheinost D, Constable RT. The individual functional connectome is unique and stable over months to years. Neuroimage. 2019; 189:676–687.

104. Hyvärinen A, Zhang K, Shimizu S, Hoyer PO. Estimation of a Structural Vector Autoregression Model Using Non-Gaussianity. Journal of Machine Learning Research. 2010; 11(56):1709–1731.

105. Jackson, E. A., El Khoudary, S. R., Crawford, S. L., Matthews, K., Joffe, H., Chae, C., & Thurston, R. C. (2016). Hot flash frequency and blood pressure: data from the Study of Women's Health Across the Nation. *Journal of Women's Health*, *25*(12), 1204-1209

106. Jacobs E, D'Esposito M. Estrogen shapes dopamine-dependent cognitive processes: Implications for women's health. J Neurosci. 2011; 31(14):5286–5293.

107. Jacobs EG, Holsen LM, Lancaster K, Makris N, Whitfield-Gabrieli S, Remington A, Weiss B, Buka S, Klibanski A, Goldstein JM. 17beta-estradiol

differentially regulates stress circuitry activity in healthy and depressed women. Neuropsychopharmacology. 2015; 40(3):566–576.

108. Jacobs EG, Weiss B, Makris N, Whitfield-Gabrieli S, Buka SL, Klibanski A, Goldstein JM. Reorganization of functional networks in verbal working memory circuitry in early midlife: The impact of sex and menopausal status. Cereb Cortex. 2016a; 27(5):2857–2870.

109. Jacobs EG, Weiss BK, Makris N, Whitfield-Gabrieli S, Buka SL, Klibanski A, Goldstein JM. Impact of sex and menopausal status on episodic memory circuitry in early midlife. J Neurosci. 2016b; 36(39):10163–10173.

110. Kim J, Frick KM. Distinct effects of estrogen receptor antagonism on object recognition and spatial memory consolidation in ovariectomized mice. Psychoneuroendocrinology. 2017; 85:110–114.

111. Kinsley, C. H., & Lambert, K. G. (2008). Reproduction-induced neuroplasticity: Natural behavioural and neuronal alterations associated with the production and care of offspring. *Journal of neuroendocrinology*, *20*(4), 515-525.

112. Kohl, J., Babayan, B. M., Rubinstein, N. D., Autry, A. E., Marin-Rodriguez, B., Kapoor, V., Miyamishi, K., Zweifel, L. S., Luo, L., Uchida, N., & Dulac, C. (2018). Functional circuit architecture underlying parental behaviour. *Nature*, *556*(7701), Article 7701.

113. Krause DN, Duckles SP, Pelligrino DA. Influence of sex steroid hormones on cerebrovascular function. J Appl Physiol. 2006; 101(4):1252–1261.

114. Kritzer MF, Creutz LM. Region and sex differences in constituent dopamine neurons and immunoreactivity for intracellular estrogen and androgen receptors in mesocortical projections in rats. J Neurosci. 2008; 28(38):9525–9535.

115. Leiva R, Bouchard T, Boehringer H, Abulla S, Ecochard R. Random serum progesterone threshold to confirm ovulation. Steroids. 2015; 101:125–129.

116. Leranth, C., Shanabrough, M., & Redmond Jr, D. E. (2002). Gonadal hormones are responsible for maintaining the integrity of spine synapses in the CA1 hippocampal subfield of female nonhuman primates. *Journal of Comparative Neurology*, *447*(1), 34-42.

117. Lisofsky N, Martensson J, Eckert A, Lindenberger U, Gallinat J, Kuhn S. Hippocampal volume and functional connectivity changes during the female menstrual cycle.Neuroimage. 2015; 118:154–162.

118. Lotze, M., Domin, M., Gerlach, F.H., Gaser, C., Lueders, E., Schmidt, C.O., Neumann, N., 2019. Novel findings from 2,838 Adult Brains on Sex Differences in Gray Matter Brain Volume. Sci. Rep. 9, 1671.

119. Maki, P. M., & Resnick, S. M. (2000). Longitudinal effects of estrogen replacement therapy on PET cerebral blood flow and cognition. *Neurobiology of aging*, *21*(2), 373-383.

120. Maki, P. M., & Thurston, R. C. (2020). Menopause and brain health: hormonal changes are only part of the story. *Frontiers in neurology*, *11*, 1074.

121. Maki, P. M., Dennerstein, L., Clark, M., Guthrie, J., LaMontagne, P., Fornelli, D., ... & Resnick, S. M. (2011). Perimenopausal use of hormone therapy is associated with enhanced memory and hippocampal function later in life. *Brain research*, *1379*, 232-243.

122. Maki, P. M., Wu, M., Rubin, L. H., Fornelli, D., Drogos, L. L., Geller, S., ... & Conant, R. J. (2020). Hot flashes are associated with altered brain function during a memory task. *Menopause*, *27*(3), 269-277.

123. Marek, S., Tervo-Clemmens, B., Calabro, F. J., Montez, D. F., Kay, B. P., Hatoum, A. S., ... & Dosenbach, N. U. (2022). Reproducible brain-wide association studies require thousands of individuals. *Nature*, *603*(7902), 654-660.

124. Martínez-García, M., Paternina-Die, M., Barba-Müller, E., Martín de Blas, D., Beumala, L., Cortizo, R., Pozzobon, C., Marcos-Vidal, L., Fernández-Pena, A., & Picado, M. (2021b). Do Pregnancy-Induced Brain Changes Reverse? The Brain of a Mother Six Years after Parturition. *Brain Sciences*, *11*(2), 168.

125. Martínez-García, M., Paternina-Die, M., Desco, M., Vilarroya, O., & Carmona, S. (2021a). Characterizing the Brain Structural Adaptations Across the Motherhood Transition. *Frontiers in Global Women's Health*, *2*(742775).

126. Mattar MG, Wymbs NF, Bock AS, Aguirre GK, Grafton ST, Bassett DS. Predicting future learning from baseline network architecture. Neuroimage. 2018; 172:107–117.

127. McEwen BS. Redefining neuroendocrinology: Epigenetics of brain-body communication over the life course. Front Neuroendocrinol. 2018; 49:8–30.

128. McEwen, B. S. (2018). Redefining neuroendocrinology: epigenetics of brain-body communication over the life course. *Frontiers in Neuroendocrinology*, *49*, 8-30.

129. Minoshima, S., Giordani, B., Berent, S., Frey, K. A., Foster, N. L., & Kuhl, D. E. (1997). Metabolic reduction in the posterior cingulate cortex in very early Alzheimer's disease. *Annals of Neurology: Official Journal of the American Neurological Association and the Child Neurology Society*, *42*(1), 85-94.

130. Morrison, J. H., Brinton, R. D., Schmidt, P. J., & Gore, A. C. (2006). Estrogen, menopause, and the aging brain: how basic neuroscience can inform hormone therapy in women. *Journal of Neuroscience*, *26*(41), 10332-10348.

131. Morrison, J. H., Brinton, R. D., Schmidt, P. J., & Gore, A. C. (2006). Estrogen, menopause, and the aging brain: how basic neuroscience can inform hormone therapy in women. *Journal of Neuroscience*, *26*(41), 10332-10348.

132. Mosconi, L., Rahman, A., Diaz, I., Wu, X., Scheyer, O., Hristov, H. W., ... & Brinton, R. D. (2018). Increased Alzheimer's risk during the menopause transition: a 3-year longitudinal brain imaging study. *PloS one*, *13*(12), e0207885.

133. Mueller, J. M., Pritschet, L., Santander, T., Taylor, C. M., Grafton, S. T., Jacobs, E. G., & Carlson, J. M. (2021). Dynamic community detection reveals transient reorganization of functional brain networks across a female menstrual cycle. *Network Neuroscience*, *5*(1), 125-144.

134. Nebel, R. A., Aggarwal, N. T., Barnes, L. L., Gallagher, A., Goldstein, J. M., Kantarci, K., ... & Mielke, M. M. (2018). Understanding the impact of sex and gender in Alzheimer's disease: a call to action. *Alzheimer's & Dementia*, *14*(9), 1171-1183.

135. Noble S, Spann MN, Tokoglu F, Shen X, Constable RT, Scheinost D. Influences on the test-retest reliability of functional connectivity MRI and its relationship with behavioral utility. Cerebral Cortex. 2017; 27(11):5415–5429.

136. Ohm, D. T., Bloss, E. B., Janssen, W. G., Dietz, K. C., Wadsworth, S., Lou, W., ... & Morrison, J. H. (2012). Clinically relevant hormone treatments

fail to induce spinogenesis in prefrontal cortex of aged female rhesus monkeys. *Journal of Neuroscience*, *32*(34), 11700-11705.

137. Orchard, E. R., Rutherford, H. J. V., Holmes, A. J., & Jamadar, S. D. (2023). Matrescence: Lifetime impact of motherhood on cognition and the brain. *Trends in Cognitive Sciences*.

138. Orchard, E. R., Ward, P. G. D., Chopra, S., Storey, E., Egan, G. F., & Jamadar, S. D. (2020). Neuroprotective Effects of Motherhood on Brain Function in Late Life: A Resting-State fMRI Study. *Cerebral Cortex*, 1270-1283.

139. Palmqvist, S., Schöll, M., Strandberg, O., Mattsson, N., Stomrud, E., Zetterberg, H., ... & Hansson, O. (2017). Earliest accumulation of β-amyloid occurs within the default-mode network and concurrently affects brain connectivity. *Nature communications*, *8*(1), 1214

140. Palombo, D. J., Amaral, R. S., Olsen, R. K., Müller, D. J., Todd, R. M., Anderson, A. K., & Levine, B. (2013). KIBRA polymorphism is associated with individual differences in hippocampal subregions: evidence from anatomical segmentation using high-resolution MRI. *Journal of Neuroscience*, *33*(32), 13088-13093.

141. Pascoal, T. A., Mathotaarachchi, S., Kang, M. S., Mohaddes, S., Shin, M., Park, A. Y., ... & Rosa-Neto, P. (2019). Aβ-induced vulnerability propagates via the brain's default mode network. *Nature communications*, *10*(1), 2353.

142. Pasqualini C, Olivier V, Guibert B, Frain O, Leviel V. Acute stimulatory effect of estradiol on striatal dopamine synthesis. J Neurochem. 1995; 65(4):1651–1657.

143. Patel AX, Bullmore ET. A wavelet-based estimator of the degrees of freedom in denoised fMRI time series for probabilistic testing of functional connectivity and brain graphs. Neuroimage. 2016; 142:14–26.

144. Paternina-Die, M., Martínez-García, M., de Blas, D. M., Noguero, I., Servin-Servet, C., Pretus, C., ... & Carmona, S. (2023). Women's neuroplasticity during gestation, childbirth, and postpartum (preprint). https://doi.org/10.21203/rs.3.rs-2723150/v1

145. Pawluski, J. L., Hoekzema, E., Leuner, B., & Lonstein, J. S. (2021). Less Can Be More: Fine Tuning the Maternal Brain. *Neuroscience &*

Biobehavioral Reviews.

146. Pawluski, Jodi L., Joseph S. Lonstein, and Alison S. Fleming. "The neurobiology of postpartum anxiety and depression." Trends in Neurosciences 40.2 (2017): 106-120.

147. Petersen N, Kilpatrick LA, Goharzad A, Cahill L. Oral contraceptive pill use and menstrual cycle phase are associated with altered resting state functional connectivity. Neuroimage. 2014; 90:24–32.

148. Pletzer, B., Harris, T. A., Scheuringer, A., & Hidalgo-Lopez, E. (2019). The cycling brain: menstrual cycle related fluctuations in hippocampal and fronto-striatal activation and connectivity during cognitive tasks. *Neuropsychopharmacology*, *44*(11), 1867-1875.

149. Plotsky PM, Owens MJ, Nemeroff CB. Psychoneuroendocrinology of depression: hypothalamic-pituitary-adrenal axis. Psychiatr Clin North Am. 1998; 21(2):293–307.

150. Poldrack RA, Laumann TO, Koyejo O, Gregory B, Hover A, Chen MY, Gorgolewski KJ,Luci J, Joo SJ, Boyd RL, Hunicke-Smith S, Simpson ZB, Caven T, Sochat V, Shine JM, Gordon E, Snyder AZ, Adeyemo B, Petersen SE, Glahn DC, et al. Long-term neural and physiological phenotyping of a single human. Nat Commun. 2015; 6:8885.

151. Pollock V, Cho DW, Reker D, Volavka J. Profile of mood states: the factors and their physiological correlates. J Nerv Ment Dis. 1979; 167(10):612–614.

152. Prendergast, B. J., Onishi, K. G., & Zucker, I. (2014). Female mice liberated for inclusion in neuroscience and biomedical research. *Neuroscience & Biobehavioral Reviews*, *40*, 1-5.

153. Pritschet, L., Santander, T., Taylor, C. M., Layher, E., Yu, S., Miller, M. B., ... & Jacobs, E. G. (2020). Functional reorganization of brain networks across the human menstrual cycle. *Neuroimage*, *220*, 117091.

154. Pritschet, L., Taylor, C. M., Santander, T., & Jacobs, E. G. (2021). Applying dense-sampling methods to reveal dynamic endocrine modulation of the nervous system. *Current opinion in behavioral sciences*, *40*, 72-78.

155. Protopopescu, X., Butler, T., Pan, H., Root, J., Altemus, M., Polanecsky, M., ... & Stern, E. (2008). Hippocampal structural changes across the menstrual cycle. *Hippocampus*, *18*(10), 985-988.

156. Puri, T. A., Richard, J. E., & Galea, L. A. M. (2023). Beyond sex differences: Short- and long-term effects of pregnancy on the brain. *Trends in Neurosciences*.

157. Qiu, L. R., Germann, J., Spring, S., Alm, C., Vousden, D. A., Palmert, M. R., & Lerch, J. P. (2013). Hippocampal volumes differ across the mouse estrous cycle, can change within 24 hours, and associate with cognitive strategies. *Neuroimage*, *83*, 593-598.

158. Rahman, A., Schelbaum, E., Hoffman, K., Diaz, I., Hristov, H., Andrews, R., ... & Mosconi, L. (2020). Sex-driven modifiers of Alzheimer risk: a multimodality brain imaging study. *Neurology*, *95*(2), e166-e178.

159. Rapp, P. R., Morrison, J. H., & Roberts, J. A. (2003). Cyclic estrogen replacement improves cognitive function in aged ovariectomized rhesus monkeys. *Journal of neuroscience*, *23*(13), 5708-5714.

160. Rechlin, R. K., Splinter, T. F., Hodges, T. E., Albert, A. Y., & Galea, L. A. (2022). An analysis of neuroscience and psychiatry papers published from 2009 and 2019 outlines opportunities for increasing discovery of sex differences. *Nature communications*, *13*(1), 2137.

161. Ritchie, S.J., Cox, S.R., Shen, X., Lombardo, M.V., Reus, L.M., Alloza, C., Harris, M.A., Alderson, H.L., Hunter, S., Neilson, E., Liewald, D.C.M., Auyeung, B., Whalley, H.C., Lawrie, S.M., Gale, C.R., Bastin, M.E., McIntosh, A.M., Deary, I.J., 2018. Sex Differences in the Adult Human Brain: Evidence from 5216 UK Biobank Participants. Cereb. Cortex 28, 2959–2975.

162. Rubinov M, Sporns O. Complex network measures of brain connectivity: Uses and interpretations. Neuroimage. 2010 Sep; 52(3):1059–1069.

163. Rubinow DR, Schmidt PJ. Gonadal steroid regulation of mood: the lessons of premenstrual syndrome. Front Neuroendocrinol. 2006; 27(2):210–216.

164. Rubinow, D. R., & Schmidt, P. J. (2019). Sex differences and the neurobiology of affective disorders. *Neuropsychopharmacology*, *44*(1), 111-128.

165. Sacher, J., Neumann, J., Okon-Singer, H., Gotowiec, S., Villringer, A., 2013. Sexual dimorphism in the human brain: evidence from neuroimaging. Magn. Reson. Imaging 31, 366–375.

166. Salehi M, Greene AS, Karbasi A, Shen X, Scheinost D, Constable RT. There is no single functional atlas even for a single individual: Functional parcel definitions change with task. NeuroImage. 2020; 208:116366.

167. Salehi M, Karbasi A, Barron DS, Scheinost D, Constable RT. Individualized functional networks reconfigure with cognitive state. Neuroimage. 2020; 206:116233.

168. Satterthwaite, T. D., Shinohara, R. T., Wolf, D. H., Hopson, R. D., Elliott, M. A., Vandekar, S. N., ... & Gur, R. E. (2014). Impact of puberty on the evolution of cerebral perfusion during adolescence. *Proceedings of the National Academy of Sciences*, *111*(23), 8643-8648.

169. Scalabrini, A., Vai, B., Poletti, S., Damiani, S., Mucci, C., Colombo, C., ... & Northoff, G. (2020). All roads lead to the default-mode network—global source of DMN abnormalities in major depressive disorder. *Neuropsychopharmacology*, *45*(12), 2058-2069.

170. Schaefer A, Kong R, Gordon EM, Laumann TO, Zuo XN, Holmes AJ, Eickhoff SB, Yeo BTT. Local-global parcellation of the human cerebral cortex from intrinsic functional connectivity MRI. Cereb Cortex. 2018; 28(9):3095–3114.

171. Schaefer, A., Kong, R., Gordon, E. M., Laumann, T. O., Zuo, X. N., Holmes, A. J., ... & Yeo, B. T. (2018). Local-global parcellation of the human cerebral cortex from intrinsic functional connectivity MRI. Cerebral cortex, 28(9), 3095-3114.

172. Scheinost, D., Finn, E. S., Tokoglu, F., Shen, X., Papademetris, X., Hampson, M., & Constable, R. T. (2015). Sex differences in normal age trajectories of functional brain networks. *Human brain mapping*, *36*(4), 1524-1535.

173. Schiller, C. E., Johnson, S. L., Abate, A. C., Schmidt, P. J., & Rubinow, D. R. (2016). Reproductive steroid regulation of mood and behavior. *Comprehensive Physiology*, *6*(3), 1135.

174. Schmidt PJ, Rubinow DR. Sex hormones and mood in the perimenopause. Ann N YAcad Sci. 2009; 1179:70–85.

175. Schmidt, P. J., Martinez, P. E., Nieman, L. K., Koziol, D. E., Thompson, K. D., Schenkel, L., ... & Rubinow, D. R. (2017). Premenstrual dysphoric disorder symptoms following ovarian suppression: triggered by change in ovarian steroid levels but not continuous stable levels. *American Journal of Psychiatry*, *174*(10), 980-989.

176. Seeley WW, Menon V, Schatzberg AF, Keller J, Glover GH, Kenna H, Reiss AL, Greicius MD. Dissociable intrinsic connectivity networks for salience processing and executive control. J Neurosci. 2007; 27(9):2349–2356.

177. Seeley, W. W., Crawford, R. K., Zhou, J., Miller, B. L., & Greicius, M. D. (2009). Neurodegenerative diseases target large-scale human brain networks. *Neuron*, *62*(1), 42-52.

178. Seitzman BA, Gratton C, Laumann TO, Gordon EM, Adeyemo B, Dworetsky A, Kraus BT, Gilmore AW, Berg JJ, Ortega M, Nguyen A, Greene DJ, McDermott KB, Nelson SM, Lessov-Schlaggar CN, Schlaggar BL, Dosenbach NUF, Petersen SE. Trait-like variants in human functional brain networks. Proc Natl Acad Sci USA. 2019; 116(45):22851–22861.

179. Sellers, K. J., Erli, F., Raval, P., Watson, I. A., Chen, D., & Srivastava, D. P. (2015). Rapid modulation of synaptogenesis and spinogenesis by 17β-estradiol in primary cortical neurons. *Frontiers in cellular neuroscience*, *9*, 137.

180. Shanmugan S, Epperson CN. Estrogen and the prefrontal cortex: towards a new understanding of estrogen's effects on executive functions in the menopause transition. Hum Brain Mapp. 2014; 35(3):847–865.

181. Shaywitz, S. E., Shaywitz, B. A., Pugh, K. R., Fulbright, R. K., Skudlarski, P., Mencl, W. E., ... & Gore, J. C. (1999). Effect of estrogen on brain activation patterns in postmenopausal women during working memory tasks. *Jama*, *281*(13), 1197-1202.

182. Shehata, H. A., & Okosun, H. (2004). Neurological disorders in pregnancy. *Current Opinion in Obstetrics and Gynecology*, *16*(2), 117-122.

183. Sheppard PAS, Choleris E, Galea LAM. Structural plasticity of the hippocampus in response to estrogens in female rodents. Mol Brain. 2019; 12(1):22.

184. Spielberger CD, Vagg PR. Psychometric properties of the STAI: A reply to Ramanaiah, Franzen, and Schill. J Pers Assess. 1984; 48(1):95–97.

185. Stam, C. J. (2014). Modern network science of neurological disorders. *Nature Reviews Neuroscience*, *15*(10), 683-695.

186. Syan, S. K., Minuzzi, L., Costescu, D., Smith, M., Allega, O. R., Coote, M., ... & Frey, B. N. (2017). Influence of endogenous estradiol, progesterone, allopregnanolone, and dehydroepiandrosterone sulfate on brain resting state functional connectivity across the menstrual cycle. *Fertility and sterility*, *107*(5), 1246-1255.

187. Taxier, L. R., Gross, K. S., & Frick, K. M. (2020). Oestradiol as a neuromodulator of learning and memory. *Nature Reviews Neuroscience*, *21*(10), 535-550.

188. Taylor CM, Pritschet L, Yu S, Jacobs EG. Applying a women's health lens to the study of the aging brain. Front Hum Neurosci. 2019; 13:224.

189. Taylor, C. M., Pritschet, L., & Jacobs, E. G. (2021). The scientific body of knowledge–Whose body does it serve? A spotlight on oral contraceptives and women's health factors in neuroimaging. *Frontiers in neuroendocrinology*, *60*, 100874.

190. Taylor, C. M., Pritschet, L., Olsen, R. K., Layher, E., Santander, T., Grafton, S. T., & Jacobs, E. G. (2020). Progesterone shapes medial temporal lobe volume across the human menstrual cycle. *NeuroImage*, *220*, 117125.

191. Thomason, M. E. (2020). Development of brain networks in utero: relevance for common neural disorders. *Biological Psychiatry*, *88*(1), 40-50.

192. Thompson TL, Moss RL. Estrogen regulation of dopamine release in the nucleus accumbens: genomic- and nongenomic-mediated effects. J Neurochem. 1994; 62(5):1750–1756.

193. Thornburg, K. L., Bagby, S. P., & Giraud, G. D. (2015). Maternal Adaptations to Pregnancy. In *Knobil and Neill's Physiology of Reproduction* (pp. 1927–1955). Elsevier, Inc.

194. Thurston, R. C., Wu, M., Chang, Y. F., Aizenstein, H. J., Derby, C. A., Barinas-Mitchell, E. A., & Maki, P. (2023). Menopausal vasomotor symptoms and white matter hyperintensities in midlife women. *Neurology*, *100*(2), e133-e141.

195. Tooley, U.A., Bassett, D.S., & Mackey, A.P. (2021). Environmental influences on the pace of brain development. Nature Reviews Neuroscience, 22, 372-384.

196. Tustison, N. J., Cook, P. A., Klein, A., Song, G., Das, S. R., Duda, J. T., ... & Avants, B. B. (2014). Large-scale evaluation of ANTs and FreeSurfer cortical thickness measurements. Neuroimage, 99, 166-179.

197. Van Dijk KR, Hedden T, Venkataraman A, Evans KC, Lazar SW, Buckner RL. Intrinsic functional connectivity as a tool for human

connectomics: Theory, properties, and optimization. Journal of Neurophysiology. 2010; 103(1):297–321.

198. Vijayraghavan S, Wang M, Birnbaum SG, Williams GV, Arnsten AFT. Inverted-U dopamine D1 receptor actions on prefrontal neurons engaged in working memory. Nat Neurosci. 2007; 10(3):376–384.

199. Wang ACJ, Hara Y, Janssen WGM, Rapp PR, Morrison JH. Synaptic estrogen receptor-alpha levels in prefrontal cortex in female rhesus monkeys and their correlation with cognitive performance. J Neurosci. 2010; 30(38):12770–12776.

200. Wang, H., Suh, J. W., Das, S. R., Pluta, J. B., Craige, C., & Yushkevich, P. A. (2012). Multi-atlas segmentation with joint label fusion. IEEE transactions on pattern analysis and machine intelligence, 35(3), 611-623.

201. Wang, Z., Liu, J., Shuai, H., Cai, Z., Fu, X., Liu, Y., ... & Yang, B. X. (2021). Mapping global prevalence of depression among postpartum women. *Translational psychiatry*, *11*(1), 543.

202. Warren SG, Juraska JM. Spatial and nonspatial learning across the rat estrous cycle. Behav Neurosci. 1997; 111(2):259–266.

203. Weis S, Hodgetts S, Hausmann M. Sex differences and menstrual cycle effects in cognitive and sensory resting state networks. Brain and cognition. 2019; 131:66–73.

204. Wilkinson, M., & Brown, R. E. (2015). *An introduction to neuroendocrinology*. Cambridge University Press.

205. Williams GV, Goldman-Rakic PS. Modulation of memory fields by dopamine D1 receptors in prefrontal cortex. Nature. 1995; 376(6541):572–575.

206. Williams, G. V., & Goldman-Rakic, P. S. (1995). Modulation of memory fields by dopamine Dl receptors in prefrontal cortex. *Nature*, *376*(6541), 572-575.

207. Woolley CS, McEwen BS. Roles of estradiol and progesterone in regulation of hippocampal dendritic spine density during the estrous cycle in the rat. J Comp Neurol. 1993; 336(2):293–306.

208. Woolley, C. S., & McEwen, B. S. (1992). Estradiol mediates fluctuation in hippocampal synapse density during the estrous cycle in the adult rat [published erratum appears in J Neurosci 1992 Oct; 12 (10)

209. Workman, J. L., Barha, C. K., & Galea, L. A. (2012). Endocrine substrates of cognitive and affective changes during pregnancy and postpartum. *Behavioral neuroscience*, *126*(1), 54

210. World Health Organization (2022). "*Maternal, newborn, child and adolescent health and ageing"*

211. Yeh, F. C., & Tseng, W. Y. I. (2011). NTU-90: a high angular resolution brain atlas constructed by q-space diffeomorphic reconstruction. *Neuroimage*, *58*(1), 91-99.

212. Yeh, F. C., Badre, D., & Verstynen, T. (2016). Connectometry: a statistical approach harnessing the analytical potential of the local connectome. *Neuroimage*, *125*, 162-171

213. Yeo, B. T., Krienen, F. M., Sepulcre, J., Sabuncu, M. R., Lashkari, D., Hollinshead, M., ... & Buckner, R. L. (2011). The organization of the human cerebral cortex estimated by intrinsic functional connectivity. Journal of neurophysiology, 106(3), 1125-1165.

214. Young EA, Kornstein SG, Harvey AT, Wisniewski SR, Barkin J, Fava M, Trivedi MH, Rush AJ. Influences of hormone-based contraception on depressive symptoms in premenopausal women with major depression. Psychoneuroendocrinology. 2007; 32(7):843–853.

215. Young EA, Korszun A. The hypothalamic-pituitary-gonadal axis in mood disorders. Endocrinol Metab Clin North Am. 2002; 31(1):63–78.

216. Yushkevich, P. A., Piven, J., Hazlett, H. C., Smith, R. G., Ho, S., Gee, J. C., & Gerig, G. (2006). User-guided 3D active contour segmentation of anatomical structures: significantly improved efficiency and reliability. *Neuroimage*, *31*(3), 1116-1128.

217. Yushkevich, P. A., Pluta, J. B., Wang, H., Xie, L., Ding, S. L., Gertje, E. C., ... & Wolk, D. A. (2015). Automated volumetry and regional thickness analysis of hippocampal subfields and medial temporal cortical structures in mild cognitive impairment. *Human brain mapping*, *36*(1), 258-287.

218. Zeydan B, Tosakulwong N, Schwarz CG, Senjem ML, Gunter JL, Reid RI, Gazzuola Rocca, L, Lesnick TG, Smith CY, Bailey KR, Lowe VJ, Roberts RO, Jack CRJ, Petersen RC, Miller VM, Mielke MM, Rocca WA, Kantarci K. Association of bilateral salpingo-oophorectomy before menopause onset with medial temporal lobe neurodegeneration. JAMA Neurol. 2019; 76(1):95–100.

219. Zsido, R. G., Heinrich, M., Slavich, G. M., Beyer, F., Masouleh, S. K., Kratzsch, J., ... & Sacher, J. (2019). Association of estradiol and visceral fat with structural brain networks and memory performance in adults. *JAMA network open*, *2*(6), e196126-e196126.

Appendix A

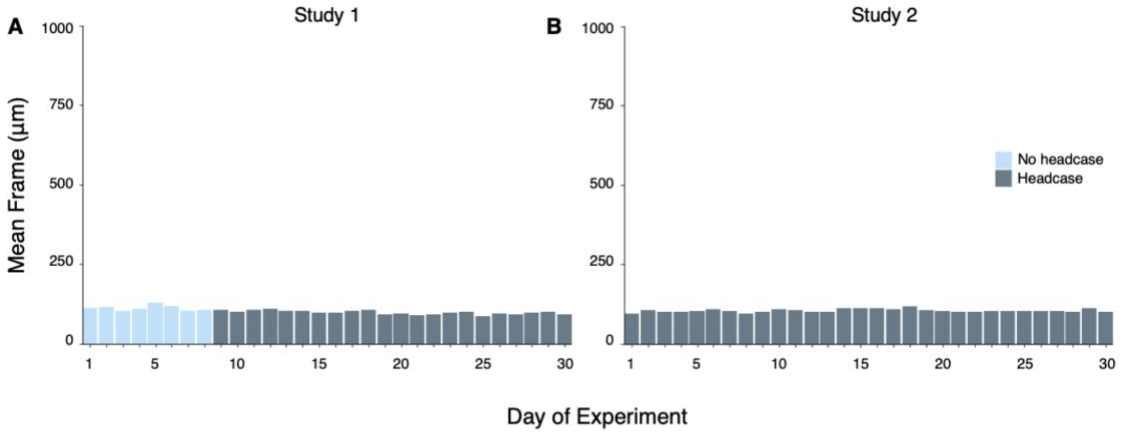

Figure S1. Head motion (mean framewise displacement) across each 30-day experiment. In Study 1 (**A**), motion on days 1-8 was limited using ample head and neck padding; on days 9-30, motion was limited using a molded headcase custom-fit to the participant's head. For both Study 1 and 2, mean framewise displacement did not exceed 130 microns.

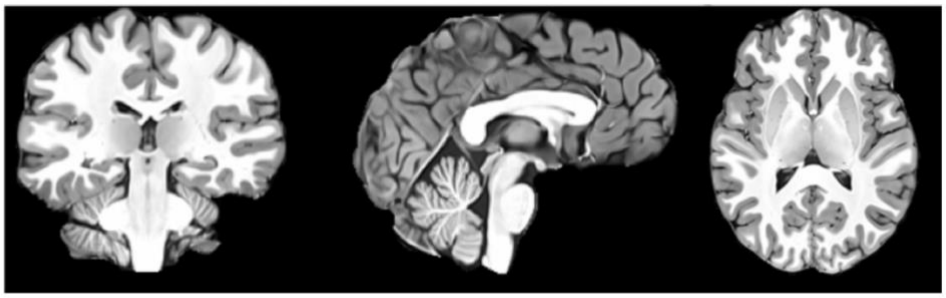

Figure S2. Subject-specific anatomical template. Functional images were registered to a subject-specific anatomical template space, created with Advanced Normalization Tools' multivariate template construction. All 30 high-resolution T_1 MPRAGE scans from Study 1 were used.

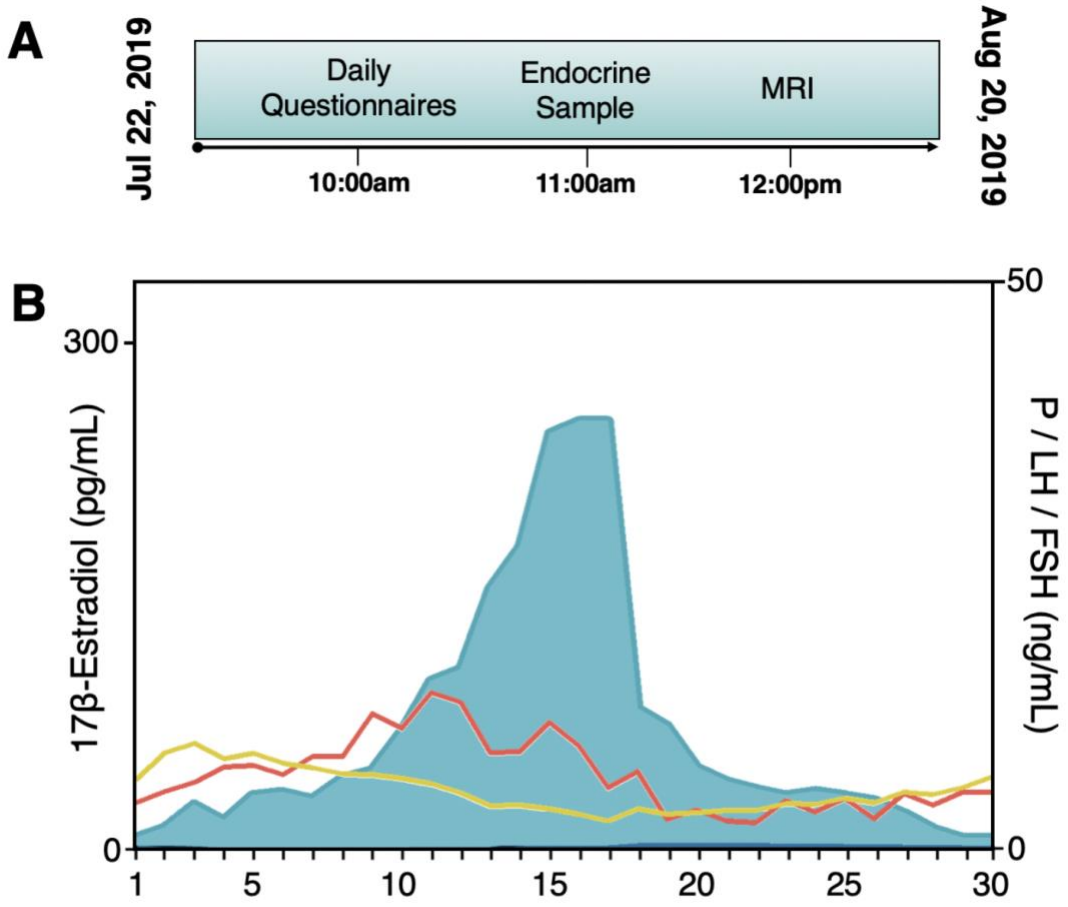

Figure S3. Experiment timeline and hormone concentrations in Study 2. (A) Endocrine and MRI data acquisition were again time-locked each day for 30 consecutive days. **(B)** Levels of estradiol (light blue), LH (red) and FSH (yellow) over the course of the experiment. Note that, while progesterone (dark blue) was pharmacologically suppressed, estradiol maintained a similar pattern of fluctuation as seen in Study 1.

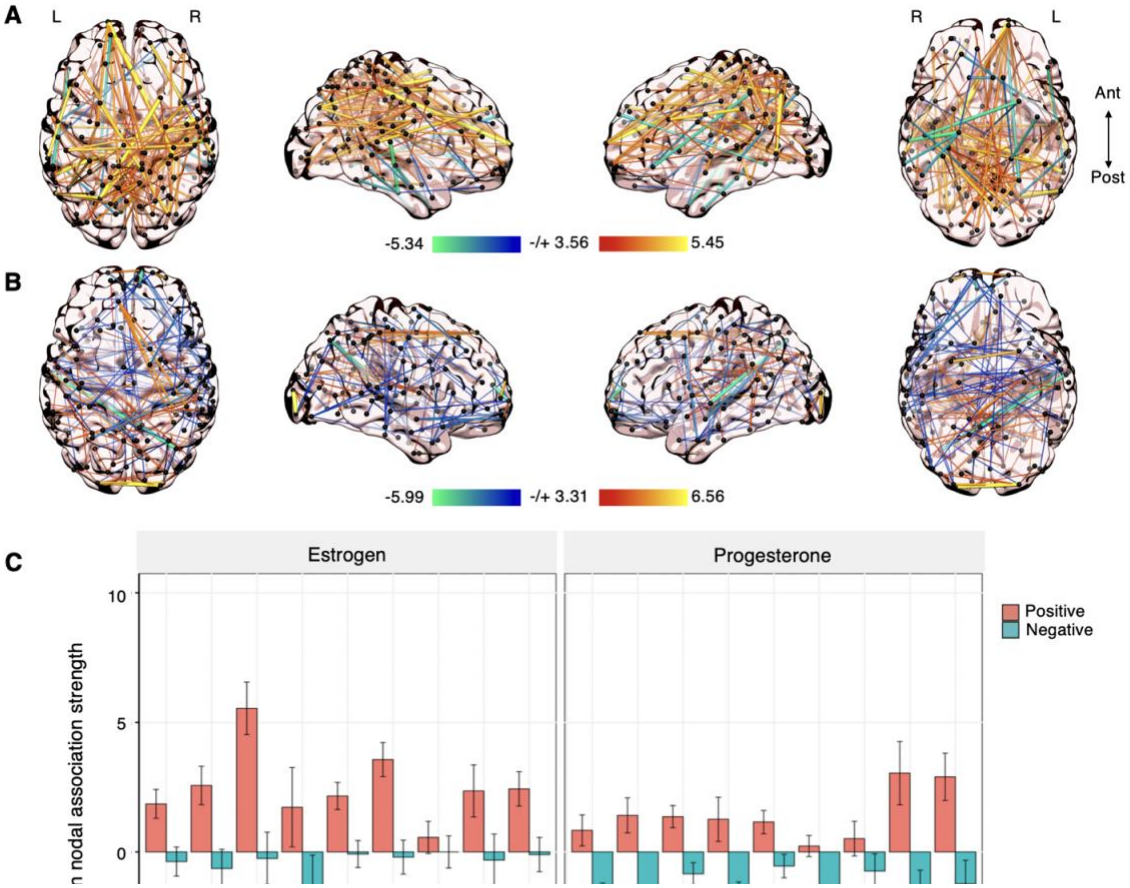

Figure S4. **Whole-brain network similarity by stage of menstrual cycle.** (A) Experiment days were divided into follicular (left) and luteal (right) stages of the cycle, and unthresholded coherence matrices were pairwise correlated with each other in order to assess inter-scan similarity in whole-brain patterns of connectivity. Fisher-Z transformed estimates are given. This revealed one session (experiment day 26) in the luteal stage that was markedly dissimilar relative to other days. (B) Mean nodal association strengths by network and hormone, after removing day 26 from the analysis shown in Figure 4. Critically, results were robust to this exclusion, suggesting no strong dependence on this session.

edge-to-edge reliability ($r = 0.61$). **(C)** While the average magnitude of brain-hormone associations differed in some networks, the overall trends remained: namely, that estradiol was associated with widespread increases in coherence.

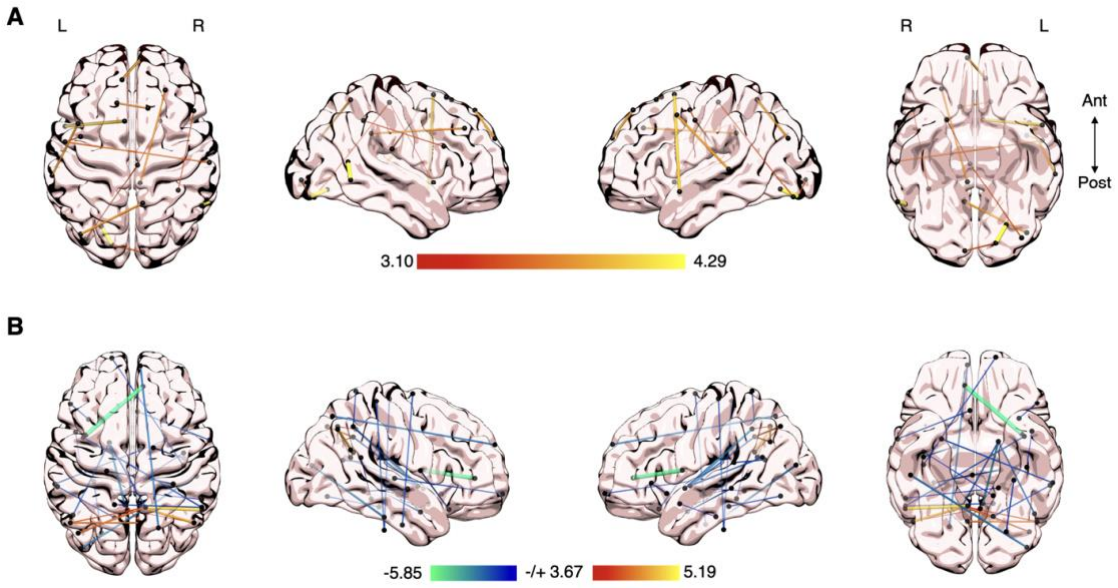

Figure S6. **The ovulatory surge in estradiol is a key modulator of whole-brain functional connectivity.** (A) Removal of the ovulation window in Study 1 (experiment days 22-24) almost entirely erases all significant associations between estradiol and edgewise coherence. (B) Removing analogously high estradiol days in Study 2 (experiment days 28-30) also has a strongly diminishing effect.

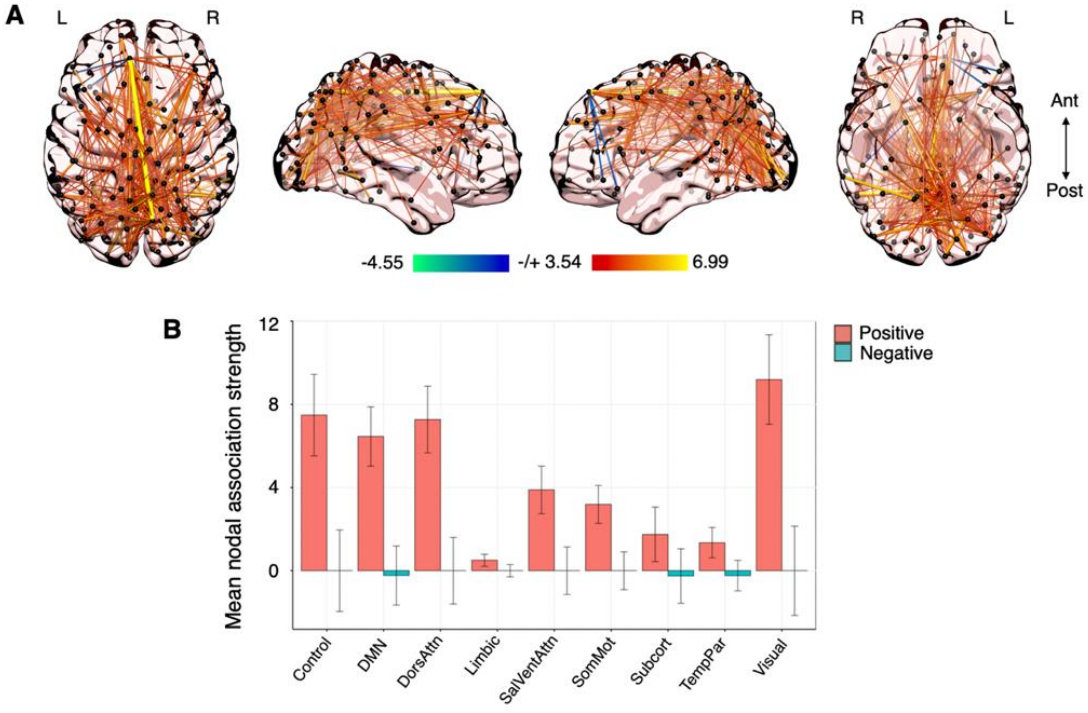

Figure S7. Whole-brain associations between coherence and estradiol persist in a replication sample (Study 2). (A) Time-synchronous associations between estradiol and coherence while progesterone was pharmacologically suppressed. Hotter colors indicate increased coherence with higher concentrations of estradiol; cool colors indicate the reverse. Results are empirically-thresholded via 10,000 iterations of nonparametric permutation testing ($p < .001$). Nodes without significant edges are omitted for clarity. **(B)** Mean nodal association strengths by network (with 95% CIs): increased concentrations of estradiol were again coincident with ubiquitous increases in resting connectivity.

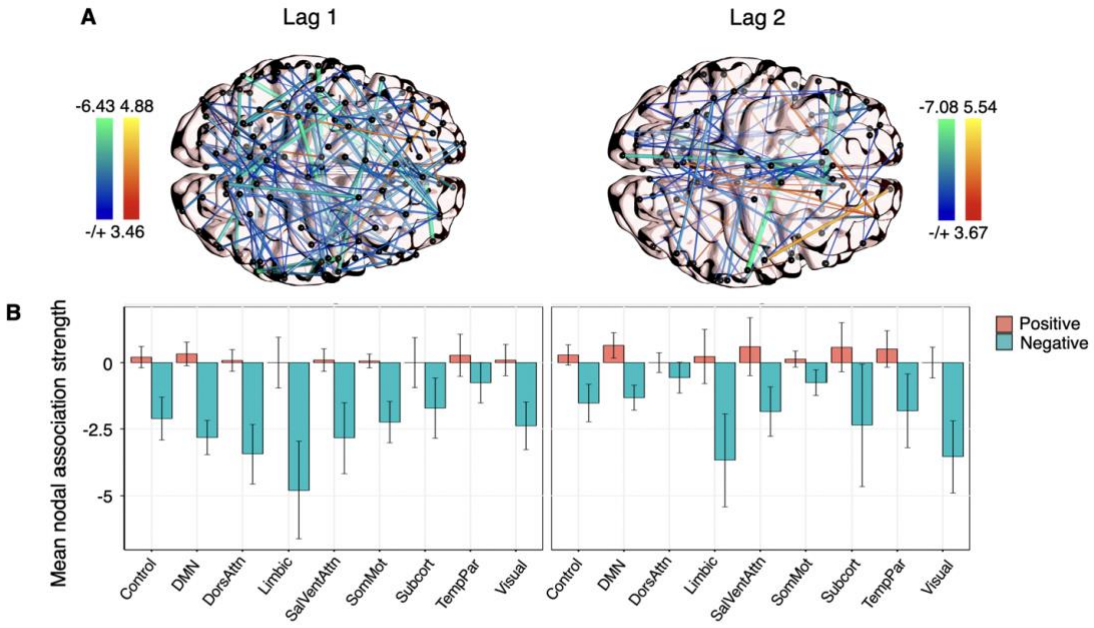

Figure S9. Estradiol shows linear dependencies on previous states of coherence (Study 1). (A) Time-lagged associations between estradiol and previous states of coherence at lag 1 (*left*) and lag 2 (*right*), derived from edgewise vector autoregressive models. Hotter colors indicate a predicted increase in estradiol given previous states of coherence; cool colors indicate the reverse. Results are empirically-thresholded via 10,000 iterations of nonparametric permutation testing ($p < .001$). Nodes without significant edges are omitted for clarity. **(B)** Mean nodal association strengths by network and time lag. Error bars give 95% confidence intervals.

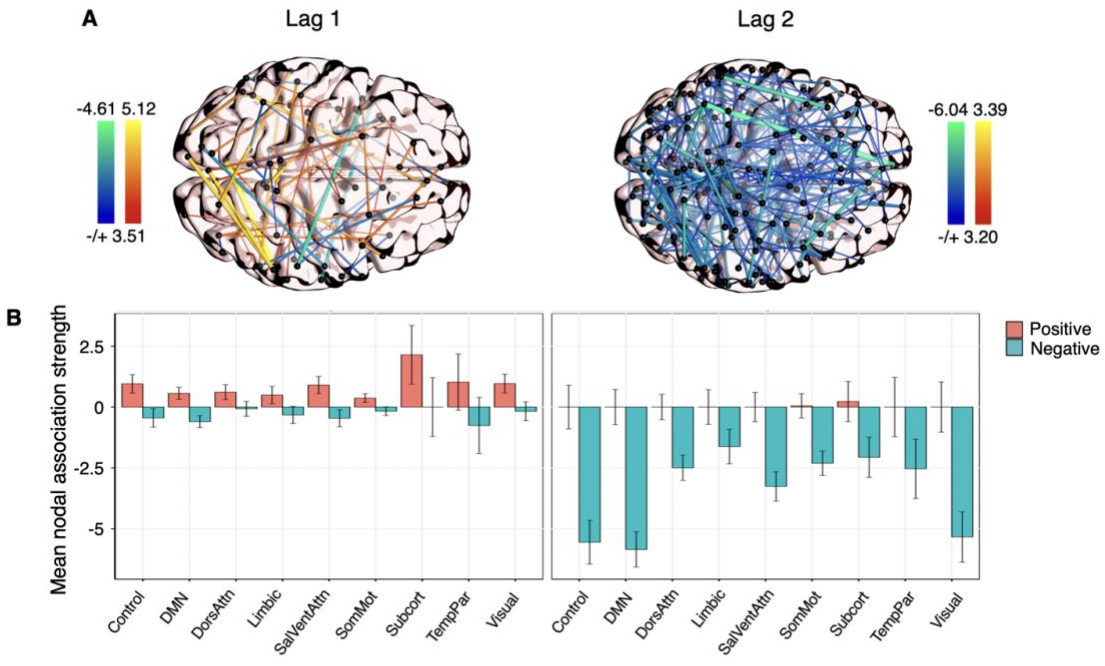

Figure S10. Autoregressive effects of edgewise coherence (Study 2). (A) Autoregressive trends in coherence at lag 1 (*left*) and lag 2 (*right*), derived from edgewise vector autoregressive models. Hotter colors indicate a predicted increase in coherence given previous states of connectivity; cool colors indicate the reverse. Results are empirically-thresholded via 10,000 iterations of nonparametric permutation testing ($p < .001$). Nodes without significant edges are omitted for clarity. **(B)** Mean nodal association strengths by network and time lag. Error bars give 95% confidence intervals.

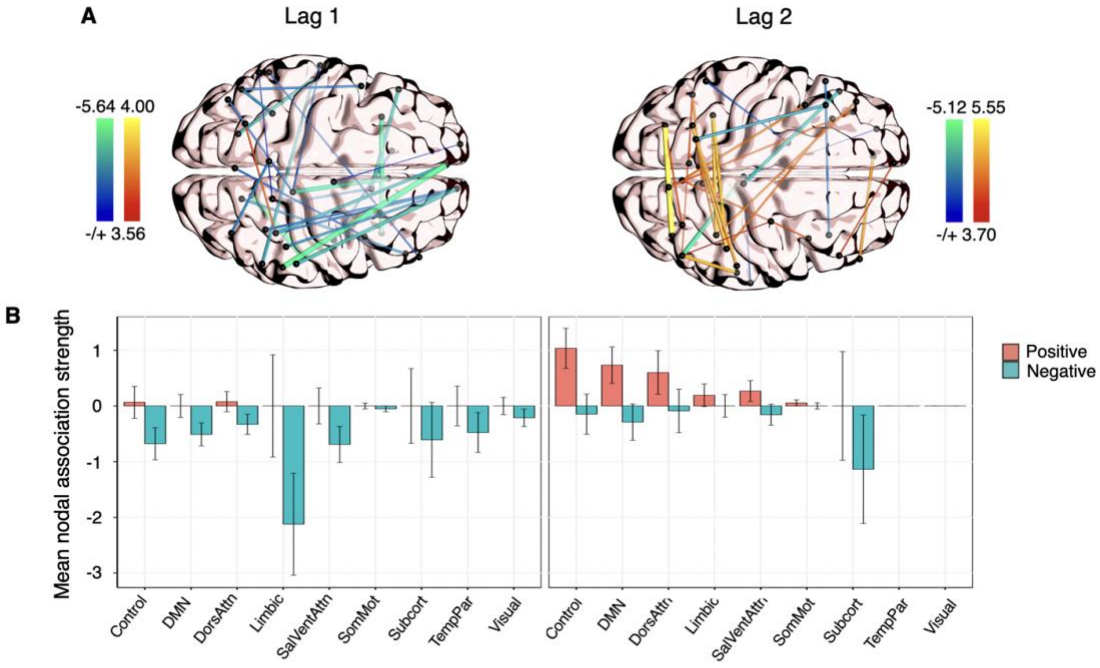

Figure S11. Estradiol shows linear dependencies on previous states of coherence (Study 2). (A) Time-lagged associations between estradiol and previous states of coherence at lag 1 (*left*) and lag 2 (*right*), derived from edgewise vector autoregressive models. Hotter colors indicate a predicted increase in estradiol given previous states of coherence; cool colors indicate the reverse. Results are empirically-thresholded via 10,000 iterations of nonparametric permutation testing ($p < .001$). Nodes without significant edges are omitted for clarity. **(B)** Mean nodal association strengths by network and time lag. Error bars give 95% confidence intervals.

Table S1. All VAR models for cross-network participation v. estradiol (Study 1).

Network	Outcome	Predictor	Estimate	*SE*	*T* (*p*)
Control	Participation	**Constant**	**0.11**	**0.18**	**0.62 (.048)**
		FCN_{t-1}	-0.15	0.19	-0.80 (.430)
		$Estradiol_{t-1}$	**-0.58**	**0.26**	**-2.21 (.036)**
		FCN_{t-2}	-0.18	0.18	-0.97 (.334)
		$Estradiol_{t-2}$	0.40	0.27	1.49 (.152)
			R^2 = 0.22 (*p* = .199); *RMSE* = 0.85 (*p* = .183)		
	Estradiol	Constant	0.01	0.12	0.11 (.691)
		FCN_{t-1}	-0.04	0.13	-0.27 (.787)
		$Estradiol_{t-1}$	**1.11**	**018**	**6.15 (< .0001)**
		FCN_{t-2}	-0.03	0.13	-0.27 (.792)
		$Estradiol_{t-2}$	**-0.51**	**0.18**	**-2.75 (.005)**
			R^2 = 0.66 (*p* = .0001); *RMSE* = 0.59 (*p* = .001)		
Default Mode	Participation	Constant	0.01	0.17	0.06 (.808)
		DMN_{t-1}	-3.13×10^{-4}	0.18	-2×10^{-3} (.998)
		$Estradiol_{t-1}$	**-0.63**	**0.26**	**-2.43 (.026)**
		DMN_{t-2}	0.09	0.18	0.53 (.599)
		$Estradiol_{t-2}$	**0.72**	**0.23**	**2.84 (.010)**
			R^2 = 0.27 (*p* = .091); *RMSE* = 0.83 (*p* = .132)		
	Estradiol	Constant	0.01	0.12	0.07 (.803)
		DMN_{t-1}	-0.08	0.12	-0.66 (.505)
		$Estradiol_{t-1}$	**1.10**	**0.18**	**6.10 (< .0001)**
		DMN_{t-2}	-0.49	0.18	0.12 (.906)
		$Estradiol_{t-2}$	**-0.49**	**0.18**	**-2.76 (.004)**
			R^2 = 0.67 (*p* < .0001); *RMSE* = 0.57 (*p* = .0004)		
Dorsal Attention	Participation	Constant	0.08	0.16	0.49 (.099)
		DAN_{t-1}	0.15	0.18	0.84 (.405)
		$Estradiol_{t-1}$	**-0.56**	**0.25**	**-2.27 (.035)**
		DAN_{t-2}	-0.29	0.17	-1.71 (.093)
		$Estradiol_{t-2}$	**0.53**	**0.24**	**2.16 (.042)**
			R^2 = 0.32 (*p* = .049); *RMSE* = 0.79 (*p* = .050)		
	Estradiol	Constant	6.88×10^{-5}	0.12	0.001 (.998)
		DAN_{t-1}	0.06	0.14	0.47 (.627)
		$Estradiol_{t-1}$	**1.12**	**0.18**	**6.12 (< .0001)**
		DAN_{t-2}	0.03	0.13	0.24 (.806)
		$Estradiol_{t-2}$	**-0.48**	**0.18**	**-2.65 (.007)**
			R^2 = 0.67 (*p* = .0001); *RMSE* = 0.59 (*p* = .0009)		

Limbic	Participation	Constant	-0.01	0.18	-0.03 (.929)
		LN_{t-1}	0.36	0.20	1.83 (.074)
		$Estradiol_{t-1}$	**-0.55**	**0.27**	**-2.06 (.050)**
		LN_{t-2}	-0.09	0.20	-0.45 (.666)
		$Estradiol_{t-2}$	**0.56**	**0.27**	**2.09 (.047)**
			R^2 = 0.27 (p = .102); *RMSE* = 0.86 (p = .235)		
	Estradiol	Constant	0.01	0.12	0.07 (.793)
		LN_{t-1}	0.07	0.13	0.49 (.624)
		$Estradiol_{t-1}$	**1.13**	**0.18**	**6.34 (< .0001)**
		LN_{t-2}	-0.14	0.13	-1.05 (.307)
		$Estradiol_{t-2}$	**-0.52**	**0.18**	**-2.89 (.003)**
			R^2 = 0.68 (p < .0001); *RMSE* = 0.58 (p = .0005)		
Salience/ Ventral Attention	Participation	Constant	-0.02	0.23	-0.12 (.715)
		SVN_{t-1}	0.15	0.20	0.73 (.488)
		$Estradiol_{t-1}$	0.28	0.99	0.29 (.782)
		SVN_{t-2}	0.11	0.22	0.51 (.625)
		$Estradiol_{t-2}$	-0.12	1.18	-0.10 (.919)
			R^2 = 0.07 (p = .80); *RMSE* = 0.96 (p = .87)		
	Estradiol	Constant	0.07	0.05	1.45 (< .0001)
		SVN_{t-1}	-0.09	0.04	-1.96 (.059)
		$Estradiol_{t-1}$	**1.31**	**0.21**	**6.27 (< .0001)**
		SVN_{t-2}	-0.01	0.05	-0.14 (.887)
		$Estradiol_{t-2}$	-0.24	0.25	-0.96 (.378)
			R^2 = 0.96 (p < .0001); *RMSE* = 0.20 (p < .0001)		
Somato-Motor	Participation	Constant	-0.08	0.22	-0.34 (.223)
		SMN_{t-1}	0.09	0.20	0.42 (.664)
		$Estradiol_{t-1}$	0.99	0.89	1.11 (.270)
		SMN_{t-2}	0.17	0.20	0.84 (.405)
		$Estradiol_{t-2}$	-0.87	1.07	-0.82 (.420)
			R^2 = 0.13 (p = .46); *RMSE* = 0.92 (p = .50)		
	Estradiol	Constant	0.07	0.05	1.25 (.003)
		SMN_{t-1}	-0.03	0.04	-0.57 (.568)
		$Estradiol_{t-1}$	**1.35**	**0.21**	**6.40 (< .0001)**
		SMN_{t-2}	-0.01	0.05	-0.29 (.767)
		$Estradiol_{t-2}$	-0.29	0.25	-1.15 (.266)
			R^2 = 0.96 (p < .0001); *RMSE* = 0.22 (p < .0001)		

Subcortical	Participation	Constant	0.04	0.19	0.21 (.344)
		SCN_{t-1}	-4.77×10^{-3}	0.19	-0.03 (.976)
		$Estradiol_{t-1}$	-0.38	0.29	-1.33 (.183)
		SCN_{t-2}	-0.03	0.19	-0.15 (.866)
		$Estradiol_{t-2}$	0.58	0.28	2.04 (.059)
			R^2 = 0.16 (p = .330); *RMSE* = 0.93 (p = .477)		
	Estradiol	Constant	0.01	0.12	0.07 (.792)
		SCN_{t-1}	0.07	0.12	0.54 (.573)
		$Estradiol_{t-1}$	**1.11**	**0.18**	**6.17 (< .0001)**
		SCN_{t-2}	0.02	0.12	0.18 (.854)
		$Estradiol_{t-2}$	**-0.50**	**0.18**	**-2.78 (.005)**
			R^2 = 0.67 (p < .0001); *RMSE* = 0.59 (p = .0009)		
Temporal Parietal	Participation	Constant	-0.04	0.24	-0.16 (.594)
		TPN_{t-1}	0.09	0.20	0.42 (.688)
		$Estradiol_{t-1}$	0.27	0.97	.28 (.79)
		TPN_{t-2}	-0.20	0.21	-0.95 (.35)
		$Estradiol_{t-2}$	-0.34	1.15	-0.28 (.79)
			R^2 = 0.05 (p = .49); *RMSE* = 0.99 (p = .96)		
	Estradiol	**Constant**	**0.07**	**0.05**	**1.45 (< .0001)**
		TPN_{t-1}	-0.04	0.04	-0.85 (.400)
		$Estradiol_{t-1}$	**1.27**	**0.20**	**6.33 (< .0001)**
		TPN_{t-2}	-0.07	0.04	-1.61 (.104)
		$Estradiol_{t-2}$	-0.22	0.24	-0.93 (.395)
			R^2 = 0.96 (p < .0001); *RMSE* = 0.20 (p < .0001)		
Visual	Participation	Constant	0.17	0.22	0.62 (.038)
		VN_{t-1}	**0.09**	**0.21**	**3.27 (.004)**
		$Estradiol_{t-1}$	0.03	0.89	-1.57 (.130)
		VN_{t-2}	0.14	0.20	-1.56 (.140)
		$Estradiol_{t-2}$	1.44	1.06	1.57 (.127)
			R^2 = 0.37 (p = .027); *RMSE* = 0.79 (p = .05)		
	Estradiol	Constant	0.06	0.05	1.23 (.003)
		VN_{t-1}	-0.05	0.05	-0.89 (.388)
		$Estradiol_{t-1}$	**1.38**	**0.21**	**6.42 (< .001)**
		VN_{t-2}	-0.02	0.05	0.30 (.776)
		$Estradiol_{t-2}$	-0.34	0.25	-1.25 (.229)
			R^2 = 0.96 (p < .0001); *RMSE* = 0.22 (p < *.0001*)		

Note. p-values empirically-derived via 10,000 iterations of nonparametric permutation testing.

Table S2. All re-test VAR models for cross-network participation v. estradiol (Study 2).

Network	Outcome	Predictor	Estimate	*SE*	*T* (*p*)
Control	Participation	Constant	-0.07	0.23	-0.31 (.296)
		FCN_{t-1}	0.02	0.20	0.12 (.905)
		$Estradiol_{t-1}$	0.76	0.94	0.81 (.429)
		FCN_{t-2}	-0.18	0.20	-0.87 (.394)
		$Estradiol_{t-2}$	-0.75	1.12	-0.67 (.510)
			R^2 = 0.08 (p = .739); *RMSE* = 0.96 (p = .834)		
	Estradiol	**Constant**	**0.07**	**0.05**	**1.41 (.001)**
		FCN_{t-1}	-0.05	0.04	-1.07 (.298)
		$Estradiol_{t-1}$	**1.31**	**0.20**	**6.61 (< .0001)**
		FCN_{t-2}	-0.07	0.04	-1.67 (.105)
		$Estradiol_{t-2}$	-0.24	0.24	-1.03 (.322)
			R^2 = 0.96 (p < .0001); *RMSE* = 0.20 (p < .0001)		
Default Mode	Participation	Constant	-0.09	0.24	-0.39 (.165)
		DMN_{t-1}	-4.00×10^{-3}	0.21	0.02 (.985)
		$Estradiol_{t-1}$	0.67	0.99	0.67 (.510)
		DMN_{t-2}	-0.12	0.21	-0.54 (.592)
		$Estradiol_{t-2}$	-0.73	1.18	-0.62 (.552)
			R^2 = 0.05 (p = .891); *RMSE* = 0.99 (p = .937)		
	Estradiol	**Constant**	**0.08**	**0.05**	**1.55 (.0002)**
		DMN_{t-1}	-0.07	0.04	-1.61 (.121)
		$Estradiol_{t-1}$	**1.25**	**0.20**	**6.11 (< .0001)**
		DMN_{t-2}	-0.06	0.04	-1.25 (.214)
		$Estradiol_{t-2}$	-0.18	0.24	-0.73 (.503)
			R^2 = 0.96 (p < .0001); *RMSE* = 0.20 (p < .0001)		
Dorsal Attention	Participation	Constant	0.07	0.24	0.27 (.347)
		DAN_{t-1}	2.00×10^{-3}	0.21	0.01 (.991)
		$Estradiol_{t-1}$	-0.31	1.01	-0.30 (.766)
		DAN_{t-2}	0.01	0.23	0.05 (.964)
		$Estradiol_{t-2}$	0.61	1.19	0.51 (.617)
			R^2 = 0.04 (p = .909); *RMSE* = 0.99 (p = .988)		
	Estradiol	**Constant**	**0.07**	**0.05**	**1.39 (.0007)**
		DAN_{t-1}	**-0.09**	**0.04**	**-2.08 (.044)**
		$Estradiol_{t-1}$	**1.27**	**0.20**	**6.22 (< .0001)**
		DAN_{t-2}	-0.04	0.05	-0.85 (.408)
		$Estradiol_{t-2}$	-0.21	0.24	-0.88 (.416)
			R^2 = 0.96 (p < .0001); *RMSE* = 0.20 (p < .0001)		

Limbic	Participation	**Constant**	**0.15**	**0.21**	**0.70 (.017)**
		LN_{t-1}	**0.49**	**0.20**	**2.39 (.029)**
		$Estradiol_{t-1}$	-1.27	0.84	-1.52 (.138)
		LN_{t-2}	-0.28	0.19	-1.47 (.155)
		$Estradiol_{t-2}$	1.54	1.01	1.53 (.144)
			R^2 = 0.24 (p = .17); *RMSE* = 0.85 (p = .160)		
	Estradiol	**Constant**	**0.07**	**0.05**	**1.27 (.002)**
		LN_{t-1}	-7.00 X 10^{-3}	0.05	-0.14 (.890)
		$Estradiol_{t-1}$	**1.33**	**0.21**	**6.25 (< .0001)**
		LN_{t-2}	-0.04	0.05	-0.84 (.406)
		$Estradiol_{t-2}$	-0.29	0.26	-1.12 (.282)
			R^2 = 0.96 (p < .0001); *RMSE* = 0.21 (p < .0001)		
Salience/ Ventral Attention	Participation	Constant	-0.02	0.23	-0.11 (.715)
		SVN_{t-1}	0.15	0.20	0.73 (.488)
		$Estradiol_{t-1}$	0.28	0.99	0.29 (.782)
		SVN_{t-2}	0.11	0.22	0.51 (.625)
		$Estradiol_{t-2}$	-0.12	1.18	-0.10 (.919)
			R^2 = 0.07 (p = .802); *RMSE* = 0.96 (p = .874)		
	Estradiol	**Constant**	**0.07**	**0.05**	**1.45 (.0002)**
		SVN_{t-1}	-0.09	0.04	-1.96 (.059)
		$Estradiol_{t-1}$	**1.31**	**0.21**	**6.26 (< .0001)**
		SVN_{t-2}	-0.01	0.05	-0.14 (.887)
		$Estradiol_{t-2}$	-0.24	0.25	-0.96 (.378)
			R^2 = 0.96 (p < .0001); *RMSE* = 0.20 (p < .0001)		
Somato-Motor	Participation	Constant	-0.08	0.22	-0.34 (.224)
		SMN_{t-1}	0.09	0.20	0.42 (.664)
		$Estradiol_{t-1}$	0.99	0.89	1.11 (.270)
		SMN_{t-2}	0.17	0.20	0.84 (.405)
		$Estradiol_{t-2}$	-0.87	1.07	-0.82 (.420)
			R^2 = 0.13 (p = .463); *RMSE* = 0.94 (p = .644)		
	Estradiol	**Constant**	**0.07**	**0.05**	**1.25 (.003)**
		SMN_{t-1}	-0.03	0.05	-0.57 (.587)
		$Estradiol_{t-1}$	**1.35**	**0.21**	**6.40 (< .0001)**
		SMN_{t-2}	-0.01	0.05	-0.29 (.767)
		$Estradiol_{t-2}$	-0.29	0.25	-1.15 (.266)
			R^2 = 0.96 (p < .0001); *RMSE* = 0.22 (p < .0001)		

Subcortical	Participation	**Constant**	**0.12**	**0.19**	**0.62 (.038)**
		SCN_{t-1}	**0.64**	**0.19**	**3.27 (.004)**
		$Estradiol_{t-1}$	-1.22	0.77	-1.57 (.130)
		SCN_{t-2}	-0.31	0.20	-1.56 (.140)
		$Estradiol_{t-2}$	1.44	0.92	1.57 (.127)
			R^2 = 0.37 (p = .026); *RMSE* = 0.80 (p = .050)		
	Estradiol	**Constant**	**0.06**	**0.05**	**1.23 (.003)**
		SCN_{t-1}	-0.05	0.05	-0.89 (.388)
		$Estradiol_{t-1}$	**1.35**	**0.21**	**6.43 (< .0001)**
		SCN_{t-2}	0.02	0.05	0.30 (.776)
		$Estradiol_{t-2}$	-0.31	0.25	-1.25 (.229)
			R^2 = 0.96 (p < .0001); *RMSE* = 0.22 (p < .0001)		
Temporal Parietal	Participation	Constant	-0.04	0.24	-0.16 (.593)
		TPN_{t-1}	0.09	0.21	0.42 (.688)
		$Estradiol_{t-1}$	0.27	0.97	0.28 (.793)
		TPN_{t-2}	-0.20	0.21	-0.95 (.356)
		$Estradiol_{t-2}$	-0.33	1.15	-0.28 (.787)
			R^2 = 0.05 (p = .876); *RMSE* = 0.99 (p = .966)		
	Estradiol	**Constant**	**-0.04**	**0.05**	**1.45 (.0003)**
		TPN_{t-1}	1.27	0.04	-0.85 (.404)
		$Estradiol_{t-1}$	**-0.07**	**0.20**	**6.33 (< .0001)**
		TPN_{t-2}	-0.22	0.04	-1.66 (.111)
		$Estradiol_{t-2}$	0.07	0.24	-0.93 (.390)
			R^2 = 0.96 (p < .0001); *RMSE* = 0.21 (p < .0001)		
Visual	Participation	**Constant**	**0.14**	**0.22**	**0.62 (.031)**
		VN_{t-1}	0.09	0.21	0.44 (.669)
		$Estradiol_{t-1}$	0.03	0.89	0.03 (.977)
		VN_{t-2}	0.14	0.20	0.71 (.485)
		$Estradiol_{t-2}$	0.17	1.06	0.16 (.876)
			R^2 = 0.05 (p = .866); *RMSE* = 0.92 (p = .573)		
	Estradiol	**Constant**	**0.06**	**0.05**	**1.22 (.003)**
		VN_{t-1}	-0.05	0.05	-1.11 (.281)
		$Estradiol_{t-1}$	**1.38**	**0.21**	**6.70 (<.0001)**
		VN_{t-2}	-0.02	0.05	-0.35 (.718)
		$Estradiol_{t-2}$	-0.34	0.25	-1.37 (.176)
			R^2 = 0.96 (p < .0001); *RMSE* = 0.21 (p < .0001)		

Note. p-values empirically-derived via 10,000 iterations of nonparametric permutation testing.

Table S3. All VAR models for global efficiency v. estradiol (Study 1).

Network	Outcome	Predictor	Estimate	*SE*	*T* (*p*)
Control	Efficiency	Constant	-0.02	0.17	-0.14 (.576)
		FCN_{t-1}	-0.13	0.18	-0.73 (.452)
		$Estradiol_{t-1}$	**0.80**	**0.27**	**2.96 (.007)**
		FCN_{t-2}	-0.12	0.19	-0.66 (.510)
		$Estradiol_{t-2}$	**-0.68**	**0.28**	**-2.47 (.023)**
			R^2 = 0.34 (*p* = .039); *RMSE* = 0.83 (*p* = .133)		
	Estradiol	Constant	3.79×10^{-3}	0.12	0.03 (.896)
		FCN_{t-1}	-0.19	0.12	-1.56 (.127)
		$Estradiol_{t-1}$	**1.17**	**0.18**	**6.41 (< .0001)**
		FCN_{t-2}	-1.83×10^{-3}	0.13	-0.04 (.967)
		$Estradiol_{t-2}$	**-0.49**	**0.19**	**-2.62 (.007)**
			R^2 = 0.69 (*p* < .0001); *RMSE* = 0.56 (*p* < .0001)		
Default Mode	Efficiency	Constant	0.04	0.15	0.28 (.279)
		DMN_{t-1}	-0.04	0.16	-0.27 (.764)
		$Estradiol_{t-1}$	**0.98**	**0.23**	**3.37 (.0003)**
		DMN_{t-2}	-0.02	0.16	-0.11 (.907)
		$Estradiol_{t-2}$	**-0.93**	**0.23**	**-4.00 (.002)**
			R^2 = 0.50 (*p* = .003); *RMSE* = 0.70 (*p* = .022)		
	Estradiol	Constant	0.01	0.12	0.09 (.729)
		DMN_{t-1}	-0.12	0.13	-0.95 (.339)
		$Estradiol_{t-1}$	**1.15**	**0.19**	**6.15 (< .0001)**
		DMN_{t-2}	-0.01	0.13	-0.08 (.930)
		$Estradiol_{t-2}$	**-0.48**	**0.19**	**-2.50 (.012)**
			R^2 = 0.67 (*p* < .0001); *RMSE* = 0.58 (*p* = .0004)		
Dorsal Attention	Efficiency	Constant	0.01	0.16	0.08 (.783)
		DAN_{t-1}	-0.11	0.18	-0.60 (.562)
		$Estradiol_{t-1}$	**0.84**	**0.25**	**3.35 (.002)**
		DAN_{t-2}	-0.10	0.18	-0.58 (.571)
		$Estradiol_{t-2}$	**-0.67**	**0.16**	**-2.57 (.017)**
			R^2 = 0.37 (*p* = .022); *RMSE* = 0.77 (*p* = .023)		
	Estradiol	Constant	0.01	0.12	0.06 (.808)
		DAN_{t-1}	-0.17	0.13	-1.29 (.207)
		$Estradiol_{t-1}$	**1.17**	**0.19**	**6.30 (< .0001)**
		DAN_{t-2}	-0.02	0.13	-0.16 (.875)
		$Estradiol_{t-2}$	**-0.48**	**0.19**	**-2.49 (.011)**
			R^2 = 0.68 (*p* < .0001); *RMSE* = 0.57 (*p* = .0004)		

Limbic	Efficiency	Constant	0.06	0.20	0.29 (.318)
		LN_{t-1}	-0.10	0.22	-0.47 (.640)
		$Estradiol_{t-1}$	0.09	0.32	0.29 (.777)
		LN_{t-2}	-0.24	0.22	-1.09 (.294)
		$Estradiol_{t-2}$	-0.10	0.32	-0.33 (.751)
			R^2 = 0.07 (p = .760); *RMSE* = 0.97 (p = .857)		
	Estradiol	Constant	0.03	0.11	0.31 (.250)
		LN_{t-1}	**-0.26**	**0.11**	**-2.26 (.035)**
		$Estradiol_{t-1}$	**1.14**	**0.17**	**6.66 (< .0001)**
		LN_{t-2}	-0.13	0.12	-1.23 (.235)
		$Estradiol_{t-2}$	**-0.48**	**0.17**	**-2.84 (.004)**
			R^2 = 0.74 (p < .0001); *RMSE* = 0.52 (p = .0001)		
Salience/ Ventral Attention	Efficiency	Constant	-0.03	0.18	-0.17 (.533)
		SVN_{t-1}	-0.05	0.19	-0.27 (.786)
		$Estradiol_{t-1}$	0.45	0.28	1.58 (.131)
		SVN_{t-2}	-0.15	0.20	-0.74 (.452)
		$Estradiol_{t-2}$	-0.47	0.28	-1.67 (.107)
			R^2 = 0.18 (p = .309); *RMSE* = 0.88 (p = .311)		
	Estradiol	Constant	-0.01	0.11	-0.07 (.787)
		SVN_{t-1}	-0.22	0.11	-1.93 (.069)
		$Estradiol_{t-1}$	**1.06**	**0.17**	**6.26 (< .0001)**
		SVN_{t-2}	-0.18	0.12	-1.57 (.126)
		$Estradiol_{t-2}$	**-0.41**	**0.27**	**-2.41 (.015)**
			R^2 = 0.73 (p < .0001); *RMSE* = 0.53 (p < .0001)		
Somato-Motor	Efficiency	Constant	0.01	0.19	0.03 (.913)
		SMN_{t-1}	-0.03	0.20	-0.17 (.856)
		$Estradiol_{t-1}$	0.53	0.30	1.75 (.093)
		SMN_{t-2}	-0.07	0.22	-0.30 (.762)
		$Estradiol_{t-2}$	-0.47	0.31	-1.52 (.140)
			R^2 = 0.15 (p = .385); *RMSE* = 0.92 (p = .553)		
	Estradiol	Constant	-0.01	0.11	-0.07 (.775)
		SMN_{t-1}	-0.21	0.11	-1.89 (.074)
		$Estradiol_{t-1}$	**1.05**	**0.17**	**6.18 (< .0001)**
		SMN_{t-2}	-0.23	0.12	-1.88 (.076)
		$Estradiol_{t-2}$	**-0.36**	**0.17**	**-2.05 (.036)**
			R^2 = 0.74 (p < .0001); *RMSE* = 0.51 (p < .0001)		

Subcortical	Efficiency	Constant	0.05	0.20	0.26 (.351)
		SCN_{t-1}	-0.05	0.20	-0.27 (.788)
		$Estradiol_{t-1}$	0.35	0.30	1.20 (.248)
		SCN_{t-2}	0.02	0.21	0.10 (.917)
		$Estradiol_{t-2}$	-0.38	0.30	-1.29 (.208)
		R^2 = 0.07 (p = .755); *RMSE* = 0.95 (p = .700)			
	Estradiol	Constant	0.01	0.12	0.06 (.823)
		SCN_{t-1}	-0.07	0.12	-0.57 (.597)
		$Estradiol_{t-1}$	**1.11**	**0.18**	**6.14 (< .0001)**
		SCN_{t-2}	-0.09	0.13	-0.69 (.493)
		$Estradiol_{t-2}$	**-0.47**	**0.18**	**-2.61 (.007)**
		R^2 = 0.67 (p < .0001); *RMSE* = 0.58 (p = .0006)			
Temporal Parietal	Efficiency	Constant	0.01	0.16	0.90 (.737)
		TPN_{t-1}	-0.21	0.18	-1.15 (.262)
		$Estradiol_{t-1}$	**0.89**	**0.26**	**3.40 (.002)**
		TPN_{t-2}	0.06	0.18	0.30 (.758)
		$Estradiol_{t-2}$	**-0.82**	**0.27**	**-3.04 (.007)**
		R^2 = 0.36 (p = .026); *RMSE* = 0.79 (p = .057)			
	Estradiol	Constant	0.02	0.12	0.19 (.477)
		TPN_{t-1}	-0.23	0.13	-1.79 (.087)
		$Estradiol_{t-1}$	**1.20**	**0.18**	**6.52 (< .0001)**
		TPN_{t-2}	-0.04	0.13	-0.28 (.783)
		$Estradiol_{t-2}$	**-0.50**	**0.19**	**-2.66 (.007)**
		R^2 = 0.70 (p < .0001); *RMSE* = 0.55 (p = .0005)			
Visual	Efficiency	Constant	0.09	0.18	0.48 (.114)
		VN_{t-1}	-0.10	0.18	-0.54 (.604)
		$Estradiol_{t-1}$	0.43	0.28	1.53 (.142)
		VN_{t-2}	-0.20	0.19	-1.02 (.321)
		$Estradiol_{t-2}$	-0.37	0.28	-1.32 (.194)
		R^2 = 0.18 (p = .307); *RMSE* = 0.86 (p = .202)			
	Estradiol	Constant	0.02	0.11	0.16 (.534)
		VN_{t-1}	-0.18	0.11	-1.62 (.120)
		$Estradiol_{t-1}$	**1.09**	**0.17**	**6.33 (< .0001)**
		VN_{t-2}	-0.19	0.12	-1.63 (.118)
		$Estradiol_{t-2}$	**-0.40**	**0.17**	**-2.30 (.019)**
		R^2 = 0.73 (p < .0001); *RMSE* = 0.53 (p = .0004)			

Note. p-values empirically-derived via 10,000 iterations of nonparametric permutation testing.

Table S4. All re-test VAR models for global efficiency v. estradiol (Study 2).

Network	Outcome	Predictor	Estimate	*SE*	*T* (*p*)
Control	Efficiency	**Constant**	**-0.12**	**0.21**	**-0.60 (.047)**
		FCN_{t-1}	-0.02	0.18	-0.10 (.921)
		$Estradiol_{t-1}$	**2.03**	**0.84**	**2.41 (.026)**
		FCN_{t-2}	-0.21	0.20	-1.06 (.292)
		$Estradiol_{t-2}$	**-2.14**	**1.02**	**-2.12 (.049)**
		R^2 = 0.23 (p = .166); *RMSE* = 0.84 (p = .156)			
	Estradiol	**Constant**	**0.08**	**0.05**	**1.49 (.0003)**
		FCN_{t-1}	0.03	0.05	0.73 (.466)
		$Estradiol_{t-1}$	**1.30**	**0.21**	**6.12 (< .0001)**
		FCN_{t-2}	0.06	0.05	1.18 (.253)
		$Estradiol_{t-2}$	-0.24	0.26	-0.95 (.367)
		R^2 = 0.96 (p < .0001); *RMSE* = 0.21 (p < .0001)			
Default Mode	Efficiency	**Constant**	**-0.19**	**0.19**	**-1.04 (.001)**
		DMN_{t-1}	0.09	0.16	0.52 (.617)
		$Estradiol_{t-1}$	**2.48**	**0.75**	**3.29 (.003)**
		DMN_{t-2}	**-0.45**	**0.19**	**-2.41 (.027)**
		$Estradiol_{t-2}$	**-2.69**	**0.91**	**-2.94 (.009)**
		R^2 = 0.38 (p = .019); *RMSE* = 0.74 (p = .011)			
	Estradiol	**Constant**	**0.08**	**0.05**	**1.44 (.0001)**
		DMN_{t-1}	0.03	0.05	0.52 (.598)
		$Estradiol_{t-1}$	**1.29**	**0.22**	**5.88 (<.0001)**
		DMN_{t-2}	0.05	0.05	0.90 (.371)
		$Estradiol_{t-2}$	-0.24	0.27	-0.90 (.400)
		R^2 = 0.96 (p < .0001); *RMSE* = 0.22 (p < .0001)			
Dorsal Attention	Efficiency	Constant	-0.06	0.20	-0.33 (.259)
		DAN_{t-1}	-0.18	0.18	-1.01 (.326)
		$Estradiol_{t-1}$	**1.88**	**0.79**	**2.37 (.026)**
		DAN_{t-2}	-0.22	0.20	-1.14 (.271)
		$Estradiol_{t-2}$	-1.64	0.94	-1.74 (.095)
		R^2 = 0.32 (p = .052); **RMSE = 0.79 (p = .045)**			
	Estradiol	**Constant**	**0.07**	**0.05**	**1.28 (.002)**
		DAN_{t-1}	0.04	0.05	0.80 (.442)
		$Estradiol_{t-1}$	**1.34**	**0.22**	**6.21 (<.0001)**
		DAN_{t-2}	0.03	0.05	0.55 (.586)
		$Estradiol_{t-2}$	-0.31	0.26	-1.20 (.253)
		R^2 = 0.96 (p < .0001); *RMSE* = 0.22 (p < .0001)			

Subcortical	Efficiency	**Constant**	**-0.19**	**0.21**	**-0.92 (.003)**
		SCN_{t-1}	0.22	0.18	1.24 (.232)
		$Estradiol_{t-1}$	**1.89**	**0.83**	**2.29 (.032)**
		SCN_{t-2}	-0.24	0.19	-1.29 (.204)
		$Estradiol_{t-2}$	**-2.22**	**1.00**	**-2.23 (.037)**
			R^2 = 0.23 (p = .172); *RMSE* = 0.85 (p = .159)		
	Estradiol	**Constant**	**0.07**	**0.05**	**1.23 (.002)**
		SCN_{t-1}	0.03	0.05	0.61 (.550)
		$Estradiol_{t-1}$	**1.37**	**0.22**	**6.41 (< .0001)**
		SCN_{t-2}	-0.01	0.05	-0.13 (.901)
		$Estradiol_{t-2}$	-0.32	0.26	-1.26 (.216)
			R^2 = 0.95 (p < .0001); *RMSE* = 0.22 (p < .0001)		
Temporal Parietal	Efficiency	**Constant**	**-0.17**	**0.22**	**-0.77 (.010)**
		TPN_{t-1}	0.16	0.20	0.83 (.412)
		$Estradiol_{t-1}$	1.82	0.93	1.95 (.059)
		TPN_{t-2}	-0.31	0.21	-1.42 (.168)
		$Estradiol_{t-2}$	-2.28	1.14	-2.00 (.057)
			R^2 = 0.16 (p = .360); *RMSE* = 0.88 (p = .286)		
	Estradiol	**Constant**	**0.06**	**0.05**	**1.17 (.004)**
		TPN_{t-1}	0.04	0.05	0.74 (.465)
		$Estradiol_{t-1}$	**1.38**	**0.23**	**6.00 (< .0001)**
		TPN_{t-2}	0.01	0.05	0.25 (.797)
		$Estradiol_{t-2}$	-0.33	0.28	-1.18 (.257)
			R^2 = 0.95 (p < .0001); *RMSE* = 0.22 (p < .0001)		
Visual	Efficiency	Constant	-0.11	0.21	-0.50 (.080)
		VN_{t-1}	-0.05	0.19	-0.27 (.792)
		$Estradiol_{t-1}$	1.34	0.84	1.59 (.126)
		VN_{t-2}	-0.09	0.19	-0.45 (.659)
		$Estradiol_{t-2}$	-1.27	1.01	-1.26 (.227)
			R^2 = 0.15 (p = .431); *RMSE* = 0.88 (p = .264)		
	Estradiol	**Constant**	**0.06**	**0.05**	**1.20 (.003)**
		VN_{t-1}	0.02	0.05	0.41 (.695)
		$Estradiol_{t-1}$	**1.38**	**0.21**	**6.60 (< .0001)**
		VN_{t-2}	-0.03	0.05	-0.69 (.499)
		$Estradiol_{t-2}$	-0.33	0.25	-1.34 (.183)
			R^2 = 0.95 (p < .0001); *RMSE* = 0.22 (p < .0001)		

Note. p-values empirically-derived via 10,000 iterations of nonparametric permutation testing.

Appendix B

Supplementary Table 1. Raw gray matter volume and correlations with gestation metrics by network

Network	Average	Range	Correlation with gestation week *N = 19*	Correlation with 17β-estradiol *N = 15*	Correlation with progesterone *N = 13*	FreeSurfer Results *corr. w/ gestation week N = 19*
Control A	0.64	0.62 – 0.67	-0.93***	-0.88***	-0.95***	-0.60**
Control B	0.67	0.66 – 0.69	-0.92***	-0.88***	-0.87***	-0.55*
Control C	0.68	0.65 - 0.70	-0.88***	-0.90***	-0.94***	-0.78***
Default Mode A	0.70	0.69 – 0.72	-0.93***	-0.93***	-0.95***	-0.76***
Default Mode B	0.70	0.69 – 0.72	-0.91***	-0.87***	-0.95***	-0.72***
Default Mode C	0.72	0.71 – 0.73	-0.69**	-0.72**	-0.86***	-0.84***
Dorsal Attention A	0.66	0.64 – 0.68	-0.91***	-0.89***	-0.97***	-0.64**
Dorsal Attention B	0.65	0.62 – 0.68	-0.95***	-0.91***	-0.97***	-0.55*
Salience Ventral Attn A	0.70	0.67 – 0.72	-0.95***	-0.91***	-0.97***	-0.92***
Salience Ventral Attn B	0.72	0.70 – 0.73	-0.92***	-0.89***	-0.92***	-0.69**
Somatomotor A	0.65	0.61 – 0.67	-0.93***	-0.88***	-0.95***	-0.76***
Somatomotor B	0.70	0.67 – 0.73	-0.92***	-0.91***	-0.95***	-0.91***
Limbic A	0.76	0.74 – 0.79	0.14	0.16	-0.11	-0.08
Limbic B	0.70	0.66 – 0.74	-0.50*	-0.67**	-0.48	-0.80***
Temporal Parietal	0.72	0.70 – 0.74	-0.89***	-0.92***	-0.97***	-0.87***
Visual Central	0.67	0.65 – 0.69	-0.72***	-0.78***	-0.82***	-0.66**
Visual Peripheral	0.70	0.69 – 0.72	-0.70**	-0.86***	-0.92***	-0.72***

FDR-corrected at $q < 0.05$; *p ≤ 0.05, **p ≤ 0.01, ***p ≤ 0.001

Supplementary Table 2. Top gray matter volume ROIs associated with gestation week

Schaefer ROI	Network	Hemisphere	T-stat (partial)
PFCd_1	ContA	Right	-5.33*
IPS_2	ContA	Left	-3.47*
PFCd_1	ContB	Left	-4.74*
PFCmp_1	ContB	Right	-3.72*
PFCmp_1	ContB	Left	-3.38*
PFCmp_1	ContB	Left	-3.38*
pCun_3	ContC	Right	-3.26*
IPL_1	DMNA	Left	-4.23*
PFCd_3	DMNA	Left	-4.05*
pCunPCC_4	DMNA	Left	-3.67*
pCunPCC_2	DMNA	Right	-3.36*
PFCd_2	DMNA	Right	-3.33*
pCunPCC_2	DMNA	Right	-3.36*
PFCd_2	DMNA	Right	-3.33*
SPL_3	DorsAttnA	Left	-3.59*
PostC_6	DorsAttnB	Right	-5.35*
PostC_3	DorsAttnB	Left	-4.95*
PostC_7	DorsAttnB	Right	-4.56*
PostC_7	DorsAttnB	Left	-4.48*
PostC_9	DorsAttnB	Left	-4.08*
PostC_8	DorsAttnB	Left	-3.96*
FEF_2	DorsAttnB	Left	-3.77*
PostC_8	DorsAttnB	Right	-3.75*
PostC_1	DorsAttnB	Left	-3.53*
FEF_3	DorsAttnB	Left	-3.41*
Ins_1	SalVentAttnA	Left	-5.22*
FrOper_3	SalVentAttnA	Right	-4.26*
ParOper_3	SalVentAttnA	Left	-3.78*
FrMed_2	SalVentAttnA	Right	-3.37*
Ins_3	SalVentAttnB	Left	-5.07*
SomMotA_11	SomMotA	Left	-4.12*
SomMotA_12	SomMotA	Left	-4.11*
SomMotA_8	SomMotA	Left	-3.76*
SomMotA_5	SomMotA	Right	-3.23*
TempPar_3	TempPar	Left	-3.40*
PHC_2	DMNC	Right	4.09*
TempPole_3	LimbicA	Right	3.54*
ExStr_2	VisCent	Left	4.43*
ExStrInf_2	VisPeri	Right	4.57*

FDR-corrected at $q < 0.05$; *$p \leq 0.05$, **$p \leq 0.01$, ***$p \leq 0.001$

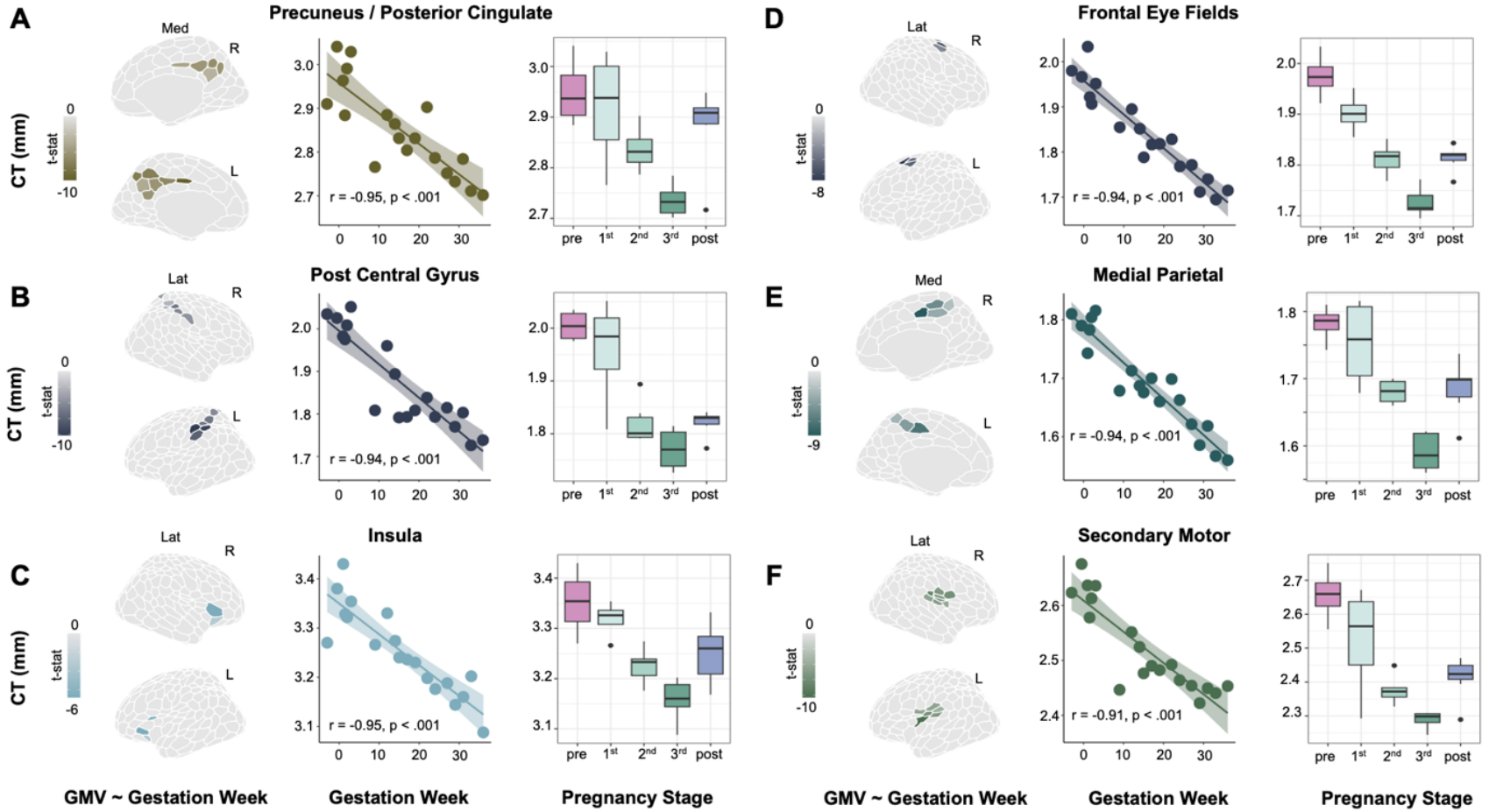

Supplementary Figure 1. Six representative regions that exhibit some of the greatest cortical thickness (CT) magnitude change across gestation, decreasing in volume at a rate greater than the global decrease. **A–F)** For each panel, we display results of a multivariate regression revealing significant associations between clustered ROI CT and gestation week (left), Pearson's product-moment correlation between the average CT of the ROIs and gestation week (middle), and summary ROI CT by pregnancy stage across the whole study (right). All statistical tests were corrected for multiple comparisons (FDR at $q < 0.05$). ROI subregions are color-coded by network affiliation (see **Fig S2**). N.b., shown here are raw data values (see **Table S4**).

Supplementary Table 3. Raw cortical thickness and associations with gestation metrics at network level

Network	**Average**	**Range**	**Correlation with gestation week** *N = 19*	**Correlation with 17β-estradiol** *N = 15*	**Correlation with progesterone** *N = 13*	**FreeSurfer Results** *corr. w/ gestation week* *N = 19*
Control A	1.87	1.75 – 2.02	-0.84***	-0.80***	-0.90***	-0.59*
Control B	2.44	2.32 – 2.65	-0.83***	-0.85***	-0.89***	-0.46
Control C	2.07	1.95 – 2.27	-0.75***	-0.80***	-0.90***	-0.83***
Default Mode A	2.69	2.57 – 2.91	-0.82***	-0.85***	-0.91***	-0.83***
Default Mode B	2.57	2.46 – 2.78	-0.80***	-0.79***	-0.85***	-0.54*
Default Mode C	2.91	2.78– 3.05	-0.40	-0.49	-0.49*	-0.81***
Dorsal Attention A	2.28	2.11 – 2.48	-0.77***	-0.82***	-0.91***	-0.46
Dorsal Attention B	1.92	1.77 – 2.12	-0.90***	-0.88***	-0.94***	-0.51
Salience Ventral Attn A	2.46	2.33 – 2.62	-0.91***	-0.91***	-0.95***	-0.93***
Salience Ventral Attn B	2.73	2.61 – 2.94	-0.86***	-0.86***	-0.91***	-0.78**
Somatomotor A	1.76	1.52 – 2.23	-0.81***	-0.81***	-0.86***	-0.62*
Somatomotor B	2.17	2.01 – 2.45	-0.89***	-0.90***	-0.93***	-0.83***
Limbic A	3.76	3.39 – 3.97	-0.32	-0.23	-0.39	-0.46
Limbic B	2.81	2.53 – 3.12	-0.59**	-0.75**	-0.66*	-0.75**
Temporal Parietal	2.66	2.46 – 2.86	-0.80***	-0.91***	-0.94***	-0.73**
Visual Central	2.24	1.89 – 2.50	-0.63**	-0.76**	-0.79**	-0.31
Visual Peripheral	2.34	2.10 – 2.50	-0.22	-0.44	-0.63*	-0.56*

FDR-corrected at $q < 0.05$; *$p \leq 0.05$, **$p \leq 0.01$, ***$p \leq 0.001$

Supplementary Table 4. Top cortical thickness ROIs associated with gestation week

Schaefer ROI	Network	Hemisphere	T-stat (partial)
PFCl_3	ContA	Left	-4.23*
PostC_2	DorsAttnB	Left	-4.94
PostC_3	DorsAttnB	Left	-4.05*
FEF_2	DorsAttnB	Left	-3.91*
FEF_3	DorsAttnB	Left	-3.90*
FEF_2	DorsAttnB	Right	-3.70*
ParMed_1	SalVentAttnA	Right	-5.72**
ParMed_1	SalVentAttnA	Left	-4.68*
Ins_2	SalVentAttnB	Left	-3.77*
Ins_1	SomB	Left	-5.22*
S2_1	SomB	Left	-4.72*
TempPole_4	LimbicA	Left	4.73*
ExStrInf_5	VisPeri	Left	3.70*
StriCal_1	VisPeri	Right	3.80*
ExStrInf_3	VisPeri	Left	3.98*
ExStrInf_2	VisPeri	Left	4.17*
ExStrInf_4	VisPeri	Right	5.73**
Rsp_2	DMNC	Left	4.04*

FDR-corrected at $q < 0.05$; *$p \leq 0.05$, **$p \leq 0.01$, ***$p \leq 0.001$, n.s. = not significant

Supplementary Table 5. Top Desikan-Killiany GMV ROIs associated with gestation week

DSK ROI	Hemisphere	T-stat (raw)	T-stat (partial)
Transverse Temporal	Bilateral	L: -8.59***, R: -5.05***	L: -4.70**, R: -3.80*
Lateral Orbital Frontal	Bilateral	L: -5.60***, R: -4.62***	L: -3.27*, R: -3.51*
Medial Orbital Frontal	Right	-6.03***	-4.80**
Lingual	Right	-4.98***	-3.58*
Posterior Cingulate	Left	-7.40***	-3.55*
Pericalcarine	Right	-2.78*	-3.44*
Precuneus	Right	-7.76***	-3.35*
Superior Temporal	Left	-7.54***	-3.26*
Insula	Right	-5.14***	-3.22*
Post Central Gyrus	Left	-7.36***	-3.04*
Pars Opercularis	Left	-7.30***	-3.00*
Superior Parietal	Left	-2.80*	2.94*
Inferior Parietal	Right	-0.70 (ns)	2.97*
Rostral Middle Frontal	Bilateral	L: -1.50 (ns), R: -2.48*	L: 3.84*, R: 3.23*
Supramarginal	Right	-1.04 (ns)	4.62**

FDR-corrected at $q < 0.05$; *$p \leq 0.05$, **$p \leq 0.01$, ***$p \leq 0.001$

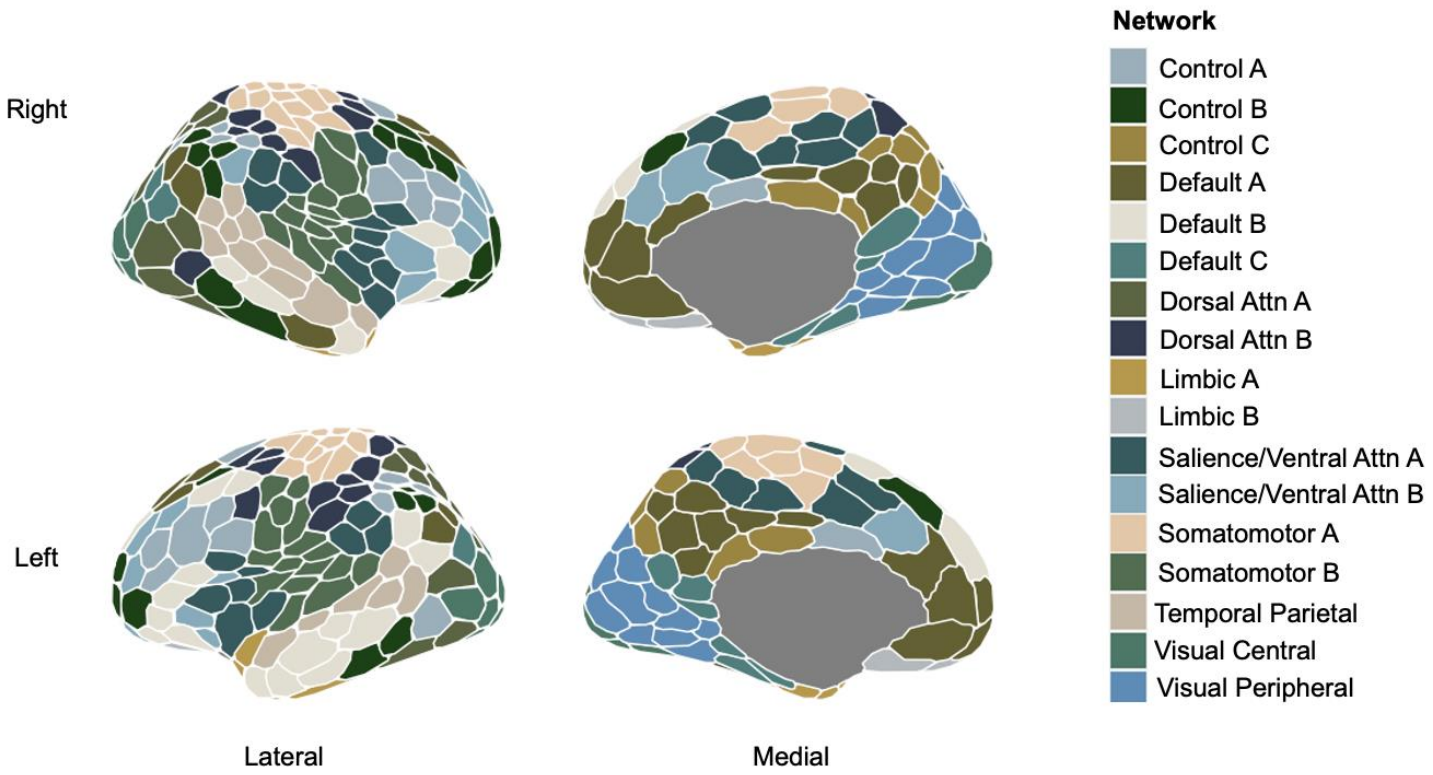

Supplementary Figure 2. The brain was parcellated into 400 cortical regions and assigned to one of eight networks based on previously identified anatomical and functional associations (Schaefer et al., 2018, Yeo et al., 2011). Colors indicate regional network membership.

Supplementary Table 6. Medial temporal subregion volumes (mm^3) and associations with gestation

	CA1	CA2/3	DG	Sub	ERC	PRC	PHC	Total Hipp
Average (SD)	507.50 (25.45)	175.63 (18.60)	497.72 (30.12)	265.33 (12.08)	735.02 (44.61)	2156.02 (67.35)	**1839.74 (76.00)**	1445.18 (74.51)
Min	462.34	144.16	451.15	244.29	643.16	2064.34	**1684.42**	1318.49
Max	554.35	202.48	561.98	281.68	836.64	2310.03	**1979.07**	1562.50
Range	92.01	58.33	110.83	37.38	193.48	245.69	**294.64**	244.01
Correlation with gest. week *p*-value *(r)*	-0.37 *n.s.*	-0.44 *n.s.*	-0.01 *n.s.*	-0.07 *n.s.*	0.29 *n.s.*	0.40 *n.s.*	**-0.78* (0.003)**	-0.25 *n.s.*
Correlation with E *p*-value *(r)*	-0.42 *n.s.*	-0.49 *n.s.*	-0.10 *n.s.*	-0.33 *n.s.*	0.30 *n.s.*	0.37 *n.s.*	**-0.79* (0.003)**	-0.35 *n.s.*
Correlation with P *p*-value *(r)*	-0.27 *n.s.*	-0.36 *n.s.*	0.02 *n.s.*	-0.20 *n.s.*	0.13 *n.s.*	0.41 *n.s.*	-0.72 *n.s.*	-0.20 *n.s.*

FDR-corrected at $q < 0.05$ | n.s.. indicates $p > 0.05$ | * remains significant with total volume correction

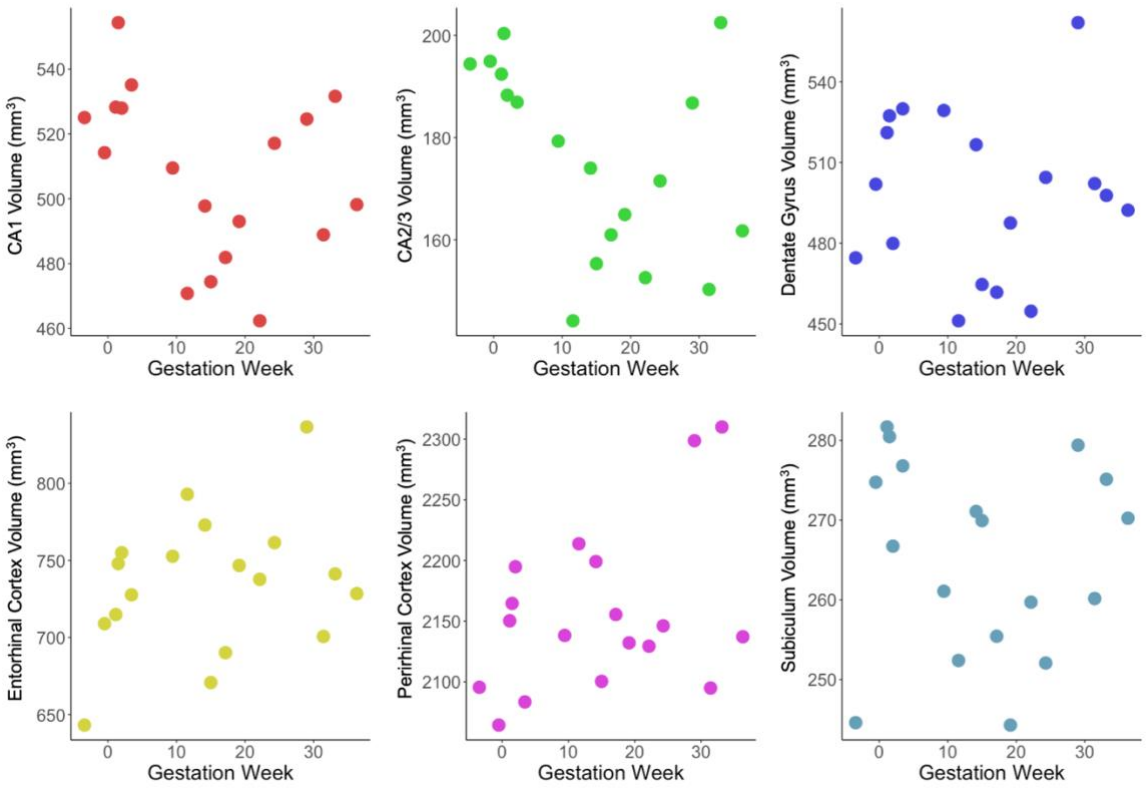

Supplementary Figure 3. Medial temporal subregion volumes across gestation, all non-significant at $p > 0.05$.

Supplementary Table 7. Tract ROIs with QA positively associated with gestation week (FDR < .001), progesterone (FDR < .001), and estradiol (FDR = .001)

	Number of tracts			Mean length (mm)			Diameter (mm)			Volume (mm^3)		
Region of Interest	*Gest Week*	*Progesterone*	*Estradiol*	*Gest Week*	*Progesterone*	*Estradiol*	*Gest Week*	*Progesterone*	*Estradiol*	*Gest Week*	*Progesterone*	*Estradiol*
Anterior_Commissure	68	_	_	62	_	_	5.4	_	_	1412	_	_
Arcuate_Fasciculus_L	559	56	12	56	58	56.3	8.8	6	3	3348	1814	333
Arcuate_Fasciculus_R	215	_	_	60	_	_	6.2	_	_	1801	_	_
Cingulum_Frontal_Parietal_L	44	_	_	56	_	_	4	_	_	703	_	_
Cingulum_Frontal_Parietal_R	64	_	_	54	_	_	4.7	_	_	951	_	_
Cingulum_Parolfactory_R	22	_	_	57	_	_	2.1	_	_	204	_	_
Corpus_Callosum_Body	854	122	41	60	58	55.9	16	8	5	11679	3012	1075
Corpus_Callosum_Forceps_Major	2247	39	29	68	58	55.9	13	5	4	9513	1044	725
Corpus_Callosum_Tapetum	2367	49	33	60	57	54.7	17	5	4	13884	1144	762
Corticopontine_Tract_Occipital_L	37	_	_	55	_	_	3.9	_	_	664	_	_
Corticopontine_Tract_Occipital_R	23	_	_	53	_	_	3.7	_	_	558	_	_
Corticopontine_Tract_Parietal_L	58	55	12	53	66	68	5.2	5	3	1133	1330	557
Corticopontine_Tract_Parietal_R	77	_	_	57	_	_	5.9	_	_	1550	_	_
Corticospinal_Tract_L	170	233	131	58	62	63.1	8.3	10	8	3161	5118	3284
Corticospinal_Tract_R	80	_	_	59	_	_	5.8	_	_	1552	_	_
Corticostriatal_Tract_Posterior_L	239	16	_	57	60	_	8.2	3	_	2972	485	
Corticostriatal_Tract_Posterior_R	110	_	_	54	_	_	7	_	_	2089	_	_
Corticostriatal_Tract_Superior_L	11	102	35	51	58	57.2	3.1	8	5	395	2886	1176
Dentatorubrothalamic_Tract_L	18	35	_	57	70	_	3.5	6	_	533	1747	_
Dentatorubrothalamic_Tract_R	24	_	_	55	_	_	3.9	_	_	635	_	_
Extreme_Capsule_L	17	16	15	55	64	62	2.1	3	3	184	600	559
Frontal_Aslant_Tract_R	30	_	_	52	_	_	3.1	_	_	389	_	_
Inferior_Fronto_Occipital_Fasciculus_L	843	_	14	59	_	52.6	11	_	3	5223	_	391
Inferior_Fronto_Occipital_Fasciculus_R	450	41	15	58	58	59.3	9.2	4	2	3869	633	263
Inferior_Longitudinal_Fasciculus_L	2297	17	12	67	55	55.5	13	3	3	8223	415	390
Inferior_Longitudinal_Fasciculus_R	603	_	_	61	_	_	10	_	_	5076	_	_
Medial_Lemniscus_L	_	69	34	_	58	55.7	_	6	5	_	1666	984
Medial_Lemniscus_R	21	27	18	56	58	57.2	3.8	4	3	620	887	453
Middle_Cerebellar_Peduncle	_	593	239	_	62	59.9	_	14	10	_	9450	4751
Middle_Longitudinal_Fasciculus_L	161	_	_	53	_	_	6	_	_	1516	_	_
Middle_Longitudinal_Fasciculus_R	115	_	_	53	_	_	5.9	_	_	1473	_	_
Superior_Longitudinal_Fasciculus1_R	21	_	_	56	_	_	3.4	_	_	499	_	_
Thalamic_Radiation_Posterior_L	26	_	_	57	_	_	4.4	_	_	891	_	_
Thalamic_Radiation_Posterior_R	56	_	_	56	_	_	5	_	_	1114	_	_

Supplementary Table 8. Full report of mean diffusivity results by tract, showing an association between gestation week (FDR < .001) and estradiol (FDR = .047)

	Number of Tracts			Mean Length			Diameter (mm)			Volume (mm^3)		
Region of Interest	*Gest Week*	*Progesterone*	*Estradiol*	*Gest Week*	*Progesterone*	*Estradiol*	*Gest Week*	*Progesterone*	*Estradiol*	*Gest Week*	*Progesterone*	*Estradiol*
Arcuate_Fasciculus_L	13	-	-	51.8	-	-	3.7	-	-	556	-	-
Cerebellum_L	27	18	29	55.1	51.6	52	3.5	3.3	4.5	537	442	835
Cerebellum_R	11	35	14	50.9	50.7	51	2.7	4.4	3.1	290	782	381
Corpus_Callosum_Body	78	-	-	53.4	-	-	6	-	-	1527	-	-
Corpus_Callosum_Forceps_Major	-	-	11		-	53.1		-	2.5		-	269
Corpus_Callosum_Tapetum	21	-	-	53.1	-	-	4.2	-	-	743	-	-
Corticospinal_Tract_L	11	-	-	51.3	-	-	3.1	-	-	381	-	-
Fornix_L	11	-	-	52.7	-	-	2.5	-	-	255	-	-
Inferior_Fronto_Occipital_Fasciculus_L	43	-	-	55.3	-	-	4.8	-	-	999	-	-
Middle_Cerebellar_Peduncle	164	31	17	53	52.9	52	6.6	3.4	3	1801	488	357
Superior_Longitudinal_Fasciculus2_L	14	-	-	53.1	-	-	2.7	-	-	303	-	-

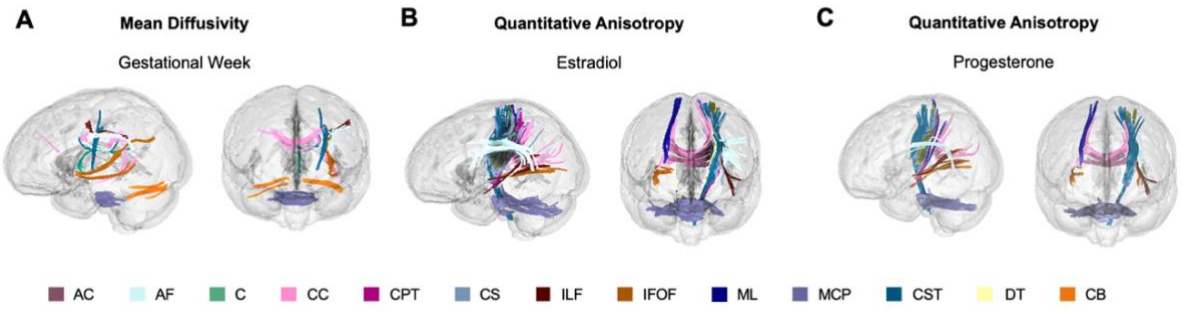

Supplementary Figure 4. Relationships between white matter integrity and gestation metrics. **A)** White matter tracts in which mean diffusivity (MD) was positively associated with gestational week (FDR q < .001). **B)** White matter tracts in which quantitative anisotropy (QA) was significantly associated with estradiol (FDR q < .001). **C)** White matter tracts in which quantitative anisotropy (QA) was significantly associated with progesterone (FDR q < .001). *Abbreviations :* AC = anterior commisure, AF = arcuate fasciculus, CC = corpus callosum, ILF = inferior longitudinal fasciculus, CS = corticostriatal tracts, CST = corticospinal tracts, CPT = corticopontine tracts, IFOF = inferior frontal occipital fasciculus, ML = medial lemniscus, MCP = middle cerebellar peduncle, DT = dentothalamic tract.

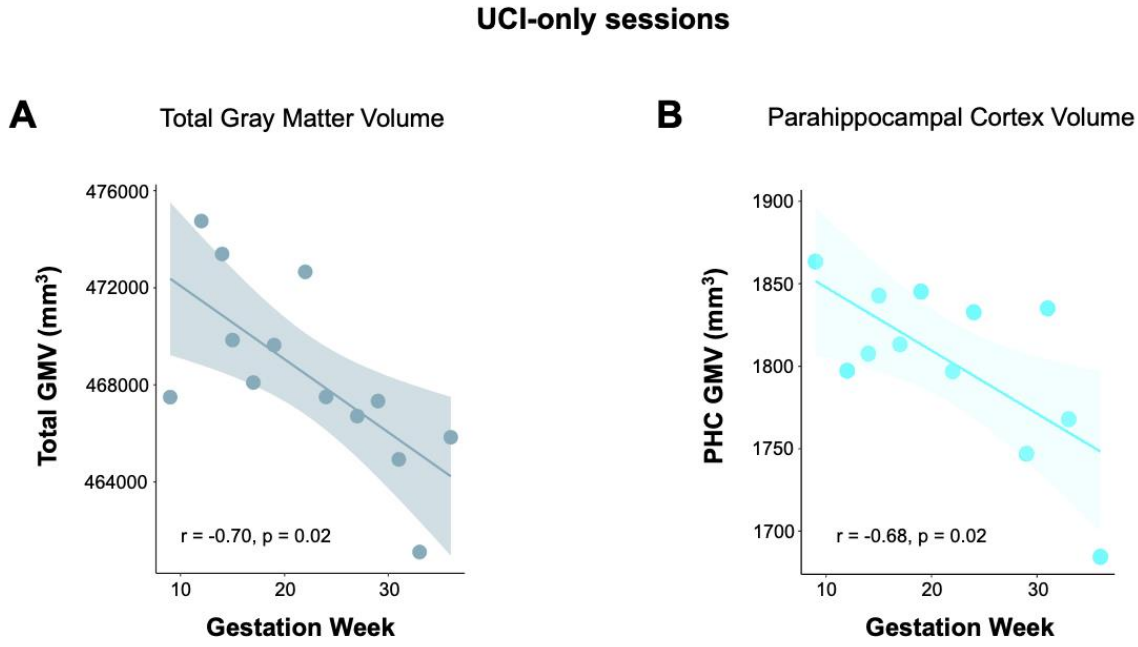

parahippocampal cortex volume.

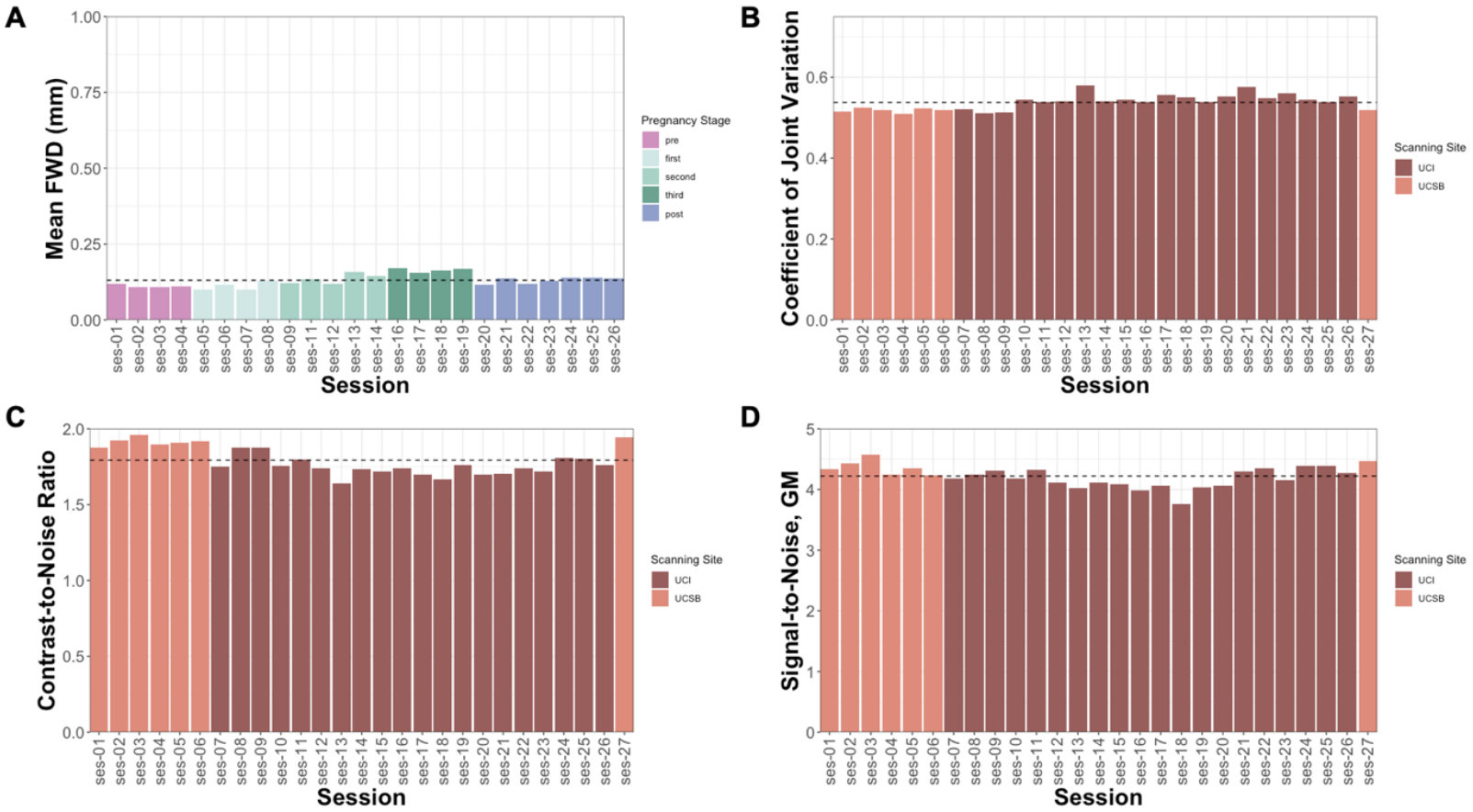

Supplementary Figure 6. Quality control estimates for this precision imaging experiment fell within standard ranges (see Esteban et al., 2017); dotted horizontal line represents the average. **A)** Mean motion (i.e., framewise displacement) estimates were derived from N=17 available resting-state scans that followed each session's whole-brain T1 MPRAGE scan. Head motion was minimal compared to a conservative 'acceptable' limit of 1mm. **B–D)** Quality control estimates derived from the *MRIQC* pipeline. **B)** Coefficient of Joint Variation is indicative of head motion and artifacts. **C)** Contrast-to-noise ratio evaluating how separated the tissue distributions of GM and WM. **D)** Signal-to-noise ratio for gray matter. Adjusting for these factors (A–D) did not alter the main findings.

Appendix C

Supplementary Table 1. Network participation predicted by menopause factors

Network	Term	Estimate	Std. Error	T-Statistic
Control A	**Intercept**	**0.64**	**0.03**	**20.24*****
	Meno Status: Peri	0.02	0.05	0.35
	Meno Status: Post	**0.16**	**0.05**	**3.35****
	Symptom Score	0.02	0.01	1.90
	Symptom X Peri	-0.02	0.01	-1.50
	Symptom X Post	**-0.03**	**0.01**	**-2.67***
				***F*(5,79) = 2.78, *p* = 0.02, R^2 = 0.15**
Control B	**Intercept**	**0.64**	**0.03**	**20.82*****
	Meno Status: Peri	0.00	0.05	0.01
	Meno Status: Post	**0.15**	**0.05**	**3.37****
	Symptom Score	0.02	0.01	2.04
	Symptom X Peri	-0.02	0.01	-1.45
	Symptom X Post	**-0.03**	**0.01**	**-2.74***
				***F(5,79)* = 3.35, *p* = 0.01, R^2 = 0.17**
Control C	**Intercept**	**0.58**	**0.04**	**14.83*****
	Meno Status: Peri	0.00	0.06	-0.07
	Meno Status: Post	**0.20**	**0.06**	**3.45****
	Symptom Score	0.03	0.01	2.08
	Symptom X Peri	-0.02	0.02	-1.18
	Symptom X Post	**-0.05**	**0.01**	**-3.20****
				***F(5,79)* = 3.28, *p* = 0.01, R^2 = 0.17**
Default A	**Intercept**	**0.61**	**0.03**	**17.45*****
	Meno Status: Peri	0.00	0.05	-0.04
	Meno Status: Post	**0.17**	**0.05**	**3.36****
	Symptom Score	0.02	0.01	1.58
	Symptom X Peri	-0.01	0.01	-0.98
	Symptom X Post	**-0.04**	**0.01**	**-2.80***
				***F(5,79)* = 3.07, *p* = 0.01, R^2 = 0.16**
Default B	**Intercept**	**0.60**	**0.04**	**17.08*****
	Meno Status: Peri	-0.01	0.05	-0.12
	Meno Status: Post	**0.18**	**0.05**	**3.47****
	Symptom Score	0.02	0.01	1.77
	Symptom X Peri	-0.02	0.01	-1.34
	Symptom X Post	**-0.04**	**0.01**	**-2.82***
				***F(5,79)* = 3.70, *p* = 0.004, R^2 = 0.19**

Default C	**Intercept**	**0.51**	**0.05**	**11.10*** **
	Meno Status: Peri	-0.02	0.07	-0.31
	Meno Status: Post	**0.16**	**0.07**	**2.38***
	Symptom Score	0.02	0.01	1.03
	Symptom X Peri	-0.01	0.02	-0.74
	Symptom X Post	-0.03	0.02	-1.53
			F(5,79) = 2.06, *p* > .05, R^2 = 0.12	
Dors A	**Intercept**	**0.64**	**0.03**	**19.33*** **
	Meno Status: Peri	-0.03	0.05	-0.66
	Meno Status: Post	**0.14**	**0.05**	**2.86***
	Symptom Score	0.02	0.01	2.14
	Symptom X Peri	-0.01	0.01	-1.13
	Symptom X Post	**-0.03**	**0.01**	**-2.63***
			***F(5,79)* = 3.17, *p* = 0.01, R^2 = 0.17**	
Dors B	**Intercept**	**0.63**	**0.03**	**19.74*** **
	Meno Status: Peri	-0.04	0.05	-0.72
	Meno Status: Post	**0.14**	**0.05**	**2.98** **
	Symptom Score	**0.03**	**0.01**	**2.73***
	Symptom X Peri	-0.02	0.01	-1.51
	Symptom X Post	**-0.04**	**0.01**	**-3.10** **
			***F(5,79)* = 3.91, *p* = 0.003, R^2 = 0.20**	
Limbic A	**Intercept**	**0.41**	**0.05**	**8.06*** **
	Meno Status: Peri	-0.03	0.08	-0.44
	Meno Status: Post	**0.28**	**0.08**	**3.65** **
	Symptom Score	0.03	0.02	1.94
	Symptom X Peri	-0.03	0.02	-1.34
	Symptom X Post	**-0.06**	**0.02**	**-3.37** **
			***F(5,79)* = 4.85, *p* < .001, R^2 = 0.23**	
Limbic B	**Intercept**	**0.38**	**0.05**	**7.33*** **
	Meno Status: Peri	0.01	0.08	0.18
	Meno Status: Post	**0.25**	**0.08**	**3.24** **
	Symptom Score	**0.04**	**0.02**	**2.61***
	Symptom X Peri	-0.04	0.02	-2.07
	Symptom X Post	**-0.06**	**0.02**	**-3.11** **
			***F(5,79)* = 3.68, *p* = 0.005, R^2 = 0.19**	
SalVentAttn A	**Intercept**	**0.56**	**0.04**	**13.25*** **
	Meno Status: Peri	-0.02	0.07	-0.25
	Meno Status: Post	**0.21**	**0.06**	**3.41** **
	Symptom Score	**0.03**	**0.01**	**2.28***
	Symptom X Peri	-0.03	0.02	-1.61
	Symptom X Post	**-0.05**	**0.02**	**-3.17** **
			***F(5,79)* = 3.84, *p* = 0.004, R^2 = 0.20**	
SalVentAttn B	**Intercept**	**0.56**	**0.04**	**13.05*** **
	Meno Status: Peri	-0.01	0.07	-0.15
	Meno Status: Post	**0.23**	**0.06**	**3.53** **

	Symptom Score	0.03	0.01	2.17
	Symptom X Peri	-0.02	0.02	-1.38
	Symptom X Post	**-0.05**	**0.02**	**-3.31****
			***F(5,79)* = 3.92, *p* = 0.003, R^2 = 0.20**	
SomMot A	**Intercept**	**0.45**	**0.05**	**9.41*****
	Meno Status: Peri	0.00	0.07	0.06
	Meno Status: Post	**0.20**	**0.07**	**2.76***
	Symptom Score	**0.04**	**0.02**	**2.40***
	Symptom X Peri	-0.03	0.02	-1.54
	Symptom X Post	**-0.05**	**0.02**	**-2.73***
			***F(5,79)* = 2.42, *p* = 0.04, R^2 = 0.13**	
SomMot B	**Intercept**	**0.45**	**0.05**	**9.27*****
	Meno Status: Peri	0.04	0.07	0.56
	Meno Status: Post	**0.23**	**0.07**	**3.23****
	Symptom Score	**0.04**	**0.02**	**2.48***
	Symptom X Peri	-0.04	0.02	-2.03
	Symptom X Post	**-0.05**	**0.02**	**-2.86***
			***F(5,79)* = 2.88, *p* = 0.02, R^2 = 0.15**	
Temp Parietal	**Intercept**	**0.55**	**0.05**	**11.98*****
	Meno Status: Peri	0.03	0.07	0.44
	Meno Status: Post	**0.19**	**0.07**	**2.80***
	Symptom Score	0.03	0.01	2.11
	Symptom X Peri	-0.04	0.02	-1.95
	Symptom X Post	**-0.04**	**0.02**	**-2.50***
			***F(5,79)* = 2.68, *p* = 0.03, R^2 = 0.14**	
Vis Central	**Intercept**	**0.49**	**0.04**	**10.93*****
	Meno Status: Peri	0.00	0.07	-0.04
	Meno Status: Post	**0.21**	**0.07**	**3.13****
	Symptom Score	**0.03**	**0.01**	**2.27***
	Symptom X Peri	-0.02	0.02	-1.38
	Symptom X Post	**-0.05**	**0.02**	**-3.21****
			***F(5,79)* = 3.00, *p* = 0.02, R^2 = 0.16**	
Vis Peripheral	**Intercept**	**0.50**	**0.04**	**11.53*****
	Meno Status: Peri	-0.03	0.07	-0.50
	Meno Status: Post	**0.21**	**0.06**	**3.23****
	Symptom Score	**0.03**	**0.01**	**2.45***
	Symptom X Peri	-0.02	0.02	-1.42
	Symptom X Post	**-0.05**	**0.02**	**-3.28****
			***F(5,79)* = 3.99, *p* = 0.002, R^2 = 0.20**	

FDR-corrected at q < 0.05; *p ≤ 0.05, **p ≤ 0.01, ***p ≤ 0.001